Norwegian University of Life Sciences
Faculty of Science and Technology (IMT)

Philosophiae Doctor (PhD)
Thesis 2019:19

Comparative analysis of heterogeneous and homogeneous neural field models

Komparativ analyse av heterogene og homogene nevrale feltmodeller

Karina Kolodina

Comparative analysis of heterogeneous and homogeneous neural field models

Komparativ analyse av heterogene og homogene nevrale feltmodeller

Philosophiae Doctor (PhD) Thesis

Karina Kolodina

Norwegian University of Life Sciences
Faculty of Science and Technology

Ås (2019)

Thesis number 2019:19
ISSN 1894-6402
ISBN 978-82-575-1583-6

Supervisory team

John Wyller, Professor (main supervisor)
Faculty of Science and Technology
Norwegian University of Life Sciences

Arkadi Ponossov, Professor (co-supervisor)
Faculty of Science and Technology
Norwegian University of Life Sciences

Anna Oleynik, Doctor (co-supervisor)
Department of Mathematics
University of Bergen, Norway

Evaluation committee

Niklas Wellander, Professor (1st opponent)
Swedish Defence Research Agency (FOI)
Lund University

Andrey Shindyapin, Professor (2nd opponent)
Department of Mathematics and Informatics
Eduardo Mondlane University, Mozambique

Bjørn Fredrik Nielsen, Professor (committee coordinator)
Faculty of Science and Technology
Norwegian University of Life Sciences

Acknowledgement

The present thesis was carried out at the Faculty of Science and Technology, Norwegian University of Life Science (NMBU) in the period of September 2015 - January 2019. The research was supported by the Norwegian University of Life Sciences and The Research Council of Norway, project number 239070.

Here I would like to thank people who made this thesis possible. First of all, I express gratitude to my main supervisor John Wyller for his patient guidance, important advice, encouragement and enthusiasm. I am very grateful to my co-supervisor Arkadi Ponossov for fruitful and stimulating discussions during the preparation phase of the papers. I deeply thank my co-supervisor Anna Oleynik for always being accessible and willing to help, for her constructive remarks and support. Anna has been taking care of me from the first days in Norway. I have learned a lot in the academic environment thanks to her. It has been a great pleasure to work with John, Arkadi and Anna. I also extend my gratitude to my colleagues at the Faculty of Science and Technology for a friendly and warm working atmosphere.

Thanks a lot to my friends in Norway and in Russia for being true friends and advisors in studies and the practicalities of everyday life.

Last but not least I would like to thank my parents and my brother for their love, supporting the choices I make, and for being so close despite being so far away. I also thank my Norwegian family for taking care of me here and encouraging me every day.

Karina Kolodina
Ås, January 2019

Abstract

The present thesis is devoted to the comparative analysis of heterogeneous and homogeneous neural field models. The motivation for this work stems from the fact that there is considerable interest in processes in neural tissue, which can underlie both natural and pathological neurobiological phenomena (e.g., orientation tuning in primary visual cortex, short term working memory, control of head direction, motion perception, visual hallucinations and EEG rhythms). The main aim of this thesis is to investigate the outcome of the analysis of a heterogeneous neural field model and its homogeneous counterpart. Another goal is to get more realistic dynamical models for the brain function which takes into account microscopic effects. Mathematically, this approach is formulated in terms of (a system of) nonlinear integro-differential equations. These models describe nonlinear interactions between neuron populations. They are used as a starting point to study traveling wave fronts, localized stationary solutions (bumps) and pattern formation.

The first part of the thesis consists of the introduction. Here we first give a short review of the neurophysical background. Secondly, we introduce the key mathematical objects of the present thesis, namely a neural field model of the Amari type and a 2-population homogenized neural field model. We also review the basic ideas of homogenization theory and the two-scale convergence method. Then we summarize the results and give ideas for future works. The second part of the thesis consists of three papers. Paper I deals with the existence and linear stability of stationary periodic bump solutions to a neural field model of the Amari type. In Paper II and III we focus on 2-population homogenized neural field models where the cortical microstructure is taken into account in the connectivity strength. We study the existence and stability of localized stationary single bump solutions (Paper II). In Paper III we investigate pattern forming processes in the same neural field model. The key methods in the present study are a pinning function technique for the existence of bumps, spectral methods and properties, block diagonalization and the Fourier decomposition method in the stability assessment and numerical simulations.

We believe that the present thesis contributes to the understanding of the brain functions, both in normal and pathological cases.

Sammendrag

I denne avhandlingen utføres en komparativ analyse av heterogene og homogene nevrale nettverksmodeller. Motivasjonen for dette arbeidet er interessen for prosesser i hjernebarken, som kan være grunnlag for både naturlige og patologiske nevrobiologiske fenomener (for eksempel i orienteringsinnstilling i den primære visuelle hjernebarken, korttidsminne, kontroll av hoderetning, bevegelsesoppfattelse, visuelle hallusinasjoner og EEG-rytmer). Hovedformålet med denne avhandlingen er å analysere en heterogen nevral nettverksmodell og dens homogene motstykke. Et annet mål er å få mer realistiske dynamiske modeller for hjernefunksjonen, som tar hensyn til mikroskopiske effekter. Disse modellene er gitt som (et system av) ikke-lineære integro-differensiallikninger. Disse modellene beskriver ikke-lineære interaksjoner mellom nevronpopulasjoner. De brukes som utgangspunkt for å studere bølgeforplantning, lokaliserte stasjonære løsninger (bumps) og mønsterdannelse.

I introduksjonen presenterer vi en oversikt over den nevrofysiologiske bakgrunnen. Videre introduserer vi de matematiske modellene som er sentrale i denne avhandlingen, det vil si en nevral nettverksmodell av Amari- typen og en homogenisert 2-populasjon nevral nettverksmodell. Vi gjennomgår også grunnbegrepene i homogeniseringsteori og toskala konvergensmetoden. Deretter oppsummerer vi resultatene og fremlegger ideer for videre arbeid. Den andre delen av denne avhandlingen består av tre artikler. Artikkel I omhandler eksistensen og den lineære stabiliteten til stasjonære periodiske bump-løsninger i en nettverksmodell av Amari-typen. I artikkel II og III fokuserer vi på en homogenisert 2-populasjons nevral nettverksmodell, hvor mikrostrukturen i hjernebarken tas med i beregningen av konnektivitetsstyrken. Vi undersøker eksistensen og stabiliteten til lokaliserte stasjonære bump-løsninger (artikkel II). I artikkel III studerer vi mønsterdannende prosesser i den samme nevrale nettverksmodellen. De sentrale metodene i denne studien er en pinning-funksjonsteknikk for eksistens av bumps. Stabilitetsanalysen er gjennomført ved hjelp av spektral metoder , blokk diagonalisering og Fouriertransformasjon og numeriske simuleringer.

Vi mener at denne avhandlingen bidrar til forståelsen av hjernens funksjoner, både under normale og patologiske omstendigheter.

List of papers

1. K. Kolodina, V. Kostrykin, A. Oleynik, *Existence and stability of periodic solutions in a neural field equation*, Submitted to Integral Equations and Operator Theory (2018).

2. K. Kolodina, A. Oleynik, J. Wyller, *Single bumps in a 2-population homogenized neuronal network model*, Physica D: Nonlinear Phenomena 370 (2018) 40-53.

3. K. Kolodina, J. Wyller, A. Oleynik, M.P. Sørensen, *Pattern formation in a 2-population homogenized neuronal network model*, Preprint (2019).

Contents

1 Introduction

1.1 Background

The human brain is a large complex biological system. There has been a tremendous interest in understanding the physiological basis of brain rhythm. The cerebral cortex is the outer layer of neural tissue $1.3 - 4.5$ mm thick. It consists of about 16 billion neurons and about 60×10^{12} connections (synapses). The cerebral cortex involved in higher functions such a memory, spatial reasoning, conscious thought and language [1, 2].

A neuron (nerve cell) as a primary component of the brain cortex consists of a cell body (soma), dendrites, and an axon, see Fig. 1. Dendrites receive electrical and chemical signals from surrounding neurons via synapses to the cell body. Hence, dendrites represent an input function. The cell body processes input data. If the total sum of input signals exceeds a certain threshold value, then the neuron fires a spike (action potential), i.e. produces an output signal. Further, a neuron transmits information through an axon to other neurons. See Fig. 2.

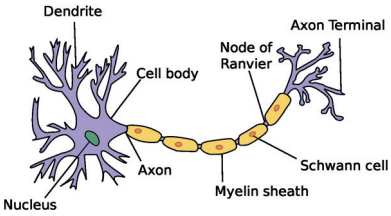

Figure 1: Anatomy of a neuron, https://en.wikipedia.org/wiki/Neuron

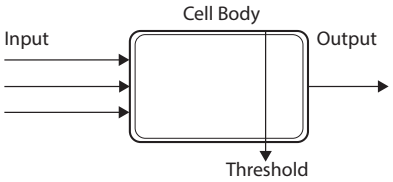

Figure 2: A schematic interpretation of the signal processing properties of a neuron.

In the simplest sense, cortical neurons can be divided into two groups: excitatory and inhibitory cells. An excitatory neuron increases the probability of an action potential occurring in a postsynaptic cell while an inhibitory neuron makes a postsynaptic neuron less likely to generate an action potential.

The first recording of the human electroencephalogram (EEG) was made by Hans Berger in 1924 [3]. It was the stimulus to develop mathematical models of cortical tissue often referred to as neural field model. In the 1950s Beurle [4] developed a continuum description of the proportion of active neurons in a random connected network. It was one of the earliest versions of such models. In the 1970s Wilson and Cowan [5, 6], Nunez [7] and Amari [8] provided the formulations for neural field models that are in common use today.

1.2 Continuous neural field model

Continuous neural field models e.g. introduced by Amari [9, 8] are used to investigate large-scale activity of neuronal population. These types of models have been used to study EEG rhythms [10], visual hallucinations [11, 12, 13], mechanisms for short term working memory (the temporary storage of information within the brain) [14, 15, 16], information processing [17, 18] and motion perception [19]. The dynamic behavior of neural field models contains of spatially and temporally periodic

patterns found in visual hallucinations, traveling waves (fronts, pulses, target wave and spirals) relevant for information processing and stationary localized structure, commonly referred to as bumps and multi-bumps, related to short term memory. In many continuum models for the propagation of electrical activity in neural tissue it is assumed that the synaptic input current is a function of the pre-synaptic firing rate function.

The simplest neural field models are expressed in terms of integro-differential equations (or systems of such equations) defined on the real line or on the plane. The corresponding nonlocal terms feature a synaptic kernel, i.e. a function that models the neuron connectivity at a macroscopic scale. The synaptic kernel is often assumed to be depended on the Euclidean distance between points on the domain and homogeneous. Experimentally it is found that most cortical neurons switch from a resting state to an active state. A resting state is characterized by a low rate of spontaneous firing whereas an active state is characterized by either tonic (regular, repetitive) firing or bursting [20]. Continuous neural field models focus on tonic firing neurons since the majority of cells in cortical networks contains this type of neurons. In this case the neural firing rates at a certain time are given by nonlinear function of the neural activity at the same time. A natural choice for firing rate is a smooth sigmoid-like function. However, neural field models can be conveniently analyzed in the limit of Heaviside firing rates. Provided the Heaviside firing rate a neuron fires maximally or not at all, depending on whether or not synaptic activity is above or below some threshold. See Bressloff [21] and the references therein.

Notice that in the present thesis one of the works is devoted to the study of stationary periodic solutions (bumps) in a continuous neural field model of the Amari type with the Heaviside function as a firing rate function. In particular, we investigate the existence of 1-bump periodic solutions of the model by applying the well-known Amari approach, see [8]. Then we analyze their linear stability by using spectral methods.

1.3 2-population neural field model of the Amari type

Let E be an excitatory population of neurons with activity level u_e and I be an inhibitory population of neurons with activity level u_i. Then the dynamics of excitatory and inhibitory interactions are modelled in a symmetric way: the population I receives impulses from all neurons of population E and vice versa. Besides, each neuron of each population receive impulses from neighbor neurons within the same population, see Fig. 3.

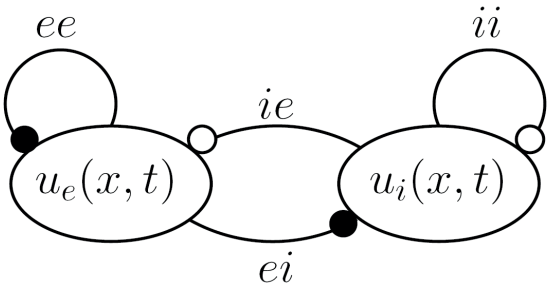

Figure 3: A schematic illustration of interactions between excitatory (E) and inhibitory (I) populations in neural field model with corresponding activity levels u_e and u_i.

In the classical 2-population models introduced by Wilson and Cowan [6], excitatory and inhibitory cells are treated the same with a single scalar number (the firing rate) associated with each neuron. Pinto and Ermentrout [22] have taken into account the activity of synaptically coupled networks of excitatory and inhibitory neurons in a single domain assuming an arrangement of synaptic connections described by "lateral inhibition" (LI) as in [8]. However their model neglects a term describing recurrent inhibition ($i \to i$) and assumes a linear firing rate function for the inhibitory population. The analysis in [22] does not support the hypothesis that sustained activity in prefrontal cortex is a result of the dynamics in a LI network. Later Blomquist *et al.* [23] generalized the model studied by Pinto and Ermentrout [22] by including a recurrent inhibitory term in the inhibitory equation as well as assuming the coupling from inhibitory to excitatory neurons to be nonlinear. Thus, the extended neural field model of excitatory and inhibitory neurons distributed in a line along of the x-axis reads:

$$\begin{aligned} \frac{\partial}{\partial t}u_e &= -u_e + \omega_{ee} \otimes P_e(u_e - \theta_e) - \omega_{ie} \otimes P_i(u_i - \theta_i) \\ \tau\frac{\partial}{\partial t}u_i &= -u_i + \omega_{ei} \otimes P_e(u_e - \theta_e) - \omega_{ii} \otimes P_i(u_i - \theta_i) \end{aligned} \tag{1}$$

where $\omega_{mn} \otimes P_m$ is the convolution of ω_{mn} and P_m $(m, n = e, i)$ defined by

$$\big(\omega_{mn} \otimes P_m(u_m - \theta_m)\big)(x,t) \equiv \int_\Omega \omega_{mn}(x - x', t)P_m(u_m(x', t) - \theta_m)dy'dx' \tag{2}$$

Here Ω is a subset of $\mathbb{R}^N$. The neurons are assumed to occupy Ω. $u_e(x,t)$ and $u_i(x,t)$ denote the synaptic input to an excitatory and inhibitory neurons, respectively, at the spatial point x and time $t > 0$. The functions $\omega_{mn}(x-x')$ $(m, n = e, i)$ describe the coupling strengths (referred to as the connectivity functions) between

neurons at positions x and x', whereas P_m $(m = e, i)$ are the firing rate functions with corresponding threshold values θ_e and θ_i of the excitatory and inhibitory neurons, respectively. The parameter τ is the relative inhibition time i.e. $\tau = \tau_i/\tau_e$ where τ_e (τ_i) is the excitatory (inhibitory) time constant.

The model (1) is often referred to as a 2-population neural field model of the Amari type.

The existence and stability of stationary localized solutions (a pair of single bumps U_e and U_i) in the 2-population model (1) with the Heaviside firing rate functions have been studied in [23]. Wyller *et al.* [24] have investigated the Turing instability and pattern forming processes within the framework (1) in one spatial dimension as a function of the steepness of the firing rate function. In particular, the stationary periodic patterns and spatiotemporal oscillations of (1) have been detected in the pattern forming process.

1.4 Homogenization and two-scale convergence

Here we give an elementary presentation of the basic ideas in the homogenization theory. Since the homogenization theory has important applications in the mathematical analysis of different physical and mechanical phenomena, we use methods of this theory to study inhomogeneous impact in the neural fields.

Homogenization is a method for modeling processes in micro inhomogeneous media, which are encountered in mechanics, physics and engineering. These processes are described by PDEs with rapidly oscillating coefficients or boundary value problems in domains with complex microstructure. Given the complexity of these processes, the best techniques to solve a wide variety of problems involve constructing appropriate macroscopic (homogenized) models.

The theory of homogenization has a long history. It has rapidly developed during the last three decades. This theory has important applications in the mathematical analysis of different physical and mechanical phenomena, see e.g. [25, 26, 27, 28]. The systematic mathematical theory of homogenization was built in [29, 30, 31, 32, 33] and so on.

Let the open bounded set $\Omega \subseteq \mathbb{R}^N$ be occupied by the heterogeneous medium and let $\partial\Omega$ be its boundary. Assume that the heterogeneities are evenly periodically distributed. Then because of the periodicity we can divide Ω into periodic cells $Y = [0, 1]^N$ with the side length ε, see Fig. 4.

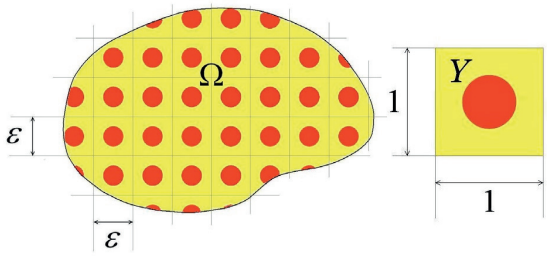

Figure 4: The sample of periodic medium with the representative Y-cell.

Mathematically we have a family of partial differentiable operators $A^\varepsilon(x) = A(\frac{x}{\varepsilon})$ with $A(y)$ being periodic with respect to $y \in Y$ and a family of solutions u^ε. For simplicity, we choose Y to be the unit cube. For a given source term f we obtain the following boundary value problem:

$$\begin{cases} -\nabla \cdot \big(A^\varepsilon(x)\nabla u^\varepsilon(x)\big) = f(x), & \text{in } \Omega \\ u^\varepsilon(x)) = 0, & \text{on } \partial\Omega. \end{cases} \tag{3}$$

The homogenization procedure is not restricted to periodically oscillating operators. Here, however, we focus on the periodically oscillating case. This allows us to use the well-known two-scale asymptotic expansion method [29, 34, 35] in order to find the precise form of the homogenized operator. With this approach we assume that the solutions u^ε can be expanded in a power series in ε of the form

$$u^\varepsilon(x) = u^0\left(x, \frac{x}{\varepsilon}\right) + \varepsilon u^1\left(x, \frac{x}{\varepsilon}\right) + \varepsilon^2 u^2\left(x, \frac{x}{\varepsilon}\right) + \dots \quad , \tag{4}$$

where each term $u^i(x, y)$ is periodic in y. Then if $\varepsilon \to 0$ the sequence of u^ε converges, in some sense, to u^0, where u^0 is the unique solution of the so-called homogenized problem

$$\begin{cases} -\nabla \cdot \big(A^0\nabla u^0(x)\big) = f, & \text{in } \Omega \\ u^0 = 0, & \text{on } \partial\Omega. \end{cases} \tag{5}$$

The two-scale asymptotic expansion method is very simple and powerful. However it is formal since, a priori, the ansatz (4) does not hold true. This method is used only to guess the form of the homogenized operator A^0. To prove the convergence of the sequence u^ε to u^0 we need other arguments. Next we provide a more efficient homogenization method that is called the two-scale convergence method [32]. Note that there are other convergence methods such as Γ-convergence (introduced by De Giorgi, [36, 37] and also [38, 39, 40, 41]), G-convergence for monotone operators (introduced by Spagnolo [42] in 1967), see e.g. [43, 29, 44, 33, 45], and H-convergence (introduced by Tartar in 1977, see [46]), where H-convergence initially is an extension of G-convergence to a wider class of problems.

Two-scale convergence method was invented by Nguetseng in 1989, see [30]. The method relies on the following theorem:

Theorem 1. *Let u^ε be a bounded sequence in $L^2(\Omega)$. There exists a subsequence, still denoted by u^ε, and a function $u^0(x, y) \in L^2(\Omega \times Y)$ such that*

$$\lim_{\varepsilon\to 0} \int_\Omega u^\varepsilon(x)\psi(x, \frac{x}{\varepsilon})dx = \int_\Omega \int_Y u^0(x, y)\psi(x, y)dydx \tag{6}$$

for any smooth function $\psi(x, y)$, which is Y-periodic in y. Such a sequence u^ε is said to two-scale converge to $u^0(x, y)$.

In 1992 Allaire [32] developed the theory further by studying some general properties of two-scale convergence. Allaire provided a simple proof of theorem 1 along with a new corrector result.

Definition: A sequence of functions u^ε in $L^2(\Omega)$ is said *two-scale converge* to a limit $u^0(x,y) \in L^2(\Omega \times Y)$ is for any function $\psi(x,y) \in L^2(\Omega; C^\infty(Y))$, where $C^\infty(Y)$ is the space of infinitely differentiable functions in $\mathbb{R}^N$ that are periodic of period Y, we have

$$\lim_{\varepsilon \to 0} \int_\Omega u^\varepsilon(x)\psi(x, \frac{x}{\varepsilon})dx = \int_\Omega \int_Y u^0(x,y)\psi(x,y)dydx. \tag{7}$$

Theorem 2. *From each bounded sequence u^ε in $L^2(\Omega)$, we can extract a subsequence, and there exists a limit $u^0(x,y) \in L^2(\Omega \times Y)$ such that this subsequence two-scale converges to u^0.*

Moreover Allaire used two-scale convergence to analyze several homogenization problems, both linear and nonlinear.

Two-scale convergence has also been generalized to n-scale convergence (or multi scale convergence) in the obvious way. In [47, 48, 49] n-scale convergence were used to study so-called reiterated homogenization.

1.5 2-population homogenized neural field model

Most studies of a 1- and 2-populations neural field models of the Amari type assume that cortical medium is homogeneous and isotropic, i.e. $\omega(x,y) = \omega(|x-y|)$. However, the best known cortical area, primary visual cortex has a periodic-like microstructure on the millimeter length-scale, reflecting the existence of various stimulus feature maps. This has motivated a number of studies to consider the effect of a periodically modulated weight distribution on wave propagation in neural field, see e.g. [50, 51, 52, 18, 53, 54, 55, 56]. It have been shown that the microstructure has an impact on the pattern forming mechanisms as well as existence and stability of traveling fronts and pulses, moreover it can give rise to a multitude of stable stationary bumps. Thus, the homogeneous isotropic modeling approach represents simplifications of the actual situation. One way to take into account the microstructure of the brain media is by using the homogenization techniques described in the previous section, see also [57, 58].

Svanstedt *et al.* [59] have provided some important results which are relevant to the theory of homogenization in connection with two-scale convergence method, for the nonlocal 1-population neural field models in one-dimensional space. A key point here is Visintin's theorem for two-scale convergence of convolution integrals [60]:

Theorem 3. *Let $p \in [1, +\infty)$, $\{u^\varepsilon\}$ be a sequence of $L^p(\Omega)$ and $\{\omega^\varepsilon\}$ be a sequence of $L^1(\mathbb{R}^N)$ such that*

$$u^\varepsilon \rightharpoonup u \quad \textit{(two-scale weak convergence) in} \quad L^p(\Omega \times Y),$$

$$\omega^\varepsilon \to \omega \quad \textit{(two-scale strong convergence) in} \quad L^1(\Omega \times Y).$$

Then

$$(u^\varepsilon \otimes \omega^\varepsilon)(x) = \int_{\mathbb{R}^N} u^\varepsilon(x')\omega^\varepsilon(x-x')dx' \rightharpoonup$$

$$(u \otimes \otimes \omega)(x,y) = \int_{\mathbb{R}^N} \int_Y u(x',y')\omega(x-x',y-y')dx'dy' \quad in \quad L^p(\Omega \times Y).$$

If moreover $u^\varepsilon \to u$ *in* $L^2(\Omega \times Y)$*, then* $u^\varepsilon \otimes \omega^\varepsilon \to u \otimes \otimes \omega$ *in* $L^2(\Omega \times Y)$*.*

Malyutina, Burlakov, Wyller and their collaborators contributed to the development of investigations on 1-population homogenized neural field models of the Amari type in one- and two-dimensional spaces, see [61, 62, 63, 64, 65, 66, 67].

Let us assume that the connectivity functions are represented as $\omega^\varepsilon_{mn}(x) = \omega_{mn}(x, x/\varepsilon)$ and have periodicity in the second variable $y = x/\varepsilon$, where the microstructure of heterogeneity is parameterized by $\varepsilon > 0$, see e.g. [68, 59, 62]. Then a 2-population heterogeneous neural field model of (1) can be expressed as the following parameterized model:

$$\begin{aligned} \frac{\partial}{\partial t}u^\varepsilon_e &= -u^\varepsilon_e + \omega^\varepsilon_{ee} \otimes P_e(u^\varepsilon_e - \theta_e) - \omega^\varepsilon_{ie} \otimes P_i(u^\varepsilon_i - \theta_i) \\ \tau\frac{\partial}{\partial t}u^\varepsilon_i &= -u^\varepsilon_i + \omega^\varepsilon_{ei} \otimes P_e(u^\varepsilon_e - \theta_e) - \omega^\varepsilon_{ii} \otimes P_i(u^\varepsilon_i - \theta_i) \end{aligned} \tag{8}$$

Applying the theory of homogenization and Theorem 3 to (8) we obtain a 2-population homogenized neural field model:

$$\begin{aligned} \frac{\partial}{\partial t}u_e &= -u_e + \omega_{ee} \otimes \otimes P_e(u_e - \theta_e) - \omega_{ie} \otimes \otimes P_i(u_i - \theta_i) \\ \tau\frac{\partial}{\partial t}u_i &= -u_i + \omega_{ei} \otimes \otimes P_e(u_e - \theta_e) - \omega_{ii} \otimes \otimes P_i(u_i - \theta_i) \end{aligned} \tag{9}$$

where the double convolution of ω_{mn} and P_m $(m, n = e, i)$ is defined by

$$\begin{aligned} &\big(\omega_{mn} \otimes \otimes P_m(u_m - \theta_m)\big)(x,y,t) \equiv \\ &\int\limits_\Omega \int\limits_Y \omega_{mn}(x-x', y-y', t)P_m(u_m(x',y',t) - \theta_m)dy'dx' \end{aligned} \tag{10}$$

and $x \in \Omega, y \in Y$ and $t > 0$.

As part of this thesis, we focus on the 2-population homogenized neural field model (9) for $\Omega = \mathbb{R}^N$ in one spatial dimension, i.e. $N = 1$. Assuming that the firing rate functions are given by the Heaviside function we study existence and linear stability of single bumps solutions in (9). The construction of bump solutions is based on a pinning function technique. The linear stability is analyzed by means of the spectral properties, block diagonalization and the Fourier decomposition method (Paper II). Then assuming that the firing rate functions are smooth functions of sigmoidal shape we investigate pattern formation in (9) (Paper III).

2 Summaries of papers

2.1 Paper I

In the first paper we focus on continuous neural field model of the Hammerstein type often referred to as the Amari model

$$\frac{\partial}{\partial t}u(x,t) = -u(x,t) + \int_{\mathbb{R}} \omega(x-y) f(u(y,t)-h)dy \tag{11}$$

To the best of our knowledge the periodic solutions of (11) have not been studied earlier except for the work by Krisner, see [69]. However, in [69] the existence of periodic solutions have been explored for a particular type of connectivity function by the ODE's method. This work motivated us, firstly, to investigate the existence of stationary 1-bump periodic solutions for general types of connectivity functions and, secondly, to develop the linear stability analysis for these solutions.

For the model (11) we assume that f is given by the Heaviside function and $\omega(x) \to 0$ as $x \to \infty$ sufficiently fast. The construction of 1-bump periodic solutions is similar to the process of construction 1-bump solutions by means Amari approach, see e.g. [8, 70]), and simpler than the ODE's method.

By analysing the spectrum of the Fréchet derivative of the corresponding Hammerstein operator we deduce that the solutions of (11) can be both linearly stable and unstable. We show that the spectrum agrees with the spectrum of an infinite block Laurent operator that can be represented as a bi-infinite matrix with constant diagonal elements. We also find analytical expression for the spectrum by means the Laurent operator's symbol defined on the unit circle. In addition we prove that the spectrum is pointwise and obtain formulas for calculating eigenvectors and eigenfunctions of the Fréchet derivative of the Hammerstein operator.

2.2 Paper II

Based on experiments there is growing evidence that there exist inhomogeneities in the primary visual cortex. Therefore, the brain cortical medium is neither homogeneous nor isotropic. According to Bressloff [50, 51] it has periodic-like microstructure. Thus, our goal is to investigate a 2-population homogenized neural field model and compare results with simpler 2-population neural field model.

In the second paper we study the existence and linear stability of single bump solutions of (9). In this work the periodic microstructure variation is modulated in both the synaptic footprint and the spatial scale of the connectivity strength:

$$\omega_{mn}(x,y) = \frac{1}{\sigma_{mn}(y)}\Phi\left(\frac{x}{\sigma_{mn}(y)}\right)$$

$$\text{with} \quad \sigma_{mn}(y) = s_{mn}(1+\alpha_{mn}\cos(2\pi y)), \quad s_{mn} > 0, \quad 0 \le \alpha_{mn} < 1.$$

The parameters α_{mn}, $m,n = e,i$ are referred to as the degrees of heterogeneity.

Under the assumption that the activation functions are modelled by the Heaviside function, we construct these solutions by means of a pinning function technique. The generic picture of solutions consists of two bumps (one narrow and one broad bump). Depending on the degrees of heterogeneity, we obtain one, two or

three single bump solutions. Next we investigate the linear stability by using the spectral properties of a Fredholm integral operator, block diagonalization and the Fourier decomposition method. For the weakly modulated case of heterogeneity ($0 < \alpha_{mn} << 1$) one of the bumps is unstable for all relative inhibition time τ in (1) whereas the second one is stable for small and moderate values of τ, consistent with the findings in the translational invariant case. In the scenario with three bumps we have at least one stable bump (maximum two stable bumps). Notice that this situation takes place only beyond the weakly modulated case.

2.3 Paper III

In the third paper we continue the investigation of 2-population homogenized neural field model (9). Here we study pattern formation (9) with smooth firing rate functions of sigmoidal shape depending on the steepness parameter. The existence theory for the constant solutions is the same as in Wyller *et al.* [24]. Then we investigate the stability of these solutions by means of a sequence of wave-number dependent invariants of 2×2-matrices representing the sequence of Fourier transformed linearized evolution equations for the perturbation imposed on the homogeneous background. The generic instability structure consists of a finite set of well-separated gain bands. The results are illustrated by examples for symmetrical exponentially decaying connectivity functions in two typical situations depending on the thresholds and inclinations of the firing rate functions (the steep and the shallow firing rate regime). We follow the linear instability into the nonlinear regime. For the weakly modulated case we typically obtain the following scenarios: In the steep firing rate regime the instability develops into a stationary periodic pattern whereas in the shallow regime we get a spatiotemporally oscillating pattern. Beyond the weakly modulated case we have a rich plethora of phenomena.

3 Discussion

3.1 Contribution

The main goal of the present thesis was to analyse a 2-population homogenized neural field model and compare the results with simpler translational invariant limit of this model. The periodic microstructure of the cortical tissue has been taken into account by means of the homogenization technique. The effect of this structure has been studied in details in Papers II and III with respect to existence and stability of bumps and pattern formation. As far as we know the homogenization technique is not widely used in neuroscience community. Nevertheless we believe that this method might be beneficial to investigate inhomogeneous structures of the cerebral cortex.

As we mentioned earlier, Papers II and III represent extensions of the works by Blomquist *et al.* [23] and Wyller *et al.* [24], respectively. All methods used in both papers for the homogenized neural field model are generalization of methods developed in cited above papers. The results obtained in the weakly modulated case of the heterogeneity parameters appear as a continuous deformation of the results in the translation invariant case. However, by increasing the degree of heterogeneity

the number of bumps and their stability as well as pattern forming process need to be analysed in some more detail.

We have also studied 1-bump periodic solutions of a continuous homogeneous neural field model of the Amari type in Paper I. Here we have worked with a more general class of the connectivity functions than in [69]. This has allowed us to address the issue of the uniqueness of the solutions to this model. Under the assumption that the firing rate function is given by the Heaviside function, we have developed the stability analysis of 1-bump periodic solutions by means of the spectral theory.

3.2 Future perspectives

In future works it is natural to extend the present 2-population homogenized neural field model into $2-D$, i.e. the connectivity kernels are defined on a two-dimensional domain (Papers II and III). That can be viewed as a step towards a more realistic description of the actual situation in the cortical tissue. Moreover, this extension can be used as a start point to study the existence and stability of multi-bump and ring solutions as well as traveling waves and fronts. Another future contribution to the present homogenized model and its generalisations to Volterra type of models is finite axonal and dendritic delays effect. After all, the framework of the corresponding homogenized problems in Papers II and III can be modeled by other types of microstructure effects and then investigated existence and stability of coherent structures as well as pattern formation.

In Papers I and II we have assumed that the firing rate functions are given by the Heaviside function. However, the result obtained in these papers can be generalized to the case of smooth sigmoid-like firing rate functions depending on steepness parameters. In particular, for the situation studied in Paper I we conjecture that 1-bump periodic solutions are robust with respect to the parameter changes in the model.

In Paper I another extension that might be interesting is to consider weight (connectivity) functions with lateral inhibition (LI), and look at the transition from unstable to stable bump and periodic solutions as the level of LI is increased. Finally, the analysis represented in Paper I can be generalized to the case of multi-bump periodic solutions and $2-D$.

References

[1] Jan H Lui, David V Hansen, and Arnold R Kriegstein. Development and evolution of the human neocortex. *Cell*, 146(1):18–36, 2011.

[2] Rand S Swenson. Review of clinical and functional neuroscience. *Dartmouth Medical School. Retrieved November*, 18:2012, 2006.

[3] Hans Berger. Über das elektrenkephalogramm des menschen. *Archiv für Psychiatrie und Nervenkrankheiten*, 98(1):231–254, 1933.

[4] Raymond L Beurle. Properties of a mass of cells capable of regenerating pulses. *Philosophical Transactions of the Royal Society of London. Series B, Biological Sciences*, pages 55–94, 1956.

[5] Hugh R Wilson and Jack D Cowan. Excitatory and inhibitory interactions in localized populations of model neurons. *Biophysical journal*, 12(1):1–24, 1972.

[6] Hugh R Wilson and Jack D Cowan. A mathematical theory of the functional dynamics of cortical and thalamic nervous tissue. *Kybernetik*, 13(2):55–80, 1973.

[7] Paul L Nunez. The brain wave equation: a model for the eeg. *Mathematical Biosciences*, 21(3-4):279–297, 1974.

[8] Shun-ichi Amari. Dynamics of pattern formation in lateral-inhibition type neural fields. *Biological cybernetics*, 27(2):77–87, 1977.

[9] Shun-Ichi Amari. Homogeneous nets of neuron-like elements. *Biological cybernetics*, 17(4):211–220, 1975.

[10] Paul L Nunez and Brian A Cutillo. *Neocortical dynamics and human EEG rhythms*. Oxford University Press, USA, 1995.

[11] Paul C Bressloff, Jack D Cowan, Martin Golubitsky, and Peter J Thomas. Scalar and pseudoscalar bifurcations motivated by pattern formation on the visual cortex. *Nonlinearity*, 14(4):739, 2001.

[12] Paul C Bressloff, Jack D Cowan, Martin Golubitsky, Peter J Thomas, and Matthew C Wiener. Geometric visual hallucinations, euclidean symmetry and the functional architecture of striate cortex. *Philosophical Transactions of the Royal Society of London B: Biological Sciences*, 356(1407):299–330, 2001.

[13] G Bard Ermentrout and Jack D Cowan. A mathematical theory of visual hallucination patterns. *Biological cybernetics*, 34(3):137–150, 1979.

[14] Patricia S Goldman-Rakic. Cellular basis of working memory. *Neuron*, 14(3):477–485, 1995.

[15] Carlo R Laing, William C Troy, Boris Gutkin, and G Bard Ermentrout. Multiple bumps in a neuronal model of working memory. *SIAM Journal on Applied Mathematics*, 63(1):62–97, 2002.

[16] Carlo R Laing and William C Troy. Two–bump solutions of amari–type models of working memory. *Physica D: Nonlinear Phenomena*, 178:190–218.

[17] G Bard Ermentrout and J Bryce McLeod. Existence and uniqueness of travelling waves for a neural network. *Proceedings of the Royal Society of Edinburgh Section A: Mathematics*, 123(3):461–478, 1993.

[18] Xiaoying Huang, William C Troy, Qian Yang, Hongtao Ma, Carlo R Laing, Steven J Schiff, and Jian-Young Wu. Spiral waves in disinhibited mammalian neocortex. *Journal of Neuroscience*, 24(44):9897–9902, 2004.

[19] Martin A Giese. *Dynamic neural field theory for motion perception*, volume 469. Springer Science & Business Media, 2012.

[20] Stephen Coombes and Paul C Bressloff. *Bursting: the genesis of rhythm in the nervous system*. World Scientific, 2005.

[21] Paul C Bressloff. Spatiotemporal dynamics of continuum neural fields. *Journal of Physics A: Mathematical and Theoretical*, 45(3):033001, 2011.

[22] David J Pinto and G Bard Ermentrout. Spatially structured activity in synaptically coupled neuronal networks: I. traveling fronts and pulses. *SIAM journal on Applied Mathematics*, 62(1):206–225, 2001.

[23] Patrick Blomquist, John Wyller, and Gaute T Einevoll. Localized activity patterns in two-population neuronal networks. *Physica D: Nonlinear Phenomena*, 206(3):180–212, 2005.

[24] John Wyller, Patrick Blomquist, and Gaute T Einevoll. Turing instability and pattern formation in a two-population neuronal network model. *Physica D: Nonlinear Phenomena*, 225(1):75–93, 2007.

[25] R Burridge, S Childress, and G Papanicolaou. Macroscopic properties of disordered media. In *Macroscopic Properties of Disordered Media*, volume 154, 1982.

[26] Carlos Conca, M Vanninathan, and J Planchard. *Fluids and periodic structures*. Wiley, 1995.

[27] Gianni Dal Maso. *Composite media and homogenization theory*. World Scientific, 1995.

[28] Jerry L Ericksen, David Kinderlehrer, Robert Kohn, and J-L Lions. *Homogenization and effective moduli of materials and media*, volume 1. Springer Science & Business Media, 2012.

[29] Lions JL Bensoussan, A and Papanicolaou G. Asymptotic analysis for periodic structures studies in mathematics and its applications, vol. 5, 1978.

[30] Gabriel Nguetseng. A general convergence result for a functional related to the theory of homogenization. *SIAM Journal on Mathematical Analysis*, 20(3):608–623, 1989.

[31] Grégoire Allaire. Homogénéisation et convergence à deux échelles. application à un problème de convection diffusion. *Comptes rendus de l'Académie des sciences. Série 1, Mathématique*, 312(8):581–586, 1991.

[32] Grégoire Allaire. Homogenization and two-scale convergence. *SIAM Journal on Mathematical Analysis*, 23(6):1482–1518, 1992.

[33] Vasilii Vasil'evich Jikov, Sergei M Kozlov, and Olga Arsen'evna Oleinik. *Homogenization of differential operators and integral functionals*. Springer Science & Business Media, 2012.

[34] Enrique Sánchez Palencia. *Non-homogeneous media and vibration theory*. Springer-Verlag, 1980.

[35] Nikolai Sergeevich Bakhvalov and G Panasenko. *Homogenisation: averaging processes in periodic media: mathematical problems in the mechanics of composite materials*, volume 36. Springer Science & Business Media, 2012.

[36] E De Giorgi-S Spagnolo. Sulla convergenza degli integrali dellenergia per operatori ellittici del secondo ordine. *Ennio De Giorgi*, page 380, 2007.

[37] E De Giorgi. Sulla convergenza di alcune successioni dintegrali del tipo dellarea. *Ennio De Giorgi*, 414, 1975.

[38] Hedy Attouch. *Variational convergence for functions and operators*, volume 1. Pitman Advanced Publishing Program, 1984.

[39] Andrea Braides. *Gamma-convergence for Beginners*, volume 22. Clarendon Press, 2002.

[40] Andrea Braides and Anneliese Defranceschi. *Homogenization of multiple integrals*, volume 12. Oxford University Press, 1998.

[41] Gianni Dal Maso. *An introduction to* Γ*-convergence*, volume 8. Springer Science & Business Media, 2012.

[42] Sergio Spagnolo. Sul limite delle soluzioni di problemi di cauchy relativi all'equazione del calore. *Annali della Scuola Normale Superiore di Pisa-Classe di Scienze*, 21(4):657–699, 1967.

[43] Grégoire Allaire, Andrea Braides, Giuseppe Buttazzo, Anneliese Defranceschi, and L Gibiansky. School on homogenization. *Lecture Notes of the Courses held at ICTP, Trieste*, pages 4–7, 1993.

[44] Doina Cioranescu and Patrizia Donato. Introduction to homogenization. 2000.

[45] Aleksandr Andreevich Pankov. *G-convergence and homogenization of nonlinear partial differential operators*, volume 422. Springer Science & Business Media, 2013.

[46] François Murat and Luc Tartar. H-convergence,séminaire danalyse fonctionnelle et numérique de luniversité dalger, mimeographed notes, 1978. english translation in topics in the mathematical modelling of composite materials (a. cherkaev and r. kohn, eds.). *Progress in Nonlinear Differential Equations and their Applications*, 31, 1994.

[47] Grégoire Allaire and Marc Briane. Multiscale convergence and reiterated homogenisation. *Proceedings of the Royal Society of Edinburgh Section A: Mathematics*, 126(2):297–342, 1996.

[48] Jacque-Louis Lions, Dag Lukkassen, Lars-Erik Persson, and Peter Wall. Reiterated homogenization of monotone operators. *Comptes rendus de l'Académie des sciences. Série 1, Mathématique*, 330(8):675–680, 2000.

[49] Jacques-Louis Lions, Dag Lukkassen, Lars-Erik Persson, and Peter Wall. Reiterated homogenization of nonlinear monotone operators. *Chinese Annals of Mathematics*, 22(01):1–12, 2001.

[50] Paul C Bressloff. Traveling fronts and wave propagation failure in an inhomogeneous neural network. *Physica D: Nonlinear Phenomena*, 155(1):83–100, 2001.

[51] Paul C Bressloff. Spatially periodic modulation of cortical patterns by long-range horizontal connections. *Physica D: Nonlinear Phenomena*, 185(3):131–157, 2003.

[52] Paul C Bressloff, Stefanos E Folias, Alain Prat, and Y-X Li. Oscillatory waves in inhomogeneous neural media. *Physical review letters*, 91(17):178101, 2003.

[53] Zachary P Kilpatrick, Stefanos E Folias, and Paul C Bressloff. Traveling pulses and wave propagation failure in inhomogeneous neural media. *SIAM Journal on Applied Dynamical Systems*, 7(1):161–185, 2008.

[54] Helmut Schmidt, Axel Hutt, and Lutz Schimansky-Geier. Wave fronts in inhomogeneous neural field models. *Physica D: Nonlinear Phenomena*, 238(14):1101–1112, 2009.

[55] Stephen Coombes and CR Laing. Pulsating fronts in periodically modulated neural field models. *Physical Review E*, 83(1):011912, 2011.

[56] Daniele Avitabile and Helmut Schmidt. Snakes and ladders in an inhomogeneous neural field model. *Physica D: Nonlinear Phenomena*, 294:24–36, 2015.

[57] Jack Xin. An introduction to fronts in random media. *SIAM Review*, 42:161, 2000.

[58] Jack Xin. An introduction to fronts in random media. *Surveys and Tutorials in the Applied Mathematical Sciences, Springer Verlag*, 2009.

[59] Nils Svanstedt and Jean Louis Woukeng. Homogenization of a wilson–cowan model for neural fields. *Nonlinear Analysis: Real World Applications*, 14(3):1705–1715, 2013.

[60] Augusto Visintin. Towards a two-scale calculus. *ESAIM: Control, Optimisation and Calculus of Variations*, 12(3):371–397, 2006.

[61] Elena Malyutina, John Wyller, and Arcady Ponosov. Two bump solutions of a homogenized wilson–cowan model with periodic microstructure. *Physica D: Nonlinear Phenomena*, 271:19–31, 2014.

[62] Nils Svanstedt, John Wyller, and Elena Malyutina. A one-population amari model with periodic microstructure. *Nonlinearity*, 27(6):1391–1417, 2014.

[63] Elena Malyutina, Arcady Ponosov, and John Wyller. Numerical analysis of bump solutions for neural field equations with periodic microstructure. *Applied Mathematics and Computation*, 260:370–384, 2015.

[64] Evgenii Burlakov, Evgeny Zhukovskiy, Arcady Ponosov, and John Wyller. Existence, uniqueness and continuous dependence on parameters of solutions to neural field equations. *Memoirs on Differential Equations and Mathematical Physics*, 65:35–55, 2015.

[65] Evgenii Burlakov, John Wyller, and Arcady Ponosov. Two-dimensional amari neural field model with periodic microstructure: Rotationally symmetric bump solutions. *Communications in Nonlinear Science and Numerical Simulation*, 32:81–88, 2016.

[66] Evgenii Burlakov, Arcady Ponosov, and John Wyller. Stationary solutions of continuous and discontinuous neural field equations. *Journal of Mathematical Analysis and Applications*, 444(1):47–68, 2016.

[67] Evgenii Burlakov, Evgeny Zhukovskiy, Arcady Ponosov, and John Wyller. On wellposedness of generalized neural field equations with delay. *arXiv preprint arXiv:1805.06754*, 2018.

[68] Stephen Coombes, Carlo Laing, Helmut Schmidt, Nils Svanstedt, and John Wyller. Waves in random neural media. *Discrete and Continuous Dynamical Systems—Series A*, 32:2951–2970, 2012.

[69] Edward P Krisner. Periodic solutions of a one-dimensional wilson-cowan type model. *Electronic Journal of Differential Equations (EJDE)[electronic only]*, 2007:Paper–No, 2007.

[70] Stephen Coombes, Peter beim Graben, Roland Potthast, and James Wright. *Neural fields: theory and applications*. Springer, 2014.

PAPER I

EXISTENCE AND STABILITY OF PERIODIC SOLUTIONS IN A NEURAL FIELD EQUATION

KARINA KOLODINA, VADIM KOSTRYKIN, AND ANNA OLEYNIK

ABSTRACT. We study the existence and linear stability of stationary periodic solutions to a neural field model, an intergo-differential equation of the Hammerstein type. Under the assumption that the activation function is a discontinuous step function and the kernel is decaying sufficiently fast, we formulate necessary and sufficient conditions for the existence of a special class of solutions that we call 1-bump periodic solutions. We then analyze the stability of these solutions by studying the spectrum of the Frechet derivative of the corresponding Hammerstein operator. We prove that the spectrum of this operator agrees up to zero with the spectrum of a block Laurent operator. We show that the non-zero spectrum consists of only eigenvalues and obtain an analytical expression for the eigenvalues and the eigenfunctions. The results are illustrated by multiple examples.

1. INTRODUCTION

The behavior of a single layer of neurons can be modeled by a nonlinear integro-differential equation of the Hammerstein type,

$$\frac{\partial}{\partial t}u(x,t) = -u(x,t) + \int_{\mathbb{R}} \omega(x-y) f(u(y,t)-h)dy. \tag{1.1}$$

Here $u(x,t)$ and $f(u(x,t)-h)$ represent the averaged local activity and the firing rate of neurons at the position $x \in \mathbb{R}$ and time $t > 0$, respectively. The parameter $h \in \mathbb{R}$ denotes the threshold of firing and $\omega(x-y)$ describes a coupling between neurons at positions x and y.

The model (1.1) belongs to a special class of models, so called neural field models, where the neural tissue is treated as a continuous structure, and is often referred to as the Amari model. Since the original paper by Amari [1], this model has been studied in numerous mathematical papers, for a review see, e.g., [2, 3] and [4]. In particular, the global existence and uniqueness of solutions to the initial value problem for (1.1) under rather mild assumptions on f and ω has been proven in [5].

In [1] Amari studied pattern formation in (1.1) for a model under the simplifying assumption that f is the unit step function H, and ω is of the "lateral-inhibitory type", i.e., continuous, integrable and even, with $\omega(0) > 0$ and having exactly one positive zero. In particular, he analyzed the existence and stability of stationary localized solutions, or so called 1-bump solutions, of the fixed point problem

$$u(x) = (\mathcal{H}u)(x), \quad (\mathcal{H}u)(x) = \int_{-\infty}^{+\infty} \omega(x-y) f(u(y)-h)dy. \tag{1.2}$$

The equations (1.1) and (1.2) have been studied with respect to various combinations of firing rate functions and connectivity functions, see [2, 6, 4]. Common examples of ω are the exponentially decaying function,

$$\omega(x) = Se^{-s|x|}, \quad S, s > 0, \tag{1.3}$$

2000 *Mathematics Subject Classification.* 45L05, 47H30, 47N60, 47G10, 47B48, 47B35.

Key words and phrases. nonlinear integral equations, sigmoid type nonlinearities, neural field model, periodic solutions, block Laurent operators.

the so-called wizard-hat function,

$$\omega(x) = S_1 e^{-s_1|x|} - S_2 e^{-s_2|x|}, \quad S_1 > S_2 > 0, \quad s_1 > s_2 > 0, \tag{1.4}$$

and the periodically modulated function

$$\omega(x) = e^{-b|x|}(b\sin(|x|)) + \cos(x)), \quad b > 0, \tag{1.5}$$

see Fig.1. In the paper we impose the following assumptions on ω.

Assumption A. *The connectivity function ω satisfies the following conditions.*

(i) $\omega(x) = \omega(-x)$

(ii) $\omega(x) \to 0$ *as* $|x| \to \infty$ *and* $|\omega(x)| \le C(1+|x|)^{-1-\delta}$, $C, \delta = \text{const} > 0$.
(iii) $\omega \in C_b^{0,1}(\mathbb{R}) \cap L_1(\mathbb{R})$.
(iv) $\int_{\mathbb{R}} \omega(x)dx =: h_0 > 0$.

One can easily check that the functions in (1.3) - (1.5) satisfy Assumption A and decrease exponentially fast as $|x| \to 0$.

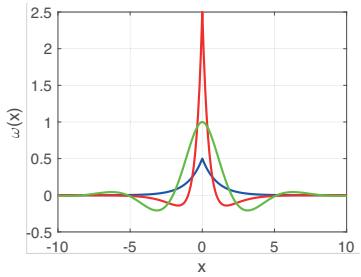

FIG. 1. Connectivity functions $\omega(x)$ given by (1.3) with $S = 0.5$, $s = 1$ (blue curve), (1.4) with $S_1 = 4$, $s_1 = 2$, $S_2 = 1.5$, $s_2 = 1$ (red curve), and (1.5) with $b = 0.5$ (green curve).

The firing rate function $f : \mathbb{R} \to [0, 1]$ is usually given as a smooth function of sigmoid shape. It is often represented by a parameterized function $f(u) = S(\beta u)$, see e.g. [7, 8, 9, 10] where $S(\beta u)$ approaches (in some specific way) the unit step function $H(u)$ as $\beta \to \infty$. One example of $f(u)$ is

$$f(u) = S(\beta u), \quad S(u) = \frac{u^p}{u^p + 1} H(u), \quad p > 1, \tag{1.6}$$

see Fig. 2.

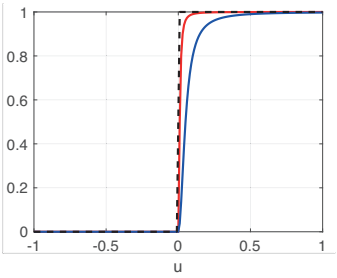

FIG. 2. Functions $f(u) = S(\beta u)$, S is as in (1.6), $p = 2$, with $\beta = 100$ (red curve) and $\beta = 20$ (blue curve) and the unit step function $H(u)$(black dashed line).

Already in his seminal paper Amari conjectured that there must exist periodic stationary solutions in the absence of bump solutions and constant solutions. He however did not pursue a further study of periodic solutions. Of course the absence of other types of stationary solutions is not necessary for periodic solutions to exist. In fact, as in some cases bump solutions can be viewed as a homoclinic orbits of an ordinary differential equation (ODE) with ω being the Green's function of its linear part, see e.g. [11], periodic solutions are very likely to co-exist with the bump solution, see [12, 13] (in Russian) and [14], and [15]. In [16, 17, 3] it has been shown numerically that stable periodic solutions of the two population version of the Amari model exist and emerge from homogeneous solutions via Turing-Hopf bifurcation. To the best of our knowledge there are no theoretical studies that address the existence of periodic solutions to (1.1) except [8], and no studies on the stability of these solutions.

Krisner in [8] studied the existence of periodic solutions to (1.1) with ω given by (1.5). In this case, any bounded solution of (1.2) is a solution of a forth order ODE, see [18] and can be studied by methods developed for ODEs. Given f as a smooth steep sigmoid function it has been shown that (1.1) has at least two periodic solution under some assumptions on the parameters. The analysis is however rather cumbersome and is not applicable for general types of ω as, e.g., (1.3) and (1.4). Thus, we would like to proceed in a different way and address the existence of periodic solutions without reformulating (1.2) as ODEs.

When f is approximated by a step function H it is possible to obtain analytical expressions for some types of stationary solutions and travelling waves, see e.g. chapter 3 in [4] and [19]. However, the operator $\mathcal{H}$ in this case is discontinuous in any classical functional space and thus, classical functional analysis tools such as e.g. generalized Picard-Lindelof theorem or Hartman-Grobman theorem, usually fail. However, many papers still conveniently assume that the model is well-posed on the considered spaces and study the stability of solutions by first approximation, see [1, 19, 20] and [21] just to name a few.

The natural way to overcome this problem is to study the model (1.1) with $f(u) = S(\beta u)$ and only use the limiting case $f = H$ to gain the knowledge about the existence and stability of solutions for large values of β. The approximation of $f = H$ with $f = S(\beta u)$ then must be properly justified. This has been successfully done for bumps solutions in [10, 22] and [23].

Our overall aim is to generalize the analysis in the mentioned papers for the periodic 1-bump solutions. In this paper we take the first crucial step towards this direction and study the limiting case $f = H$.

The paper organized as follows: Section 2 contains the notation we use. In Section 3 we give the definition of 1-bump periodic solutions and study their existence by means of the Amari approach. We formulate necessary and sufficient conditions for the existence of 1-bump periodic

solutions and show that for $\omega \geq 0$ there is a unique solution for each period $T > 0$. Section 4 is dedicated to the linear stability of 1-bump periodic solutions. We show that the spectrum of the corresponding linearized operator $\mathcal{H}$ can be obtained as the spectrum of an infinite block Laurent (or bi-infinite block Toeplitz) operator. We give an analytical expression for the spectrum in terms of the symbol of the Laurent operator and discuss ways how it can be calculated numerically. We prove that the spectrum consists only of eigenvalues and give a formula for calculating eigenfunctions. The results in Section 3 and Section 4 are illustrated for the case of ω given by (1.3) and (1.4). Section 5 contains conclusions and remarks.

2. NOTATIONS

For the convenience of the readers we give a list of functional spaces and specify other notations we use.

- S^1 is the unit circle.
- i is the imaginary unit.
- $\overline{z}$ is the complex conjugate of $z \in \mathbb{C}$.
- $cl(\Omega)$ is the closure of a set Ω.
- $\|\cdot\|_{op}$ denotes the operator norm.
- $C_b^{0,1}(\mathbb{R})$ is the space of all Lipschitz continuous bounded functions on $\mathbb{R}$ equipped with the norm

$$\|f\|_{C_b^{0,1}(\mathbb{R})} = \sup_{x,y\in\mathbb{R}} \frac{|f(x)-f(y)|}{|x-y|}, \quad x \neq y.$$

- $\ell_p^m(\mathbb{Z})$ is the Banach space of sequences with entries from $\mathbb{R}^m$ where $1 \leq p \leq \infty$ and $m \in \mathbb{N}$ equipped with the norm

$$\|x\|_{\ell_p^m(\mathbb{Z})} = \left(\sum_{k\in\mathbb{Z}} \|x_k\|^p\right)^{1/p}, \quad 1 \leq p < \infty$$

and

$$\|x\|_{\ell_\infty^m(\mathbb{Z})} = \sup_{k\in\mathbb{Z}} \|x_k\|, \quad p = \infty,$$

where $\|\cdot\|$ is any norm in $\mathbb{R}^m$.

- $\ell_p^{m\times m}(\mathbb{Z})$ is the space of sequences where components are matrices m by m on $\mathbb{R}$, equipped with the norm

$$\|A\|_{\ell_p^{m\times m}(\mathbb{Z})} = \left(\sum_{k\in\mathbb{Z}} \|A_k\|_{op}^p\right)^{1/p}, \quad 1 \leq p < \infty$$

and

$$\|A\|_{\ell_\infty^{m\times m}(\mathbb{Z})} = \sup_{k\in\mathbb{Z}} \|A_k\|_{op}, \quad p = \infty.$$

- $\mathcal{W}(S^1)$ is the Wiener space of functions defined on S^1 (continuous functions whose Fourier coefficients is an $\ell_1(\mathbb{Z})$ sequence) equipped with the norm

$$\|f\|_{\mathcal{W}} = \sum_{k\in\mathbb{Z}} |a_k|,$$

where a_k are the Fourier coefficients of f.

- $\mathcal{W}^{m\times m}(S^1)$ is the Wiener space of m by m matrix functions defined on S^1 equipped with the norm

$$\|\varphi\|_{op} = \max_{1\leq i\leq m} \sum_{j=1}^{m} \|\varphi_{ij}\|_{\mathcal{W}}.$$

- $\sigma(L)$ is the spectrum of the linear operator L.

• $\rho(L)$ is the resolvent of the linear operator L.

3. Existence of 1-bump periodic solutions

We consider a particular type of periodic solution that we call a 1-bump periodic solution, due to its shape on one considered period, that is, $u(x) \geq h$ on a (connected) interval and $u(x) < h$ otherwise. Krisner in [8] proved the existence of the same type of periodic solutions for ω given in (1.5). Below we define the class of periodic functions that we intent to consider.

Definition 3.1. *Let $h \in \mathbb{R}$, and $u(x)$ be a continuous periodic function defined on $\mathbb{R}$ with a period $T > 0$. We say that $u(x)$ is a* 1-bump periodic *function with period T, or simply 1-bump periodic, if there is a translation of $u(x)$, say $p(x) = u(x - c)$, with the following properties:*

(i) *It has two symmetric intersection, say at $x = \pm a$ with the straight line $y = h$, i.e., $p(\pm a) = h$.*

(ii) *It lies above $y = h$ for all $x \in (-a, a)$ and below for $x \in [-T/2, T/2] \setminus [-a, a]$, i.e., $p(x) > h$ for $x \in (-a, a)$ and $p(x) < h$ for $x \in [-T/2, T/2] \setminus [-a, a]$.*

If in addition $u \in C^1_b(\mathbb{R})$ with $p'(\pm a) \neq 0$ then we say that $u(x)$ is regular.

We illustrate the definition above in Fig.3

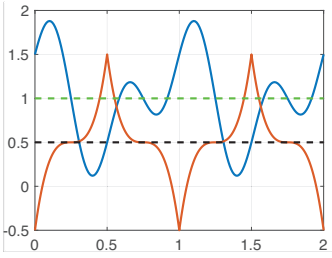

FIG. 3. The function corresponding to the blue curve is the regular 1-bump periodic if $h = 0.5$ and is not a 1-bump periodic if $h = 1$. The red curve corresponds to the 1-bump periodic function for both $h = 0.5$ and $h = 1$. Here we assume that the functions given by blue and red curves both have period $T = 1$.

A small perturbation of a regular 1-bump periodic function in $C^{0,1}_b(\mathbb{R})$ does not destroy the 1-bump structure of the function. We formulate it as the lemma below.

Lemma 3.2. *Let $h \in \mathbb{R}$ and $T > 0$ be fixed and $p(x)$ be a regular 1-bump periodic function with $p(\pm a) = h$, $0 < a < T/2$. Then there exists $\varepsilon > 0$ such that any $v \in B_\varepsilon(u_p) := \{v| : \|v - u_p\|_{C^{0,1}} < \varepsilon\}$ has exactly two intersection with the straight line $y = h$ on each of the intervals $(-T/2 + kT, T/2 + kT)$, $k \in \mathbb{Z}$, i.e., there are $a_\pm(\varepsilon, k) \in (-T/2 + kT, T/2 + kT)$ such that $v(a_\pm(\varepsilon, k)) = h$. Moreover $a_\pm(\varepsilon, k) \to \pm a + kT$ as $\varepsilon \to 0$ and $v(x) > h$ for $x \in (a_-(\varepsilon, k), a_+(\varepsilon, k))$ and $v(x) < h$ for $x \in [-T/2 + kT, T/2 + kT] \setminus (a_-(\varepsilon, k), a_+(\varepsilon, k))$.*

Proof. The proof goes in line with the proof of Lemma 3.6 in [24]. □

Definition 3.3. *A (regular) 1-bump periodic function which is a solution to* (1.2) *we call a (regular) 1-bump periodic solution to* (1.1).

We notice that any solution to (1.2) is translation invariant, i.e., if $u(x)$ is a solution to (1.2) then so is $u(x-c)$ for any $c \in \mathbb{R}$. Thus, without loss of generality we can simply consider $p(x) = u(x)$ in (ii) of Definition 3.1.

Given that f is a unit step function, a 1-bump periodic solution can be expressed as

$$u_p(x) = \sum_{k\in\mathbb{Z}} \int_{-a+kT}^{a+kT} \omega(x-y)dy = \sum_{k\in\mathbb{Z}} \int_{-a}^{a} \omega(x-y+Tk)dy \tag{3.1}$$

where $a \in (0, T/2)$ is the root of $u_p(a) = h$.

We notice here that the critical cases $a = 0$ and $a = T/2$ correspond to the constant solutions $u_p(x) = 0$ and $u_p(x) = h_0$ where $h_0 = \int_{\mathbb{R}} \omega(y)dy > 0$. This serves as a motivation to consider $h \in (0, h_0)$. Further we will show that for some connectivity functions the condition $h \in (0, h_0)$ is sufficient for the existence of a 1-bump periodic solution.

It is easy to see that the function in (3.1) is periodic. Indeed,

$$u_p(x+T) = \sum_{k\in\mathbb{Z}} \int_{-a}^{a} \omega(x-y+T(k+1))dy = u_p(x).$$

Moreover, due to Assumption A (i), it is even

$$\begin{aligned} u_p(-x) &= \sum_{k\in\mathbb{Z}} \int_{-a}^{a} \omega(-x-y+Tk)dy = \sum_{k\in\mathbb{Z}} \int_{-a}^{a} \omega(-x+y+Tk)dy \\ &= \sum_{k\in\mathbb{Z}} \int_{-a}^{a} \omega(x-y-Tk)dy = u_p(x). \end{aligned}$$

From Assumption A(ii) we obtain the following estimate

$$\max_{\substack{x\in[-T/2,T/2]\\ y\in[-a,a]}} |\omega(x-y+Tk)| \le C\alpha_k, \quad k \in \mathbb{Z},$$

where

$$\alpha_k = \begin{cases} 1, & k = 0, \\ (1+T|k|-a-T)^{-1-\delta}, & |k| \ge 1. \end{cases}$$

Since $\sum\limits_{k\in\mathbb{Z}} \alpha_k$ converges, the series $\sum\limits_{k\in\mathbb{N}} \omega(x+Tk)$ converges absolutely and uniformly on $[-a-T/2, a+T/2]$. Due to periodicity of this series, it converges absolutely and uniformly on any bounded interval to an even periodic function

$$\omega_p(x;T) := \sum_{k\in\mathbb{Z}} \omega(x-Tk) \tag{3.2}$$

that has the antiderivative

$$W_p(x;T) := \int_0^x \omega_p(y;T)dy = \sum_{k\in\mathbb{Z}} \int_0^x \omega(y-kT)dy. \tag{3.3}$$

Using the notations above we obtain

$$u_p(x) = \int_{-a}^{a} \omega_p(x-y;T)dy \tag{3.4}$$

or, equivalently,

$$u_p(x) = W_p(x+a;T) - W_p(x-a;T) \tag{3.5}$$

where a is then given as

$$W_p(2a;T) = h. \tag{3.6}$$

Thus, the procedure of finding 1-bump periodic solutions becomes analogous to the one of finding 1-bump solutions proposed by Amari in [1] where instead of ω and W we use ω_p and W_p, respectively. Namely, first we find a from (3.6). Then we verify that the function in (3.5) is indeed a 1-bump periodic function. As the function u_p is even and periodic, it is enough to consider the interval $[0, T/2]$. We summarize this in a theorem.

Theorem 3.4. *The function $u_p(x)$ given by* (3.5) *is a periodic solution to* (1.1) *if and only if the following three conditions hold*

(1) $u_p(a) = h$, *or equivalently,* $W_p(2a; T) = h$, *for some* $0 < a < T/2$,
(2) $u_p(x) > h$ *for all* $x \in (0, a)$,
(3) $u_p(x) < h$ *for all* $x \in (a, T/2]$.

Similarly as for the bump solutions, it is not generally possible to verify the conditions of the theorem above without additional information about ω. However, for a particular choice of ω the verification procedure is rather simple.

Observe that from (3.5) $u_p \in C^1_b(\mathbb{R})$. Then we calculate

$$u_p'(x) = \omega_p(x + a; T) - \omega_p(x - a; T) \tag{3.7}$$

and

$$|u_p'(a)| = \omega_p(0; T) - \omega_p(2a; T). \tag{3.8}$$

Hence, if u_p is a 1-bump periodic solution, $\omega_p(0; T) \geq \omega_p(2a; T)$ must be satisfied. Then for $\omega \geq 0$ we can simplify conditions of Theorem (3.4).

Lemma 3.5. *Let $T > 0$ be arbitrary and ω satisfies Assumption A. Then for any $0 < h < h_0$ the equation $u_p(a) = h$ possesses at least one solution $a \in (0, T/2)$. If $\omega \geq 0$ and can have only isolated zeros then such $a = a(T)$ is unique and the corresponding u_p is a 1-bump regular periodic solution provided that $\omega_p(2a(T); T) < \omega_p(0; T)$.*

Proof. Since the function $W_p(x; T)$ is continuous and $W_p(0; T) = 0$ and $W_p(T; T) = h_0 > 0$, there is at least one solution to the equation $W_p(2a; T) = h$ with $0 < a < T/2$.

Assume now that $\omega \geq 0$ and does not have non isolated zeros. Then $W_p(x; T)$ is strictly monotone increasing on $[0, T/2]$. Indeed,

$$\frac{d}{dx} W_p(x; T) = \omega_p(x; T) = \sum_{k \in \mathbb{Z}} \omega(x + Tk) \geq 0$$

and may have only isolated zeros. This implies the uniqueness of a as a function of T. The final statement follows from (3.8) and uniqueness of a. □

For more general function ω number of 1-bump periodic solution may vary with the period. In the next section we give several examples of ω, T and h for which the solutions do not exist, exist and are unique or non-unique.

3.1. **Examples.** We consider two examples of the connectivity functions given in (1.3) and (1.4) where most of the calculations can be done analytically.

Indeed, for ω given by (1.3) we get $h_0 = 2S/s$,

$$\omega_p(x; T) = S\psi(x \bmod T; s), \text{ and } W_p(x) = \frac{2S}{s} \left\lfloor \frac{x}{T} \right\rfloor + S\Psi(x \bmod T; s)$$

where

$$\psi(x; s) = \frac{\exp(-sx) + \exp(-s(T - x))}{1 - \exp(-sT)} \tag{3.9}$$

$$\Psi(x; s) = \frac{\exp(s(x - T)) - \exp(-sx) - \exp(-sT) + 1}{s(1 - \exp(-sT))}, \tag{3.10}$$

see Fig.4(a).

From Lemma 3.5 the equation $W_p(2a;T) = h$, $h \in (0, h_0)$ possesses a unique solution $0 < a(T) < T/2$. Moreover, $\omega_p(0;T) = 2S/(1-\exp(-sT))$ and $\omega_p(2a;T) = (\exp(-2sa) + \exp(-s(T-2a)))/(1-\exp(-sT))$ and thus, $\omega_p(2a;T) < \omega_p(0;T)$ for any $T > 0$ which implies that $u_p(x)$ is a 1-bump regular periodic solution, see Fig.3.

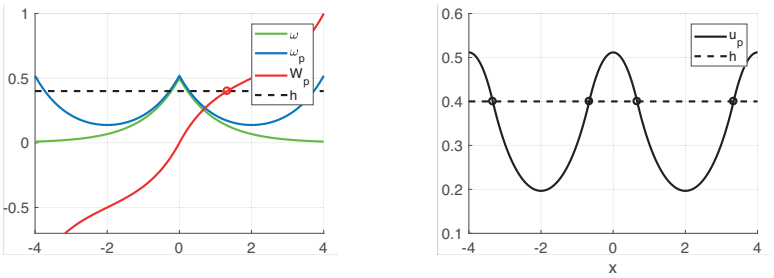

(a) (b)

FIG. 4. (a)The function ω given in (1.3) with $S = 0.5$, $s = 1$ and the corresponding ω_p and W_p with $T = 4$. The intersection point corresponds to $a = 0.6633$ (rounded up to 4 decimals) and $h = 0.4$. (b) 1-periodic bump solution (3.5) with W_p as in (a).

For ω given by (1.4) we find $h_0 = 2(S_1/s_1 - S_2/s_2)$,

$$\omega_p(x;T) = S_1\psi(x \bmod T; s_1) - S_2\psi(x \bmod T; s_2) \tag{3.11}$$

and

$$W_p(x;T) = \left(\frac{2S_1}{s_1} - \frac{2S_2}{s_2}\right)\left\lfloor \frac{x}{T}\right\rfloor + S_1\Psi(x \bmod T; s_1) - S_2\Psi(x \bmod T; s_2) \tag{3.12}$$

with ψ and Ψ given as in (3.9)-(3.10), see Fig. 5.

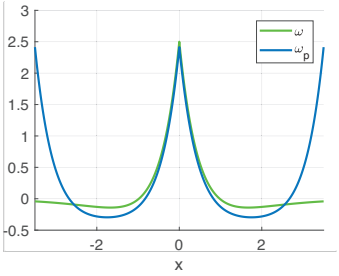

FIG. 5. The function ω given by (1.4) with parameters $S_1 = 4$, $s_1 = 2$, $S_2 = 1.5$, $s_2 = 1$ and the corresponding ω_p and W_p , see (3.11)-(3.12) with $T = 3.5$.

The equation $W_p(2a;T) = h$, $h \in (0, h_0)$ has one, two, or three solutions depending on T. That is for the parameter values $S_1 = 4$, $s_1 = 2$, $S_2 = 1.5$, $s_2 = 1$ and $h = 0.4$, it has one solution for $T < T_1 := 2.4997$, two solutions for $T = T_1$ and three solutions for $T > T_1$, see

Fig.6. The value $T_1 = 2.4997$ is obtained numerically and is rounded up to four decimals. It turns out that all of u_p correspond to 1-periodic bump solutions, see Fig.7 -Fig.8 .

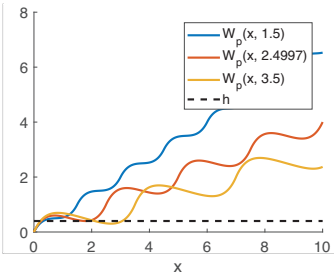

FIG. 6. The function W_p in (3.12) with parameters $S_1 = 4$, $s_1 = 2$, $S_2 = 1.5$, $s_2 = 1$ for different periods T and the fixed threshold value $h = 0.4$.

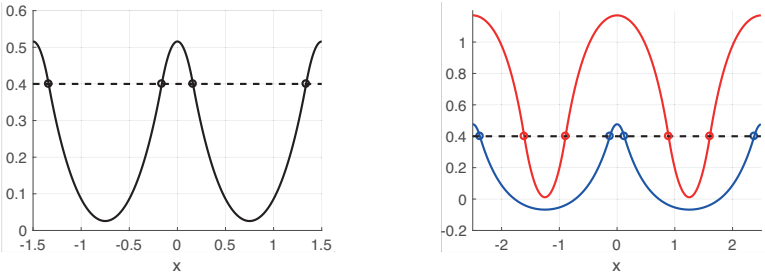

(a) (b)

FIG. 7. (a) 1-bump periodic solutions (3.5) with $T = 1.5$. The intersection point corresponds to $a = 0.1619$ and $h = 0.4$. (b) 1-bump periodic solutions (3.5) with $T = 2.4997$. The intersection points correspond to $a_1 = 0.1243$, $a_2 = 0.8919$ and $h = 0.4$. (All the approximated values are rounded up to 4 decimals.)

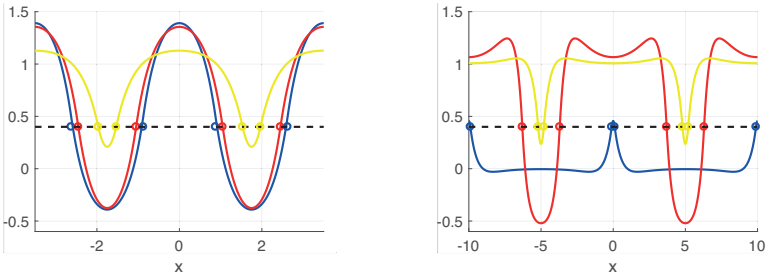

(a) (b)

FIG. 8. (a) 1-bump periodic solutions (3.5) with $T = 3.5$. The intersection points correspond to $a_1 = 0.1113$, $a_2 = 1.0494$ and $a_3 = 1.5281$, and $h = 0.4$. (b) 1-bump periodic solutions (3.5) with $T = 7$. The intersection points correspond to $a_1 = 0.1046$, $a_2 = 2.2792$ and $a_3 = 3.3036$ and $h = 0.4$. (All the approximated values are rounded up to 4 decimals.)

There are parameters S_1, S_2, and s_1, s_2 that $W_p(2a;T) = h$ have two solutions for $h > h_0$ and some $T > 0$. For example, for $S_1 = 3$, $s_1 = 2$, $S_2 = 1.4$, $s_2 = 1$, and $h = 0.25$ this situation occurs when $T > 2.116$, see Fig. 9. These solutions correspond to the 1-bump periodic solutions, see Fig. 10. We however do not aim to study this particular case of the connectivity function in detail. Thus, we will further restrict our attention to the case $h < h_0$, see Fig. 6.

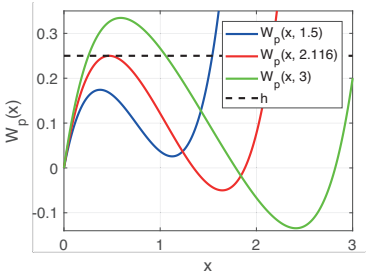

FIG. 9. The function $W_p(x;T)$ in (3.12) with parameters $S_1 = 3$, $s_1 = 2$, $S_2 = 1.4$, $s_2 = 1$, for different periods T and the fixed threshold value $h = 0.25$.

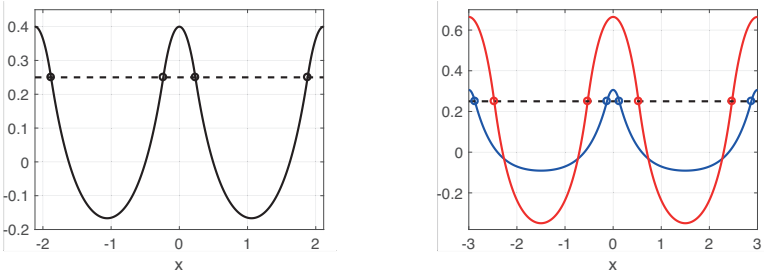

(a) (b)

FIG. 10. (a) 1−bump periodic solution (3.5) with $T = 2.116$. The point of tangency corresponds to $a = 0.2352$ and $h = 0.25$. (b) 1−bump periodic solutions (3.5) with $T = 3$. The intersection points correspond to $a_1 = 0.1272$, $a_2 = 0.5288$ and $h = 0.25$. (All the approximated values are rounded up to 4 decimals.)

4. STABILITY OF 1-BUMP PERIODIC SOLUTIONS

In this section we study linear stability of regular 1-bump periodic solutions. We first obtain the Fréchet derivative of the Hammerstein operator defined in (1.2) and then study its spectrum.

Lemma 4.1. *Let $h, T > 0$ be fixed and u_p be a 1-bump periodic solution of* (1.1)*. The Fréchet derivative of the operator $\mathcal{H} : C_b^{0,1}(\mathbb{R}) \to C_b^{0,1}(\mathbb{R})$ at u_p exists and is given as*

$$(\mathcal{H}'(u_p)v)(x) = \frac{1}{|u_p'(a)|}\sum_{k\in\mathbb{Z}}(\omega(x+a-kT)v(-a+kT) + \omega(x-a-kT)v(a+kT)).$$

Proof. Due to Lemma 3.2 and periodicity of u_p the proof in [10] for bumps can be easily adopted here. □

We would like to emphasize that the regularity condition on u_p, that is $|u_p'(a)| > 0$, is necessary in order for the Fréchet derivative to exists.

Next we show how the spectrum of the operator $\mathcal{H}'(u_p)$ relates to the spectrum of a Laurent block operator, or in some literature, bi-infinite block Toeplitz operator, see e.g. [25] and [26, 27].

Let $\ell_p^m(\mathbb{Z})$ be a Banach space of sequences with entries from $\mathbb{R}^m$, see Section 2.

The block Laurent operator $L : \ell_p^m(\mathbb{Z}) \to \ell_p^m(\mathbb{Z})$ can be represented as an bi-infinite matrix with constant diagonal elements, that is, $L = (A_{i-j})_{i,j\in\mathbb{Z}}$ giving

$$L = \begin{pmatrix} \ddots & & & & \\ & A_0 & A_{-1} & A_{-2} & \\ & A_1 & A_0 & A_{-1} & \\ & A_2 & A_1 & A_0 & \\ & & & & \ddots \end{pmatrix}, \quad A_k \in \mathbb{R}^{m\times m}. \tag{4.1}$$

The representation (4.1) means that the action of L is given by

$$\left(L\,(x_n)_{n\in\mathbb{Z}}\right) = (y_n)_{n\in\mathbb{Z}}, \quad y_j = \sum_i A_{i-j}x_j.$$

For $p = 1, \infty$ we have

$$\|L\|_{op} = \sum_{k\in\mathbb{Z}} \|A_k\|_{op}. \tag{4.2}$$

Theorem 4.2. *The nonzero spectrum of the operator $\mathcal{H}'(u_p) : C_b^{0,1}(\mathbb{R}) \to C_b^{0,1}(\mathbb{R})$ (see Lemma 4.1) agrees with that of the Laurent block operator $L : \ell^2_\infty(\mathbb{Z}) \to \ell^2_\infty(\mathbb{Z})$ defined by*

$$A_k = \frac{1}{|u_p'(a)|}\begin{pmatrix} \omega(kT) & \omega(-2a+kT) \\ \omega(2a+kT) & \omega(kT)\end{pmatrix}. \tag{4.3}$$

Moreover, any eigenfunction $v(x)$ of $\mathcal{H}'(u_p)$ (if exists) corresponds to the eigenfunction $\mathrm{v} = (\mathrm{v}_k)_{k\in\mathbb{Z}}$ of L where

$$\mathrm{v}_k = (v(-a+kT), v(a+kT))^T, \quad k \in \mathbb{Z},$$

and for a given eigenfunction v of L that corresponds to a non-zero eigenvalue, we can calculate the eigenfunction of $\mathcal{H}'(u_p)$ as

$$v(x) = \frac{1}{\lambda}\frac{1}{|u_p'(a)|}\sum_{k\in\mathbb{Z}} (\omega(x+a-kT)\mathrm{v}_k^{(1)} + \omega(x-a-kT)\mathrm{v}_k^{(2)}.$$

Proof. First of all we observe that L is a bounded operator on $\ell^2_\infty(\mathbb{Z})$ since

$$\|L\|_{op} = \frac{1}{|u_p'(a)|}\sum_{k\in\mathbb{Z}} (|\omega(kT)| + \max\{|\omega(\pm 2a + kT)|\}) < \infty$$

due to Assumption A.

A number $\lambda \in \mathbb{C}$ is in the resolvent set of the operator $\mathcal{H}'(u_p)$ if and only if the equation

$$\mathcal{H}'(u_p)\xi - \lambda\xi = w$$

has a solution ξ for any w, where ξ and w belong to the complexified $C_b^{0,1}(\mathbb{R})$.

Thus, if $\lambda \in \mathbb{C}$ is in the resolvent set of the operator $\mathcal{H}'(u_p)$, then for any $k \in \mathbb{Z}$ the system of equations

$$(\mathcal{H}'(u_p)\xi)(a+kT) - \lambda\xi(a+kT)\xi = w(a+kT),$$
$$(\mathcal{H}'(u_p)\xi)(-a+kT) - \lambda\xi(-a+kT)\xi = w(-a+kT)$$

possesses a solution. Hence, λ is in the resolvent set of the operator L.

Conversely, assume that $\lambda \neq 0$ is in the resolvent set of the operator L. Then for any arbitrary w the values $\xi(a+kT)$ and $\xi(-a+kT)$ of the solution to $\mathcal{H}'(u_p)\xi - \lambda\xi = w$ are determined. For arbitrary $x \in \mathbb{R}$ we set

$$\xi(x) = \frac{1}{\lambda}((\mathcal{H}'(u_p)\xi)(x) - w(x)).$$

It is straightforward to verify that $\xi \in C_b^{0,1}$ and solves $\mathcal{H}'(u_p)\xi - \lambda\xi = w$. We have shown that the resolvent sets of $\mathcal{H}'(u_p)$ and L agree up to the point $\lambda = 0$. Thus, their spectra agree up to the point $\lambda = 0$ as well. The second part of the statement follows from above. □

The reader can find more information about Laurent operators and their properties in [25] and more recent studies [27, 26]. The results concerning in particular the spectrum of Laurent operators can be found in [28]. Finally, as the spectrum of Laurent operator on $\ell^m_2(\mathbb{Z})$ is given by the spectrum of the corresponding matrix valued multiplication operator we refer to [29] where the spectrum of the latter operator is studied. For the original paper on the Toeplitz and Laurent operators see [30]. Since the eigenvalue 0 does not have any impact on the stability of u_p, we now turn to the study of the Laurent operator in (4.1) with elements as in (4.3).

As $(A_k)_{k\in\mathbb{Z}} \in \ell_1^{2\times 2}(\mathbb{Z})$ we can define a matrix function $\Phi : S^1 \to \mathbb{R}^{2\times 2}$ as

$$\Phi(z) = \sum_{k\in\mathbb{Z}} A_k z^k, \quad z \in S^1, \tag{4.4}$$

where S^1 is the unit circle. The power series is uniformly convergent and thus the function Φ is continuous on S^1. The function Φ is called a symbol or a defining function of L. It is easily observed that Φ belongs to the Weiner algebra of all periodic functions with absolutely summable sequence of Fourier coefficients, that is $\Phi \in \mathcal{W}^{2\times 2}(S^1)$. Via the Fourier transform the Banach algebra of all block Laurent operators on $\ell^2_\infty(\mathbb{Z})$ is isomorphic to $\mathcal{W}^{2\times 2}(S^1)$.

We prove the following important result.

Theorem 4.3. (i) *The spectrum of the block Laurent operator $L : \ell^m_\infty(\mathbb{Z}) \to \ell^m_\infty(\mathbb{Z})$ is given as*

$$\sigma(L) = \bigcup_{z\in S^1} \sigma(\Phi(z)) \tag{4.5}$$

where $\Phi(z)$ is the symbol (4.4) *of L.*

(ii) *The spectrum $\sigma(L)$ is pointwise, and the eigenvectors $\mathrm{v}_\lambda = (v_k(\lambda))_{k\in\mathbb{Z}}$ of L can be calculated as*

$$\mathrm{v}^{(k)}_\lambda = \bar{z}^k w(z_\lambda) \tag{4.6}$$

where $z_\lambda \in S^1$ is such that $\lambda \in \sigma(\Phi(z_\lambda))$, and $w(z_\lambda)$ is the corresponding eigenvalue of the matrix $\Phi(z_\lambda)$.

Proof. To prove the first statement we recall that invertibility (and Fredholmness) of operators on the Wiener algebra is independent on underlying space, see [31, 32] and references therein. That is, the spectrum of $L : \ell^m_p(\mathbb{Z}) \to \ell^m_p(\mathbb{Z})$, does not depend on $1 \le p \le \infty$, and is given by all the values $\lambda \in \mathbb{C}$ such that $\det(\Phi(z) - \lambda I) = 0$ for some $z \in S^1$, see [25, 28] and [29].

To prove the second statement let $\lambda \in \sigma(L)$. From (4.5) there exists $z_\lambda = \exp(i\theta_\lambda)$, $\theta_\lambda \in [0, 2\pi)$ such that

$$\det(\Phi(z_\lambda) - \lambda I) = 0.$$

Thus, there exists an eigenvector $w(z_\lambda) \in \mathbb{C}^m$ such that

$$\Phi(z_\lambda) w(z_\lambda) = \lambda w(z_\lambda).$$

Let us define $v \in \ell^m_\infty(\mathbb{Z})$ as follows

$$v = \{v_k\}_{k\in\mathbb{Z}}, \quad v_k = e^{-\mathrm{i}k\theta_\lambda} w(z_\lambda).$$

It is easy to check that $v \in \ell^m_\infty(\mathbb{Z})$ and is the eigenfunction of the Laurent operator L corresponding to λ. Indeed, for the nth row we have

$$\begin{aligned}(Lv)_n &= \sum_{k\in\mathbb{Z}} A_{k-n} e^{\mathrm{i}k\theta_\lambda} w(z_\lambda) = \sum_{l\in\mathbb{Z}} A_l e^{\mathrm{i}(n+l)\theta_\lambda} w(z_\lambda) = \\ &= e^{\mathrm{i}n\theta_\lambda} \sum_{l\in\mathbb{Z}} A_l e^{\mathrm{i}l\theta_\lambda} w(z_\lambda) = e^{\mathrm{i}n\theta_\lambda} \Phi(z_\lambda) = e^{\mathrm{i}n\theta_\lambda} \lambda w(z_\lambda) = \\ &= \lambda v_n.\end{aligned}$$

□

Next, we describe some properties of the symbol Φ that corresponds to the Laurent operator (4.3).

Lemma 4.4. *The matrix $\Phi(z)$ in* (4.4) *with A_k given by* (4.3) *is self-adjoint and $\overline{\Phi(z)} = \Phi(\bar{z})$, $z \in S^1$.*

Proof. The second property follows directly from (4.4) and $\omega(x)$ being real. To show that $\Phi(z)$ is self-adjoint let $\theta \in [0, 2\pi)$. Then we have

$$\overline{\Phi(z)^T} = \sum_{k\in Z} \begin{pmatrix} \omega(kT) & \omega(2a+kT) \\ \omega(-2a+kT) & \omega(2kT) \end{pmatrix} e^{-\mathrm{i}k\theta} = \sum_{m\in Z} \begin{pmatrix} \omega(-mT) & \omega(2a-mT) \\ \omega(-2a-mT) & \omega(-mT) \end{pmatrix} e^{\mathrm{i}m\theta} = \Phi(z)$$

as $\omega(x)$ is symmetric, see Assumption A(i). □

From Lemma 4.4 and Theorem 4.3(i) the spectrum of L, and consequently of $\mathcal{H}'(u_p)$, is real and

$$\sigma(L) = \bigcup_{z\in S^1} (\lambda_{1,2}(z)) \tag{4.7}$$

where

$$\lambda_1(z) = \Phi_{11}(z) - |\Phi_{12}(z)| \text{ and } \lambda_2(z) = \Phi_{11}(z) + |\Phi_{12}(z)| \tag{4.8}$$

and $\Phi_{ij}(z)$ are the entries of the symbol matrix $\Phi(z)$. Moreover, it is enough to consider only half of the circle, that is, $z = e^{\mathrm{i}\theta}$ with $\theta \in [0, \pi]$.

Let now $z_\lambda = e^{\mathrm{i}\theta}$ in Theorem 4.3(ii) with $\theta/(2\pi)$ being a rational number from $[0, 0.5]$, i.e. $\theta/(2\pi) = p/q$, $p \cup \{0\}$, $q \in \mathbb{N}$ where p and q are in the lowest terms. Then from (4.6) the corresponding eigenvector v is $(1+q)$-periodic. If $\lambda \neq 0$ then from Theorem 4.2, the eigenfunction v of $\mathcal{H}'(u_p)$ is $(1+q)T$-periodic. Thus, we can calculate the spectrum even without calculating the symbol Φ. We summarize it as a theorem.

Theorem 4.5. *The spectrum of the operator L is given as*

$$\sigma(L) = cl\left(\bigcup \sigma\left(L(1+q)\right)\right)$$

where $L(1+q)$, $q = 1, 2, ...,$ are $2(1+q) \times 2(1+q)$ matrices given as

$$L(1+q) = \begin{pmatrix} B_0 & B_1 & B_2 & ... & B_q \\ B_q & B_0 & B_1 & ... & B_{q-1} \\ \vdots & \vdots & \vdots & \vdots & \vdots \\ B_1 & B_2 & B_3 & ... & B_0 \end{pmatrix}$$

where

$$B_n = \frac{1}{|u_p'(a)|} \begin{pmatrix} \omega_p(nT; (1+q)T) & \omega_p(-2a+nT; (1+q)T) \\ \omega_p(2a+nT; (1+q)T) & \omega_p(nT; (1+q)T) \end{pmatrix}, n = 0, ..., q.$$

We illustrate Theorem 4.5 in Fig.12(b) for ω as in (1.3).

When $q = 0$ we readily calculate $L(1) = B_0$ where

$$B_0 = \frac{1}{u_p'(a)} \begin{pmatrix} \omega_p(0; T) & \omega_p(2a; T) \\ \omega_p(2a; T) & \omega_p(0; T) \end{pmatrix},$$

has the eigenvalues

$$\lambda_{1,2} = \frac{\omega_p(0; T) \pm \omega_p(2a; T)}{\omega_p(0; T) - \omega_p(2a; T)} \tag{4.9}$$

or, equivalently, $\lambda_1 = 1$ and $\lambda_2 = 1 + 2\omega_p(2a; T)/|\omega_p(0; T) - \omega_p(2a; T)|$.

These eigenvalues are similar to the ones obtained for bump solutions. Indeed, for a bump solution one can compute the corresponding eigenvalues of the Fréchet operator (at a bump solution) as $\mu_1 = 1$ and $\mu_2 = 1 + 2\omega(2a)/|\omega(0) - \omega(2a)|$, see e.g.[33]. The first eigenvalue $\lambda_1 = 1$ ($\mu_1 = 1$) corresponds to the translation of the solution, see [33]. Thus, for the bump solutions, the sign of $\omega(2a)$ will define the linear stability. In the case of 1-bump periodic solutions, $\omega_p(2a; T) > 0$ implies instability. Thereby, we immediately conclude that for excitatory connectivity functions ω 1-bump periodic solutions are always unstable.

If $\omega_p(2a; T) < 0$ the eigenvalues of $L(2)$, then $L(3)$ and etc., must be calculated. The structure of $L(1 + q)$ could be useful in exploring spectrum if the analytic expression for Φ is not available.

As we aim at studying Lyapunov stability of 1-bump periodic solutions for (1.1) with smooth sigmoid like function f by deriving spectral asymptotic, the eigenvalue 1 ideally must be isolated and have multiplicity one. We believe that the second condition could be satisfied under some additional assumptions on ω_p, including $\omega_p(2a; T) \neq 0$. The first condition, however, is never satisfied. Thus one must employ more detailed analysis of spectral convergence than in the case of bump solutions [23]. However, this is out of the scope of this paper.

In the next section we apply the theory above to study linear stability of the 1-bump periodic solutions from Section 3.1.

4.1. **Examples.** Define the auxiliary functions

$$\alpha(\theta; s, T) = \frac{\sinh(sT)}{\cosh(sT) - \cos(\theta)} \tag{4.10}$$

and

$$\beta(\theta; s, T) = \frac{\sinh(2as)e^{-\mathrm{i}\theta} + \sinh(s(T - 2a))}{\cosh(sT) - \cos(\theta)}. \tag{4.11}$$

Then, for ω as in (1.3) we obtain

$$\Phi(e^{\mathrm{i}\theta}) = \frac{S}{|u_p'(a)|} \begin{pmatrix} \alpha(\theta; s) & \overline{\beta(\theta; s)} \\ \beta(\theta; s) & \alpha(\theta; s) \end{pmatrix}.$$

In Fig. 12(a) we plot $\lambda_1(e^{\mathrm{i}\theta})$ and $\lambda_2(e^{\mathrm{i}\theta})$ as functions of θ, $\theta \in [0, 2\pi)$ for $T = 4$ and the parameters as in Fig.4. As $\lambda_i(z) - 1 < 0$ the 1-bump periodic solution is linearly unstable. It can be shown that this is always the case for all admissible parameters and any $T > 0$. Indeed, for $S = 0.5$ and $s = 1$, we obtain $a \to -0.5 \log(|2h - 1|)$ as $T \to \infty$ and $\lambda_1 \to 1$ while $\lambda_2 \to 1/h - 1 > 1$. We notice that these values could be obtained by passing the limit in (4.9). In Fig.11 we plot the minimum and maximum of $\lambda_2(e^{\mathrm{i}\theta})$ (red curves) and $\lambda_1(e^{\mathrm{i}\theta})$ (blue curves) for different T. As $T \to 0$, $\max_\theta \lambda_2(e^{\mathrm{i}\theta}) \to \infty$.

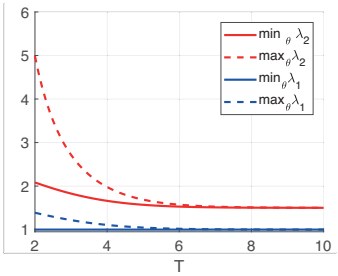

FIG. 11. Bounds for $\sigma(L)$ in (4.7) depending on T when ω is given by (1.3) with $S = 0.5$, $s = 1$, and $h = 0.4$.

In order to illustrate Theorem 4.5, we plot the eigenvalues of the matrices $L(n)$ for $n = 6$, $n = 10$ and $n = 50$ in Fig. 12(b).

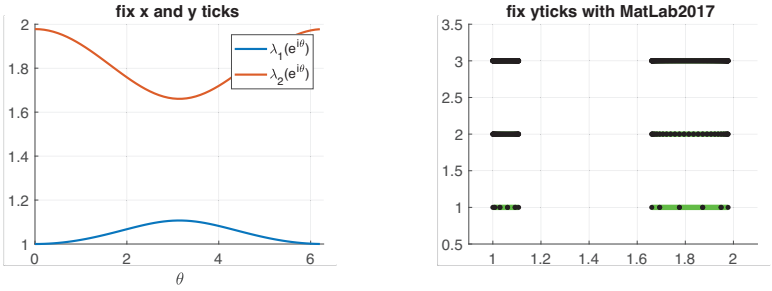

(a) (b)

FIG. 12. (a) The eigenvalues $\lambda_{1,2}(e^{\mathrm{i}\theta})$ as functions of θ when ω is given by (1.3) with parameters $S = 0.5$, $s = 1$, $h = 0.4$ and $T = 4$. (b) The eigenvalues of the matrices $L(n)$ for $n = 6$, $n = 20$ and $n = 50$ (black dots) with the same parameters as in (a).

Let us consider ω in (1.4). We readily find

$$\Phi(e^{\mathrm{i}\theta}) = \frac{1}{|u_p'(a)|}\begin{pmatrix} S_1\alpha(\theta,s_1,T) - S_2\alpha(\theta,s_2,T) & \overline{S_1\beta(\theta,s_1,T) - S_2\beta(\theta,s_2,T))} \\ S_1\beta(\theta,s_1,T) - S_2\beta(\theta,s_2,T) & S_1\alpha(\theta,s_1,T) - S_2\alpha(\theta,s_2,T) \end{pmatrix}$$

with $u_p'(a)$ given by (3.8).

For this case we have different cases depending on T, see Table 1.

Parameters	Number of solutions	Stability
$0 < T < T_1$	One solution $u_{p,1}$	Unstable
$T = T_1$	Two solutions $u_{p,1}$ and $u_{p,cr}$	Unstable
$T \in (T_1, T_2)$	Tree solutions $u_{p,i}$	Unstable
$T \geq T_2$	Tree solutions $u_{p,i}$	$u_{p,1}, u_{p,3}$ are unstable, $u_{p,2}$ is stable

TABLE 1. $u_{p,k} = u_p(x; a_i)$, $i = 1, 2, 3$ are 1-bump periodic solutions for $a_1 \leq a_2 \leq a_3$. For parameters $S_1 = 4$, $s_1 = 2$, $S_2 = 1.5$, $s_2 = 1$ and $h = 0.4$ we have $T_1 = 2.4997$, $T_2 = 3.3320$ and examples of $u_{p,\cdot}$ given in Fig. 7-Fig. 8.

The solution $u_{p,1}$ is always unstable, see Table 1. Similarly to the previous examples, we plot spectral bounds in Fig. 13. In Fig. 13(b) we plot the boundaries of $\lambda_1(z)$ to illustrate that at $T = T_1$ the eigenvalue becomes less than 1, which in this case does not effect the stability of the solution.

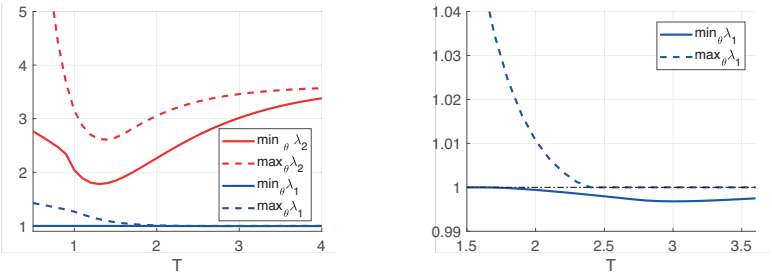

(a) (b)

FIG. 13. Bounds for $\sigma(L)$ when $u_p = u_{p,1}$, depending on T. Here ω is given by (1.4) with $S_1 = 4$, $s_1 = 2$, $S_2 = 1.5$, $s_2 = 1$ and $h = 0.4$, see Table 1.

The period $T = T_1$ corresponds to the critical situation where the new linearly unstable solution $u_{p,cr}$ appears, and splits into two unstable solutions $u_{p,2}$ and $u_{p,3}$ for $T = T_1 + \varepsilon$, $\varepsilon > 0$. The spectrum of L in this case has no spectral gap, see Fig. 14.

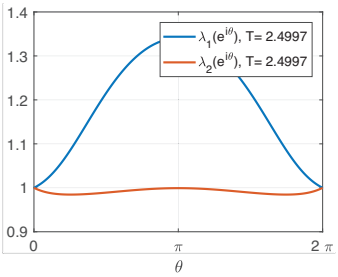

FIG. 14. The eigenvalues $\lambda_1(e^{\mathrm{i}\theta})$ and $\lambda_1(e^{\mathrm{i}\theta})$ when $u_p = u_{p,cr}$. Here ω is given as in (1.4) with $S_1 = 4, s_1 = 2, S_2 = 1.5, s_2 = 1, h = 0.4$, the critical period value $T = T_1 = 2.4997$ giving $\sigma(L) = [9.8460, 1.3403]$ (all the approximated values are rounded up to 4 decimals).

For the solution $u_{p,2}$ we plot the bifurcation diagram in Fig. 15. The red curves corresponds to the minimum and maximum of λ_2 and blue to the minimum and maximum values of λ_1 for different T. From (4.8) the spectrum of $\mathcal{H}'(u_{p,2})$ lies in between of red and blue curves.

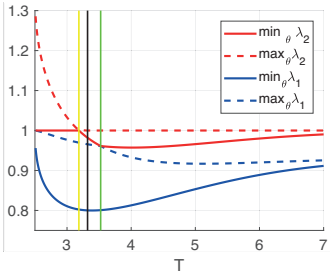

FIG. 15. Bounds for $\sigma(L)$, when $u_p = u_{p,2}$, depending on T. The marked values corresponds to $T = 3.1849$ (yellow), $T = 3.3320$ (black) and $T = 3.5243$ (green) (all the values are rounded up to 4 decimals). Here ω is given as in (1.4) with $S_1 = 4, s_1 = 2, S_2 = 1.5, s_2 = 1, h = 0.4$, see Table 1.

The point $T = 3.1849$ in Fig.15 seemingly appears as a bifurcation point. This is however not the case and $T = 3.1849$ only corresponds to the situation when minimum of $\lambda_2(e^{\mathrm{i}\theta})$ becomes negative. In order to clarify this point we plot $\lambda_2(e^{\mathrm{i}\theta})$ for $T = 3.18$, $T = 3.1849$ in Fig. 16(a). We also plot $\lambda_2(e^{\mathrm{i}\theta})$ for $T = 3.25$ and the bifurcation point $T = T_2 = 3.3320$ in Fig. 16(a). For $T = 3.5243$ the spectrum is again a connected set $\sigma(L) = [0.8007, 1]$, see Fig.16(b).

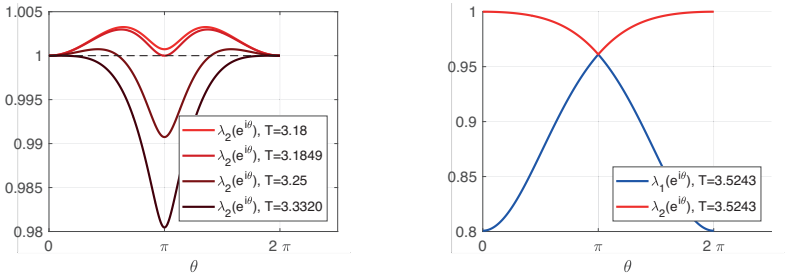

(a) (b)

FIG. 16. The eigenvalue $\lambda_2(e^{i\theta})$ in (a) and $\lambda_{1,2}(e^{i\theta})$ in (b) when $u_p = u_{p,2}$, see Table 1 for different T. Here ω is given as in (1.4) with $S_1 = 4, s_1 = 2$, $S_2 = 1.5$, $s_2 = 1$, $h = 0.4$.

Similarly, we plot the spectral bounds for $u_{p,3}$ in Fig.17.

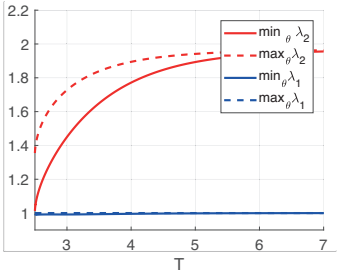

FIG. 17. Bounds for $\sigma(L)$ when $u_p = u_{p,3}$, depending on T, see Table 1. Here ω is given as in (1.4) with $S_1 = 4, s_1 = 2$, $S_2 = 1.5$, $s_2 = 1$, $h = 0.4$.

As $T \to \infty$ the limiting values could be calculated from (4.9) once the limiting expression for $a(T)$ is obtained. The calculations however are cumbersome and we omit them here. The numerical calculations however indicate, as illustrated in Fig.13, 15 and 17, that there are no stability changes for larger period T.

We plot examples of $\lambda_1(e^{i\theta})$ and $\lambda_2(e^{i\theta})$ as functions of θ for $T = 1.5$,$T = 3.2$ and $T = 3.5$ for every solution $u_{p,i}$, $i = 1, 2, 3$, in Fig. 18-20.

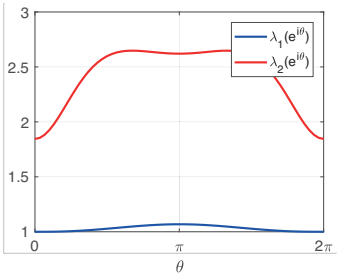

FIG. 18. The eigenvalues $\lambda_{1,2}(e^{\mathrm{i}\theta})$ when $u_p = u_{p,1}$. Here ω is given as in (1.4) with $S_1 = 4, s_1 = 2, S_2 = 1.5, s_2 = 1, h = 0.4$, and $T = 1.5$. The resulting spectrum $\sigma(L) = [1, 1.0684] \cup [1.8449, 2.6479]$

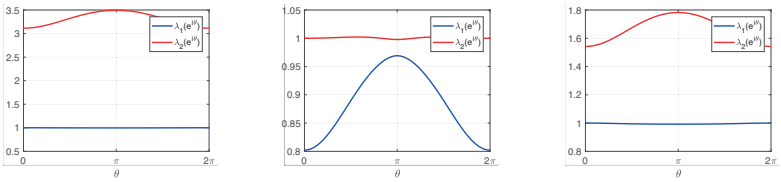

(a) (b) (c)

FIG. 19. The eigenvalues $\lambda_{1,2}(e^{\mathrm{i}\theta})$ for $u_p = u_{p,1}$ in (a), $u_p = u_{p,2}$ in (b) and $u_p = u_{p,3}$ in (c). Here ω is given as in (1.4) with $S_1 = 4, s_1 = 2, S_2 = 1.5, s_2 = 1, h = 0.4$, and $T = 3.2$. The corresponding spectra are $\sigma(L) = [0.9969, 1] \cup [3.1147, 3.4945]$, $\sigma(L) = [0.8020, 0.9692] \cup [0.9978, 1.0022]$ and $\sigma(L) = [0.9921, 1] \cup [1.5419, 1.7825]$, respectively. (All the approximated values are rounded up to 4 decimals).

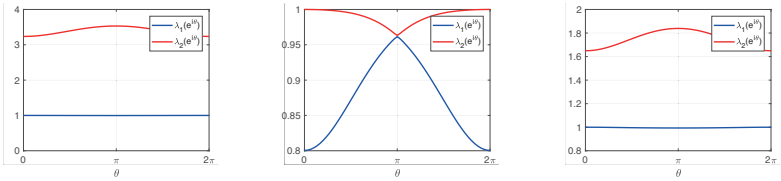

FIG. 20. The eigenvalues $\lambda_{1,2}(e^{\mathrm{i}\theta})$ for $u_p = u_{p,1}$ in (a), $u_p = u_{p,2}$ in (b) and $u_p = u_{p,3}$ in (c). Here ω is given as in (1.4) with $S_1 = 4, s_1 = 2, S_2 = 1.5, s_2 = 1, h = 0.4$, and $T = 3.5$. The corresponding spectra are $\sigma(L) = [0.9973, 1] \cup [3.2365, 3.5318]$, $\sigma(L) = [0.8005, 0.9616] \cup [0.9633, 1]$ and $\sigma(L) = [0.9934, 1] \cup [1.6494, 1.8390]$, respectively. (All the approximated values are rounded up to 4 decimals).

5. Conclusions and outlook

In the present paper we have studied the existence of stationary periodic solutions, the so-called 1-bump periodic solutions, of the Amari model, and their linear stability. We have restricted the choice of the firing rate function to the Heaviside function. This allowed us to obtain an almost explicit description of the solutions when the connectivity functions ω are sufficiently localized symmetric interactions with positive total mass. We have shown that the analysis of the existence then boils down to analysing the behaviour of the T-periodic function $\omega_p(x;T)$, obtained as the infinite sum of $\omega(x+kT)$, on the half period interval. Once ω_p is given, this analysis is in fact even simpler than the analysis of the existence for 1-bump solutions as in [**?**]. The main difficulty here is that, in most cases, ω_p has no analytic expression and has to be approximated. Despite that, the considered approach of constructing solutions is still simpler than the ODE-method proposed in [8]. In addition, it allows us to address the uniqueness of solutions and is not restricted to a particular type of ω. To illustrate the method we have constructed 1-bump periodic solutions for different types of ω.

The choice of the Heaviside function also enabled us to analyse the spectral stability of the solutions, which is the main contribution of this paper. This was done by analysing the spectrum of a Laurent block operator which, we have proved, possesses almost the same eigenvalues as the Fréchet derivative of the operator in consideration. We have shown that the model (1.1) can have both linearly stable and unstable periodic solutions for some connectivity functions. When ω is of the excitatory type, the periodic solutions are always unstable.

In order to draw the conclusions about Lyapunov stability of the solutions based on their linear stability, the firing rate function f must be smooth enough, which is not the case here. We conjecture that the existence and stability results would hold for steep sigmoid like functions f, see (1.6). To prove this conjecture one can proceed in the way similar to [10] and [23]. It is not possible to apply the results from the mentioned papers directly since the eigenvalue $\lambda = 1$ of the Fréchet derivative of the operator defined by (1.2) is not isolated. However, the stability analysis in Section 4 shows that the spectrum is pointwise and the eigenfunctions can be calculated, which gives a possibility of studying the dynamics of solutions on a central manifold. We plan to address this problem in our future work.

Another topic that we have not properly addressed in this paper, is the coexistence of the localized and periodic solutions with different stability properties. The combination of the ODE-methods [11, 18, 15] with the results obtained here could be used to investigate this interesting problem.

Finally, we would like to mention that the analysis presented here could be generalized to the case of N-bump periodic solutions and several dimensions.While the stability analysis could be extended without much changes, the major difficulty is to obtain the necessary and sufficient conditions for the existence of regular solutions and to find their intersections with the threshold.

6. Acknowledgements

The authors are grateful to Professor Arcady Ponosov and John Wyller (Norwegian University of Life Sciences) for fruitful discussions during the preparation phase of this paper. We thank Professor Mårten Gulliksson (Örebro University) for constructive criticism of the manuscript. This research work was supported by the Norwegian University of Life Sciences and The Research Council of Norway, project number 239070.

References

1. Shun-ichi Amari. Dynamics of pattern formation in lateral-inhibition type neural fields. *Biological cybernetics*, 27(2):77–87, 1977.
2. Stephen Coombes. Waves, bumps, and patterns in neural field theories. *Biological cybernetics*, 93(2):91–108, 2005.

3. Bard Ermentrout. Neural networks as spatio-temporal pattern-forming systems. *Reports on progress in physics*, 61(4):353, 1998.
4. Stephen Coombes, Peter beim Graben, Roland Potthast, and James Wright. *Neural Fields: Theory and Applications*. Springer, 2014.
5. Roland Potthast and Peter Beim Graben. Existence and properties of solutions for neural field equations. *Mathematical Methods in the Applied Sciences*, 33(8):935–949, 2010.
6. Bard Ermentrout. The analysis of synaptically generated traveling waves. *Journal of Computational Neuroscience*, 5(2):191–208, 1998.
7. Stephen Coombes and Helmut Schmidt. Neural fields with sigmoidal firing rates: approximate solutions. *Discrete and Continuous Dynamical Systems. Series S*, 2010.
8. Edward P Krisner. Periodic solutions of a one dimensional wilson-cowan type model. *Electronic Journal of Differential Equations*, 2007(102):1–22, 2007.
9. Carlo R Laing, William C Troy, Boris Gutkin, and G Bard Ermentrout. Multiple bumps in a neuronal model of working memory. *SIAM Journal on Applied Mathematics*, 63(1):62–97, 2002.
10. Anna Oleynik, Arcady Ponosov, Vadim Kostrykin, and Alexander V Sobolev. Spatially localized solutions of the hammerstein equation with sigmoid type of nonlinearity. *Journal of Differential Equations*, 261(10):5844–5874, 2016.
11. A.J. Elvin, C.R. Laing, R.I. McLachlan, and M.G. Roberts. Exploiting the hamiltonian structure of a neural field model. *Physica D: Nonlinear Phenomena*, 239(9):537 – 546, 2010. Mathematical Neuroscience.
12. L.P. Šil'Nikov. A case of the existence of a denumerable set of periodic motions. *Sov. Math. Dokl. 6*, pages 163–166, 1965.
13. L.P. Šil'Nikov. A contribution to the problem of the structure of an extended neighborhood of a rough equilibrium state of saddle-focus type. *Mathematics of the USSR-Sbornik*, 10(1):91, 1970.
14. Paul Glendinning and Colin Sparrow. Local and global behavior near homoclinic orbits. *Journal of Statistical Physics*, 35(5):645–696, Jun 1984.
15. Robert L Devaney. Homoclinic orbits in hamiltonian systems. *Journal of Differential Equations*, 21(2):431 – 438, 1976.
16. Paul C Bressloff. Spatiotemporal dynamics of continuum neural fields. *Journal of Physics A: Mathematical and Theoretical*, 45(3):033001, 2011.
17. John Wyller, Patrick Blomquist, and Gaute T. Einevoll. Turing instability and pattern formation in a two-population neuronal network model. *Physica D: Nonlinear Phenomena*, 225(1):75 – 93, 2007.
18. Edward P Krisner. The link between integral equations and higher order odes. *Journal of mathematical Analysis and Applications*, 291(1):165–179, 2004.
19. S. Coombes and M. R. Owen. Evans functions for integral neural field equations with heaviside firing rate function. *SIAM Journal on Applied Dynamical Systems*, 3(4):574–600, 2004.
20. Patrick Blomquist, John Wyller, and Gaute T Einevoll. Localized activity patterns in two-population neuronal networks. *Physica D: Nonlinear Phenomena*, 206(3):180–212, 2005.
21. Anna Oleynik, John A. Wyller, Tom Tetzlaff, and Gaute T. Einevoll. Stability of bumps in a two-population neural-field model with quasi-power temporal kernels. *Nonlinear Analysis: Real World applications*, 12(6):30733094, 2011.
22. Evgenii Burlakov, Arcady Ponosov, and John Wyller. Stationary solutions of continuous and discontinuous neural field equations. *Journal of Mathematical Analysis and Applications*, 444(1):47–68, 2016.
23. Vadim Oleynik, Anna Kostrykin and Alexander Sobolev. Lyapunov stability of bumps in a one-population neural field equation. work in progress, 2015.
24. Anna Oleynik, Arcady Ponosov, and John Wyller. On the properties of nonlinear nonlocal operators arising in neural field models. *Journal of Mathematical Analysis and Applications*, 398(1):335–351, 2013.
25. Israel Gohberg, Seymour Goldberg, and Marius A. Kaashoek. *Classes of Linear Operators*, volume 2 of *63*. Birkhuser Basel, 1 edition, 1993.
26. Arthur Frazho and Wisuwat Bhosri. *An operator perspective on signals and systems*, volume 204. Springer Science & Business Media, 2009.
27. Cornelis VM van der Mee, Sebastiano Seatzu, and Giuseppe Rodriguez. Spectral factorization of bi-infinite multi-index block toeplitz matrices. *Linear algebra and its applications*, 343:355–380, 2002.
28. Lothar Reichel and Lloyd N Trefethen. Eigenvalues and pseudo-eigenvalues of toeplitz matrices. *Linear algebra and its applications*, 162:153–185, 1992.
29. Robert Denk, Manfred Mller, and Christiane Tretter. The spectrum of the multiplication operator associated with a family of operators in a banach space. In Karl-Heinz Frster, editor, *Operator theory in Krein spaces and nonlinear eigenvalue problems*, pages 103–116. Birkhuser, Basel, 2006.
30. Otto Toeplitz. Zur theorie der quadratischen und bilinearen formen von unendlichvielen veränderlichen. *Mathematische Annalen*, 70(3):351–376, 1911.

31. Marko Lindner. Fredholmness and index of operators in the wiener algebra are independednt on the underlying space. *Operators and matrices*, 2(2):297–306, 2008.
32. Markus Seidel. Fredholm theory for band-dominated and related operators: a survey. *Linear Algebra and its Applications*, 445:373–394, 2014.
33. Vadim Kostrykin and Anna Oleynik. On the existence of unstable bumps in neural networks. *Integral equations and operator theory*, 75(4):445–458, 2013.

K. KOLODINA, FACULTY OF SCIENCE AND TECHNOLOGY, NORWEGIAN UNIVERSITY OF LIFE SCIENCES, P.O. BOX 5003, N-1432 ÅS, NORWAY
E-mail address: karina.kolodina@nmbu.no

V. KOSTRYKIN, FB 08 - INSTITUT FÜR MATHEMATIK, JOHANNES GUTENBERG-UNIVERSITÄT MAINZ, STAUDINGER WEG 9, 55099 MAINZ, GERMANY
E-mail address: kostrykin@mathematik.uni-mainz.de

A. OLEYNIK, FACULTY OF SCIENCE AND TECHNOLOGY, NORWEGIAN UNIVERSITY OF LIFE SCIENCES, P.O. BOX 5003, 1432 ÅS, NORWAY
Current address: Department of Mathematics, University of Bergen, Postboks 7803, 5020 Bergen, Norway
E-mail address: anna.oleynik@uib.no

PAPER II

Single bumps in a 2-population homogenized neuronal network model

Karina Kolodina[a,*], Anna Oleynik[a,b], John Wyller[a]

[a] *Department of Mathematical Sciences and Technology, Norwegian University of Life Sciences, P.O. Box 5003, N-1432 Ås, Norway*
[b] *Present address: Department of Mathematics, University of Bergen, P.O. Box 7803, N-5020 Bergen, Norway*

[*] Corresponding author
Email address: karina.kolodina@nmbu.no (Karina Kolodina)

Preprint submitted to Elsevier *November 11, 2017*

Abstract

We investigate existence and stability of single bumps in a homogenized 2-population neural field model, when the firing rate functions are given by the Heaviside function. The model is derived by means of the two-scale convergence technique of Nguetseng in the case of periodic microvariation in the connectivity functions. The connectivity functions are periodically modulated in both the synaptic footprint and in the spatial scale. The bump solutions are constructed by using a pinning function technique for the case where the solutions are independent of the local variable. In the weakly modulated case the generic picture consists of two bumps (one narrow and one broad bump) for each admissible set of threshold values for firing. In addition, a new threshold value regime for existence of bumps is detected. Beyond the weakly modulated regime the number of bumps depends sensitively on the degree of heterogeneity. For the latter case we present a configuration consisting of three coexisting bumps. The linear stability of the bumps is studied by means of the spectral properties of a Fredholm integral operator, block diagonalization of this operator and the Fourier decomposition method. In the weakly modulated regime, one of the bumps is unstable for all relative inhibition times, while the other one is stable for small and moderate values of this parameter. The latter bump becomes unstable as the relative inhibition time exceeds a certain threshold. In the case of the three coexisting bumps detected in the regime of finite degree of heterogeneity, we have at least one stable bump (and maximum two stable bumps) for small and moderate values of the relative inhibition time.

Keywords: Neural field models, homogenization theory, existence and stability of bumps.

1. Introduction

The coupled system of nonlocal field equations

$$\begin{aligned} \frac{\partial}{\partial t}u_e &= -u_e + \omega_{ee} \otimes P_e(u_e - \theta_e) - \omega_{ie} \otimes P_i(u_i - \theta_i) \\ \tau\frac{\partial}{\partial t}u_i &= -u_i + \omega_{ei} \otimes P_e(u_e - \theta_e) - \omega_{ii} \otimes P_i(u_i - \theta_i) \end{aligned} \tag{1}$$

has been proposed by Blomquist *et al.* [1] as a generic model for interaction between populations of excitatory and inhibitory neurons. Here $f \otimes g$ is the spatial convolution of f and g defined as

$$[f \otimes g](x) = \int_\Omega f(x - x')g(x')dx', \quad \Omega \subseteq \mathbb{R}^N$$

u_e and u_i denote the membrane potentials of excitatory and inhibitory elements, respectively, at the spatial point x and time t. The region Ω is the spatial region occupied by the neurons. The functions ω_{mn} $(m, n = e, i)$ model the coupling strengths (referred to as the connectivity functions) in the network, while P_m $(m = e, i)$ are the firing rate functions. The parameter τ is the relative inhibition time i.e. $\tau = \tau_i/\tau_e$ where τ_e (τ_i) is the excitatory (inhibitory) time constant, while θ_e and θ_i are the threshold values for firing of the excitatory and the inhibitory neurons, respectively. The model (1) presupposes that the cortical medium is homogeneous and isotropic. It is one of the simplest models for the spatiotemporal variation of the neural activity in cortical networks. These networks are modelled as a continuous sheet of neurons where the typical spatial and temporal scales of the activity are assumed to be much larger than the corresponding neuronal scales.

Since the seminal works of Amari [2, 3, 4], 1- and 2-population neural field models have been subject to a vast number of studies. See also Bressloff [5] and the references therein. They are expected to capture the brain activity on the macroscale level. However, as most of these models presuppose that the cortical structure is homogeneous and isotropic, they do not take into account the microscopic fine structure of the cortex. This means that modelling frameworks like (1) represent simplifications of the actual situation. It is therefore necessary to develop a mathematical machinery which makes it

possible to investigate waves and stationary activity patterns in neural media with microscopic fine structure. One way of doing this is by using so-called *homogenization techniques* [6, 7, 8, 9]. In Bressloff [10] fronts propagating through a cortical medium with a periodically modulated microstructure are studied. The coupling between periodic micro level structure of the cortex and nonlocal mean field description has also been investigated in the works [11, 12, 13, 14, 15, 16]. It turns out that the detailed microstructure has an impact on pattern forming mechanisms as well as existence and stability of traveling fronts and pulses. A typical feature observed in the works [10, 11, 12, 13, 14, 15, 16] is that the fronts slow down when the degree of heterogeneity increases. The fronts cannot propagate if the heterogeneity exceeds a certain threshold. In the papers [17, 18, 19, 20, 21] the focus is existence and stability of single- and 2-bumps within the framework of a homogenized 1-population neural field model, where one allows for periodic microstructure variation in both the synaptic footprint and the spatial scale of the connectivity strength. We notice here that most studies of bumps/traveling fronts in inhomogeneous media use 1-population models as modelling frameworks. As far as we know, it is rare in between studies of 2-population nonlocal neural field models with inhomogeneities.

This serves as a background and motivation for the present study. The starting point is the 2-population neuronal network model

$$\begin{aligned} \frac{\partial}{\partial t}u_e^{(\varepsilon)} &= -u_e^{(\varepsilon)} + \omega_{ee}^{(\varepsilon)} \otimes P_e(u_e^{(\varepsilon)} - \theta_e) - \omega_{ie}^{(\varepsilon)} \otimes P_i(u_i^{(\varepsilon)} - \theta_i) \\ \tau\frac{\partial}{\partial t}u_i^{(\varepsilon)} &= -u_i^{(\varepsilon)} + \omega_{ei}^{(\varepsilon)} \otimes P_e(u_e^{(\varepsilon)} - \theta_e) - \omega_{ii}^{(\varepsilon)} \otimes P_i(u_i^{(\varepsilon)} - \theta_i) \end{aligned} \tag{2}$$

which generalizes the 2-population neuronal network model (1). Here Ω is a subset of $\mathbb{R}^N$, $u_e^{(\varepsilon)}$ and $u_i^{(\varepsilon)}$ describe the membrane potentials of an excitatory and an inhibitory neural element, respectively, at position x and time t. P_e and P_i are non-negative firing rate functions and ω_ε given as $\omega_{mn}^{(\varepsilon)}(x) = \omega_{mn}\left(x, \frac{x}{\varepsilon}\right)$ the connectivity kernel which by assumption is periodic in the second variable $y = x/\varepsilon$. We refer to the model (2) as the *heterogeneous 2-population neural field model*.

By employing the same arguments as in Coombes *et al.* [17] and Svanstedt *et al.* [18], we conclude that $u_e^{(\varepsilon)}$ and $u_i^{(\varepsilon)}$ of the Cauchy problem of

this model converge to the solution u_e and u_i of the Cauchy problem of the nonlocal nonlinear diffusion model

$$\begin{aligned} \frac{\partial}{\partial t}u_e &= -u_e + \omega_{ee} \otimes\otimes P_e(u_e - \theta_e) - \omega_{ie} \otimes\otimes P_i(u_i - \theta_i) \\ \tau\frac{\partial}{\partial t}u_i &= -u_i + \omega_{ei} \otimes\otimes P_e(u_e - \theta_e) - \omega_{ii} \otimes\otimes P_i(u_i - \theta_i) \end{aligned} \tag{3}$$

as $\varepsilon \to 0$ in the two-scale sense. Here $f \otimes\otimes g$ is the *double convolution* of f and g defined by

$$[f \otimes\otimes g](x,y) \equiv \int_\Omega \int_Y f(x - x', y - y')g(x', y')dy'dx' \tag{4}$$

where $x \in \Omega$, $y \in \mathbb{R}^N$, $t > 0$ in the two-scale sense. Here $Y = [0,1]^N$ is the period cell in $\mathbb{R}^N$. We refer to this model as the *homogenized 2-population neural field model*. The key tools for proving this result is the multiscale convergence technique of Nguetseng [8, 9] together with Visintins theorem for two-scale convergence of convolution integrals [22].

Notice that it is possible to design the firing rate functions and the connectivity kernels in the nonlocal models (1)-(3) in such a way that the corresponding Cauchy problem is globally well-posed. In order to prove this fact one proceeds in a way analogous to Potthast *et al.* [23] for well-posedness in the Banach space of bounded continuous functions and Faye *et al.* [24] in the case of well-posedness in L^2-spaces on bounded spatial domains.

A characteristic feature of the homogenized neural field model (3) (as well as in the works [17, 18, 19, 20, 21]) is the appearance of the double convolution integrals of the type (4) describing the nonlocal effects. We notice here that there is a notable structural difference between the homogenized neural field models in these works (as well as the model (3)) and in the papers [10, 11, 12, 13, 14, 15, 16]). Here the following should be noted: First of all, we have not seen a derivation of the modelling frameworks like (3) and the homogenized 1-population models investigated in [17, 18, 19, 20, 21] by using standard perturbation techniques. Secondly, we are not aware of any attempts to justify rigorously the usage of standard homogenization techniques to nonlocal neural field models by means of functional analytical based convergence arguments. Multi-scale convergence techniques and

standard perturbation expansions yield in some cases the same leading order approximations of PDE problems with strong heterogeneities, thus showing that standard perturbation techniques are rigorously justified for these local problems. They seem not capable, however, of giving the correct leading order approximations when handling nonlocal neural field models. The problem consists of dealing with convergence of convolution integrals containing microscale variation in a rigorous manner. Homogenization theory based on functional analytic based multi-scale convergence technique offers a rigorous approach to this problem.

Our main goal is to investigate existence and stability of y-independent, single bumps within the framework of the homogenized 2-population model (3) in the Heaviside limit H of the firing rate functions P_m, $m = e, i$ in one spatial dimension i.e. $N = 1$ in (3). This means that the period cell Y is given by $Y = [0, 1]$.

The connectivity kernels ω_{mn} are expressed in terms of the scaling function Φ and the footprint functions σ_{mn}, $m, n = e, i$ as

$$\omega_{mn}(x, y; \alpha_{mn}) = \frac{1}{\sigma_{mn}(y; \alpha_{mn})} \Phi\left(\frac{x}{\sigma_{mn}(y; \alpha_{mn})}\right). \tag{5}$$

Here

$$\sigma_{mn}(y; \alpha_{mn}) = s_{mn}(1 + \alpha_{mn} \cos(2\pi y)), \quad s_{mn} > 0, \quad 0 \leq \alpha_{mn} < 1 \tag{6}$$

This means that the connectivity kernels are assumed to be periodically modulated in both the spatial scale and the synaptic footprints. The parameters α_{mn}, $m, n = e, i$ are referred to as the heterogeneity parameters. Notice that we recover the translational invariant case when $\alpha_{mn} = 0$. The scaling function Φ is assumed to be even, positive, normalized and with a bounded continuous derivative i.e.

$$\Phi(\xi) = \Phi(-\xi), \quad \Phi(\xi) \geq 0, \quad \int_{\mathbb{R}} \Phi(\xi) d\xi = 1, \quad \Phi \in BC^1(\mathbb{R}) \tag{7}$$

Notice that the normalization condition implies that the connectivity functions are normalized i.e.

$$\int_{\mathbb{R}} \int_{Y} \omega_{mn}(x, y; \alpha_{mn}) dy dx = \int_{\mathbb{R}} \Phi(\xi) d\xi = 1 \tag{8}$$

In all the numerical computations, we will let the scaling function Φ be given as the Gaussian function

$$\Phi(\xi) = \frac{1}{\sqrt{\pi}} \exp(-\xi^2) \tag{9}$$

Just as in Blomquist *et al.* [1], we allow for the situation where $\theta_e \neq \theta_i$.

The existence of bumps is determined by means of the mapping technique in exactly the same way in Blomquist *et al.* [1]. The uniqueness issue is resolved by interpreting the solutions of pinning equations as intersection points between level curves with the threshold values as the level curve constants. Contrary to the translation invariant case we show that the model (3) can produce more than two bumps given the heterogeneity parameters α_{mn} are large enough. We then derive a framework for analyzing the stability of the bumps in a way analogous to [25, 26, 27] for single bumps in 2 spatial dimension, Kollár *et al.* [28] for the spectral stability of vortex solutions to the Gross-Pitaevski equation in a 2-dimensional spatial configuration, Svanstedt *et al.* [20] for the stability of single bump solutions in a homogenized 1-population neural field model and Malyutina *et al.* [19] for the stability of the 2-bump solutions of a homogenized 1-population neural field equation. This framework is based on the spectral properties of a Fredholm integral operator, block diagonalization of this operator and the Fourier decomposition method. This approach produces an infinite sequence of Evans functions corresponding to the modes in the Fourier-expansion for the perturbations. Each Evans function can be written as a product of quadratic polynomials in the growth/decay rates with a structure identical to the translational invariant case treated in Blomquist *et al* [1]. In Theorem 4 the estimate on the eigenvalue number for the matrices is derived. We justify the linearization approach using the notion of Frechét derivatives.

The present study complements the works [18], [19], [21] and [17].

The paper is organized as follows:

In Section 2 we construct single bumps of the homogenized 2-population model which are independent of the microvariable y. In Section 3 we develop the framework for analyzing the stability of these bumps. Both in Section 2 and Section 3 we demonstrate the numerical results by assuming the scaling

function of the connectivity kernels to be the Gaussian function (9). Section 4 contains of conclusions and outlook.

2. Single bumps of the homogenized 2-population model.

We observe that stationary, y-independent solutions U_m $(m = e, i)$ of the homogenized 2-population model (3) must satisfy the fixed point problem

$$\begin{aligned} U_e &= \langle \omega_{ee} \rangle \otimes H(U_e - \theta_e) - \langle \omega_{ie} \rangle \otimes H(U_i - \theta_i) \\ U_i &= \langle \omega_{ei} \rangle \otimes H(U_e - \theta_e) - \langle \omega_{ii} \rangle \otimes H(U_i - \theta_i) \end{aligned} \tag{10}$$

if they exist. Here $f \otimes g$ is the spatial convolution of f and g defined as

$$[f \otimes g](x) = \int_{\mathbb{R}} f(x - x')g(x')dx'$$

and $\langle \omega_{mn} \rangle$ is the mean value of the connectivity kernel ω_{mn} over the period of the second variable y i.e.

$$\langle \omega_{mn} \rangle(x; \alpha_{mn}) \equiv \int_Y \omega_{mn}(x, y; \alpha_{mn})dy \tag{11}$$

Here we will focus on localized stationary solutions of (10), referred to as *bumps*. As the bumps are independent of the local scale y, the fixed point problem (10) appears from the translational invariant case simply by making the replacement $\omega_{mn} \to \langle \omega_{mn} \rangle$. Therefore the theory for positioning the bumps in our case is identical with what we get for the translational invariant case. Thus we can assume that positioned about the origin, without loss of generality. Notice that the translational invariance is reflected in the property that the spectrum of the operator in Section 3 for the stability problem always contains zero.

Hence, in accordance with this, we define a single bump $U = (U_e, U_i)$ in the present modelling framework in the following way:

1. Spatial symmetry: $U_m(x) = U_m(-x)$ for $m = e, i$.

2. There are a unique positive numbers a_e and a_i such that

$$U_e(\pm a_e) = \theta_e, \quad U_i(\pm a_i) = \theta_i$$

and

$$U_e(x) > \theta_e \quad \text{for} \quad |x| < a_e$$

$$U_e(x) < \theta_e \quad \text{for} \quad |x| > a_e$$

$$U_i(x) > \theta_i \quad \text{for} \quad |x| < a_i$$

$$U_i(x) < \theta_i \quad \text{for} \quad |x| > a_i$$

3. $\lim_{|x|\to\infty} U_m(x) = 0$ for $m = e, i$.

The numbers a_e and a_i are referred to as *the excitatory and the inhibitory pulse widths*, respectively.

In order to construct the bumps, we proceed in a way analogous to Amari [4], Blomquist *et al.* [1] and Folias *et al.* [29]. We introduce the anti-derivatives W_{mn} of $\langle\omega_{mn}\rangle$ defined by

$$W_{mn}(x;\alpha_{mn}) = \int_0^x \langle\omega_{mn}\rangle(z;\alpha_{mn})dz, \quad m,n = e,i \tag{12}$$

The components U_e and U_i of the bumps can now formally be written as

$$\begin{aligned} U_e(x;\alpha_e) = {} & W_{ee}(a_e - x;\alpha_{ee}) + W_{ee}(a_e + x;\alpha_{ee}) \\ & -W_{ie}(a_i - x;\alpha_{ie}) - W_{ie}(a_i + x;\alpha_{ie}) \end{aligned} \tag{13}$$

$$\begin{aligned} U_i(x;\alpha_i) = {} & W_{ei}(a_e - x;\alpha_{ei}) + W_{ei}(a_e + x;\alpha_{ei}) \\ & -W_{ii}(a_i - x;\alpha_{ii}) - W_{ii}(a_i + x;\alpha_{ii}) \end{aligned} \tag{14}$$

where α_e and α_i are the *heterogeneity vectors*

$$\alpha_e = \begin{bmatrix} \alpha_{ee} \\ \alpha_{ie} \end{bmatrix}, \quad \alpha_i = \begin{bmatrix} \alpha_{ei} \\ \alpha_{ii} \end{bmatrix}$$

Since $0 \leq \alpha_{mn} < 1$ by assumption, $\alpha_m \in [0,1)^2$, $m = e, i$.

Necessary conditions for the existence of single bumps hence read

$$\begin{aligned} f_e(a;\alpha_e) &= \theta_e \\ f_i(a;\alpha_i) &= \theta_i \end{aligned} \tag{15}$$

where the functions f_e and f_i are given as

$$\begin{aligned} f_e(a;\alpha_e) &\equiv W_{ee}(2a_e;\alpha_{ee}) - W_{ie}(a_e + a_i;\alpha_{ie}) + W_{ie}(a_e - a_i;\alpha_{ie}) \\ f_i(a;\alpha_i) &\equiv W_{ei}(a_e + a_i;\alpha_{ei}) - W_{ei}(a_i - a_e;\alpha_{ei}) - W_{ii}(2a_i;\alpha_{ii}) \end{aligned} \tag{16}$$

Here we have introduced the *pulse width vector*

$$a = \begin{bmatrix} a_e \\ a_i \end{bmatrix}$$

We refer to the system (15) as the *system of pinning equations*. Notice that the set of pinning equations gives a necessary (but not sufficient) condition for the existence of bumps. This means that it is necessary to emphasize the non-existence result: If the pinning equation system (15)-(16) has no solution for which both components a_e and a_i are positive, then bumps do not exist. Just as in Blomquist *et al.* [1], the investigation of this system is conveniently divided into the following two problems:

1. (*Existence issue.*) In Subsection 2.1 we derive necessary conditions existence of bumps. This problem is resolved by means of an extension of the mapping technique introduced in Blomquist *et al.* [1]

2. (*Uniqueness issue.*) In Subsection 2.2 we study the uniqueness of bump solutions. In contrast to the existence issue (which a global problem) this question is local issue which is solved by means of the inverse function theorem.

2.1. Existence of single bumps.

Our aim is to determine the set of threshold values θ_e, θ_i for which the system (15) has at least one solution. In order to do that we make use of the mapping technique developed in Blomquist *et al.* [1].

We proceed as follows: Introduce the 4-vector

$$\alpha = \begin{bmatrix} \alpha_e \\ \alpha_i \end{bmatrix}$$

where α_e and α_i are the heterogeneity vectors for the excitatory and the inhibitory population, respectively. We notice that

$$\alpha \in \mathcal{A} \equiv [0,1)^4$$

Let Σ denote the first quadrant in the a_e, a_i - plane i.e.

$$\Sigma = \{(a_e, a_i) \in \mathbb{R}^2; a_e, a_i > 0\}$$

We then introduce the 4-parameter family of vector fields $\{F_\alpha\}_{\alpha \in \mathcal{A}}$ acting on Σ defined by

$$F_\alpha(a) = \begin{bmatrix} f_e(a; \alpha_e) \\ f_i(a; \alpha_i) \end{bmatrix}$$

Let θ be the threshold vector

$$\theta = \begin{bmatrix} \theta_e \\ \theta_i \end{bmatrix}$$

and let I be the set

$$I = \{(\theta_e, \theta_i) \in \mathbb{R}^2; 0 < \theta_e \leq 1, 0 < \theta_i \leq 1\} \tag{17}$$

The system of pinning equations (15) now reads

$$F_\alpha(a) = \theta, \quad \theta \in I \tag{18}$$

The subset of threshold values in I for which (18) has at least one solution is referred to as the set of admissible threshold values.

From Blomquist *et al.* [1] we know that there always is a subset J of admissible threshold values in I i.e. that (18) has at least one solution $a = a_0$ for $\alpha = 0$, provided the connectivity functions ω_{mn} are continuous:

$$F_0(a_0) = \theta, \quad \theta \in J \tag{19}$$

For the weakly modulated case ($0 < \alpha_{mn} \ll 1, m, n = e, i$), we end up with the same result, as the following theorem shows:

Theorem 1. *Assume that the scaling function Φ of the connectivity kernels ω_{mn}, $m, n = e, i$, satisfies (7) and that the synaptic footprint functions σ_{mn} are given by* (6)*. Then the following holds true:*

1. *The set $F_\alpha(\Sigma)$ is bounded for all $\alpha \in \mathcal{A}$.*

2. *The vectorfield $F_\alpha : \Sigma \to \mathbb{R}^2$ is smooth for all $\alpha \in \mathcal{A}$.*

3. *If the Jacobian $D_a F_0(a_0)$ is non-singular where a_0 is a solution of (19), then the intersection between $F_\alpha(\Sigma)$ and I is non-empty i.e. there is a $k \in [0, 1)$ such that*

   $$F_\alpha(\Sigma) \cap I \neq \emptyset$$

   for $\alpha \in \mathcal{A}_k$ where

   $$\mathcal{A}_k \equiv \{\alpha \in \mathcal{A}; 0 \leq \alpha_{mn} < k\}$$

Proof. The proof is divided into three parts:

1. (*Boundedness.*) From the conditions imposed on the connectivity kernels ω_{mn} we have that the anti-derivatives W_{mn} are monotonically increasing and odd. This property together with the normalization condition (8) imply that

   $$|W_{mn}(x; \alpha_{mn})| \leq \frac{1}{2}$$

   The triangle inequality hence yields the uniform bounds

   $$f_e(a; \alpha_e) = W_{ee}(2a_e; \alpha_{ee}) + W_{ie}(a_e - a_i; \alpha_{ie}) - W_{ie}(a_e + a_i; \alpha_{ie})$$

   $$\leq W_{ee}(2a_e; \alpha_{ee}) \leq \frac{1}{2}$$

   $$f_i(a; \alpha_i) = W_{ei}(a_e + a_i; \alpha_{ei}) - W_{ei}(a_i - a_e; \alpha_{ei}) - W_{ii}(2a_i; \alpha_{ii})$$

$$\leq W_{ei}(a_e + a_i; \alpha_{ei}) + W_{ei}(a_e - a_i; \alpha_{ei})$$
$$\leq 2 \max_{x_\pm = a_e \pm a_i} W_{ei}(x_\pm; \alpha_{ei}) \leq 1$$

for the pinning functions f_e and f_i from which it follows that $F_\alpha(\Sigma)$ is bounded for all $\alpha \in \mathcal{A}$.

2. (*Smoothness.*) Continuity of the scaling functions Φ implies that the anti-derivatives W_{mn} defined by (12) are smooth functions, from which it follows that the pinning functions f_e and f_i are smooth on Σ. This argument holds true for all $\alpha \in \mathcal{A}$. Thus the vectorfield $F_\alpha : \Sigma \to \mathbb{R}^2$ is smooth for all $\alpha \in \mathcal{A}$.

3. (*Non-empty intersection and continuous dependence on α*) The vector fields $F_\alpha : \Sigma \to \mathbb{R}^2$ induces a mapping $F : \Sigma \times \mathcal{A} \to \mathbb{R}^2$ defined by

$$F(a, \alpha) = F_\alpha(a) \tag{20}$$

Since by Fubinis theorem, the anti-derivative W_{mn} of the mean value $\langle \omega_{mn} \rangle$ can be expressed as

$$W_{mn}(\xi; \alpha_{mn}) = \int_Y \int_0^{\xi/\sigma_{mn}(y;\alpha_{mn})} \Phi(z) dz dy$$

we conclude that the pinning functions f_e and f_i defined by (16) are smooth functions of the heterogeneity parameters α_{mn}. Hence the mapping $F : \Sigma \times \mathcal{A} \to \mathbb{R}^2$ is smooth. The pinning condition (18) reads

$$F(a, \alpha) = \theta \tag{21}$$

From (19)

$$F(a_0, 0) = \theta, \quad \theta \in J$$

for at least one solution $a = a_0$. Since by assumption the Jacobian $D_a F(a_0, 0)$ is non-singular, the implicit function theorem implies that (21) has a unique solution which is a smooth function of α for some α-subset $\mathcal{A}_k$ of $\mathcal{A}$.

□

The implicit function theorem also implies that the solution of (21) satisfies the continuity property ($m = e, i$)

$$a_m(\alpha) \to a_m(0) \quad \text{as} \quad \alpha \to 0$$

The conditions (5) imposed on the connectivity functions ω_{mn} imply that the mean value of these functions, $\langle \omega_{mn} \rangle(x, \alpha)$ are uniformly continuous with respect to α. Hence we arrive at the following corollary:

Corollary 1. *The bump solutions depend continuously on α i.e.*

$$||U(\alpha) - U_0||_{BC^1(\mathbb{R})} \to 0 \quad as \quad \alpha \to 0 \tag{22}$$

Here $U_\alpha \equiv (U_e(\alpha), U_i(\alpha))$, $U_0 \equiv (U_e(0), U_i(0))$ and $BC^1(\mathbb{R})$ the Banach space of bounded, smooth functions on $\mathbb{R}$.

The results summarized in Theorem 1 and Corollary 1 imply that there is a set of threshold values for which the pinning equations (15)-(16) have at least one solution in the weakly modulated case ($0 < \alpha_{mn} \ll 1$), and hence that excitatory and inhibitory single bumps exist since the corresponding solution of (18) yields a function that crosses threshold only at the appropriate crossings. Just as in Blomquist *et al.* [1], we can show that there exist admissible threshold values which produce narrow inhibitory bumps ($0 \leftarrow a_i \ll a_e$) and finite width excitatory bumps. Moreover, we will find that narrow excitatory bumps ($0 \leftarrow a_e \ll a_i$) cannot coexist with inhibitory bumps in this parameter regime. Thus we can conclude that the results obtained in the translational invariant case ($\alpha_{mn} = 0$) carry over to the weakly modulated case ($0 < \alpha_{mn} \ll 1$) at least with respect to the existence of bumps.

We observe from the proof of the boundedness of the pinning functions f_e and f_i that f_e approaches $1/2$ and f_i approaches 1 for large a_e and small a_i. This means that the set of admissible threshold values is located in the set $0 < \theta_e \leq 1/2$ and $0 < \theta_i \leq 1$.

In order to study the effect of heterogeneity on the bumps in some detail, we make use the same connectivity kernel and the same set of input parameters as in Blomquist *et al.* [1]. These parameters are listed in Table 1 as Set 1.

Parameters	s_{ee}	s_{ei}	s_{ie}	s_{ii}	θ_e	θ_i
Set 1	0.35	0.48	0.60	0.69	0.12	0.08
Set 2	0.35	0.48	0.60	0.69	0.12	0.16

Table 1: Sets of parameters used in the numerical runs underlying Fig. 1 and Fig. 13, where s_{mn} for $(m, n = e, i)$ represent mean synaptic footprints, see (6), and θ_m $(m = e, i)$ threshold values. The scaling function Φ of the connectivity kernels ω_{mn} is given as Gaussian function (9).

Let us consider an example of the weakly modulated case where we use the parameters in Set 1 in Table 1.

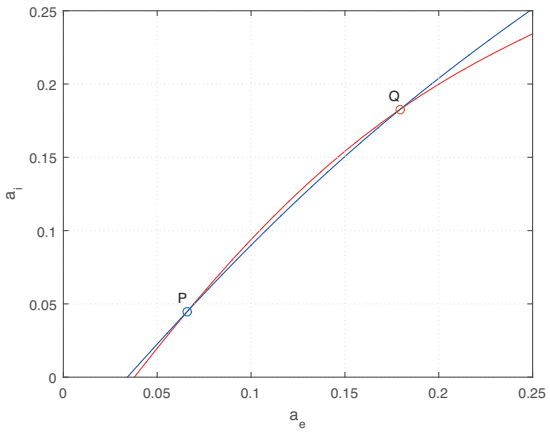

Figure 1: The intersection of level curves (15)-(16) in the weakly modulated case. $f_e = \theta_e$ (red curve) and $f_i = \theta_i$ (green curve) with the parameters in Set 1 in Table 1, $\alpha_{ee} = 0.01$, $\alpha_{ie} = 0.01$, $\alpha_{ei} = 0.025$ and $\alpha_{ii} = 0.025$ as input parameters. The points P and Q correspond to the narrow and broad bump, respectively.

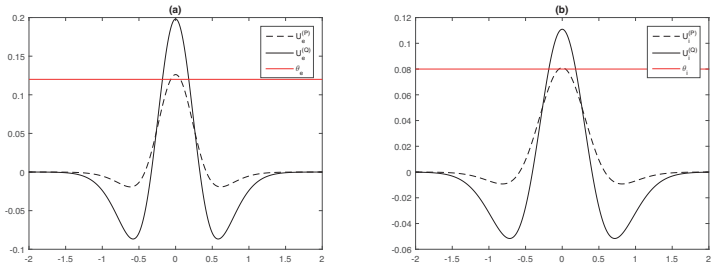

Figure 2: Excitatory components (a) and inhibitory components (b) of the bumps corresponding to the intersections P and Q of level curves in Fig. 1. The pulse width coordinates are given as $P : (a_e, a_i) = (0.1794, 0.1827)$ and $Q : (a_e, a_i) = (0.0660, 0.0448)$.

The results summarized in Fig. 1 and Fig. 2 are consistent with our theoretical predictions in the weakly modulated case: The generic picture which emerges consists of two bumps per admissible threshold value, just as in the translational invariant case [1].

Let us consider the translational invariant limit ($\alpha = 0$) of our model in some detail. Just as in Blomquist *et al.* [1], we plot the image set $F_\alpha(\Sigma)$ in the threshold value plane for $\alpha = 0$. The result is summarized in Fig. 3. In addition to the region producing bumps identified in Blomquist *et al.* [1], we also find a new region for existence of bumps. The former one is referred to as Region A whereas the new region for bumps is called Region B. It turns out that for threshold values (θ_e, θ_i) selected from Region A or Region B the number of solutions of the corresponding pinning equations $f_e = \theta_e, f_i = \theta_i$ is equal to 2. The number of bumps produced is also equal to 2.

Fig. 3 displays the boundaries of Region A and Region B. The curves H_1 and H_6 correspond to tangency of the level curves $f_e = \theta_e$ and $f_i = \theta_i$. These curves are constructed in the following way: We construct positive solutions of the system of equations

$$\begin{aligned} \det[D_a F](a, \alpha) &= 0 \\ f_e(a; \alpha_e) &= \theta_e \end{aligned} \tag{23}$$

for $\theta_e \in (0, 1/2]$. We then compute the corresponding θ_i-value for $\theta_i \in (0, 1]$

using the component equation $\theta_i = f_i(a; \alpha_i)$ of the pinning system (15). The curve H_2 corresponds to the situation where $a_i \to 0$ for the narrow bump. The curve H_3 corresponds to the situation where $a_e \to \infty$. In the region with boundaries given by H_2 and H_3 we have detected only one intersection point between level curves which corresponds to one single bump. However, for threshold values close to H_2 in that region, the level curves have 2 intersection points but one of the intersection point does not produce a bump due to the fact that $U_i(0) < \theta_i$. Notice that if $\theta_e > U_e(0)$ and $\theta_i > U_i(0)$, the system of pinning equations (15) has either no solution or not a unique positive solution. Thus the curves H_5 and H_4 defined by $U_e(0) = \theta_e$ and $U_i(0) = \theta_i$, respectively, give the boundary between the region of existence and non-existence of bumps in Region B.

Next we study the change of the image set $F_\alpha(\Sigma)$ with the degree of heterogeneity. Let us first consider the weakly modulated case. Fig. 4 shows that the image set $F_\alpha(\Sigma)$ in this case appears as a continuous deformation of the set $F_{\alpha=0}(\Sigma)$ depicted in Fig. 3, in agreement with the predictions of Theorem 1. Fig. 5 displays an example of intersection between the level curves $f_e = \theta_e$ and $f_i = \theta_i$ in the weakly modulated case. In Fig. 6 the corresponding bumps are depicted. As expected, the Region A and Region B possess the same property with respect to the number of solutions of the pinning equations $f_e = \theta_e$, $f_i = \theta_i$ and the number of bumps, as in the translational invariant regime.

Due to the fact that the four heterogeneity parameters α_{mn} $(m, n = e, i)$ can be changed independently of each other, we expect a rich plethora of phenomena to take place beyond the weakly modulated regime. Fig. 7 demonstrates possible outcomes for the image set $F_\alpha(\Sigma)$ beyond the weakly modulated regime. In the computations underlying the plot in this figure we have assumed the heterogeneity parameters α_{mn} to have moderate values, except for α_{ei}. In Fig. 7 we have the same two regions, Region A and Region B, in the threshold value plane just as in the translational invariant and the weakly modulated case. We notice that Region B has become slimmer as compared with what we observed in the regime $0 \leq \alpha_{mn} \ll 1$. By increasing α_{ei} the positions of the curves H_3, H_4 and H_5 can be swapped. In Fig. 7 the curve H_5 is located below the curve H_3 for some threshold values. In this case this takes place for θ_e less than 0.084. The curves H_2, H_3 and H_5 together form the boundary of a new region termed Region C. Region C produces at

least 1 and maximum 3 solutions of the pinning equations (15)-(16). Here each solution corresponds to a bump. We now give a numerical example on bumps in the regime with a mix of moderate and large values of the heterogeneity parameters, i.e. in the situation corresponding to the $*$ marked point in Fig. 7. Interestingly, we detect 3 intersection points between the level curves $f_e = \theta_e$ and $f_i = \theta_i$ in this case. The outcome of this computation is displayed in Fig. 8. These intersections produce 3 bumps (Fig. 9). For heterogeneity parameters α beyond the weakly modulated regime the shapes of the level curves change.

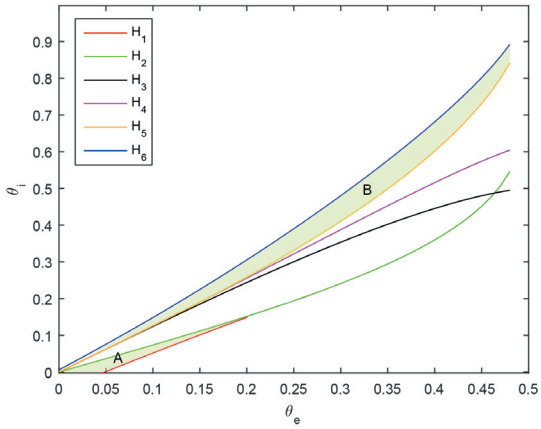

Figure 3: The image set $F_\alpha(\Sigma)$ in the translational invariant case ($\alpha = 0$). The synaptic footprints given as in Table 1 and the heterogeneity parameters $\alpha = 0$. Green shaded regions (Region A and Region B) produce two bumps (narrow and broad bump). The curves H_1 and H_6 correspond to only one bump produced by the non-transversal intersection between the level curves $f_e = \theta_e$ and $f_i = \theta_i$. The curve H_2 corresponds to the situation where $a_i \to 0$ for the narrow bump. The curve H_3 corresponds to the asymptotic state $a_e \to \infty$. The curves H_5 and H_4 correspond to $U_e(0) = \theta_e$ and $U_i(0) = \theta_i$, respectively.

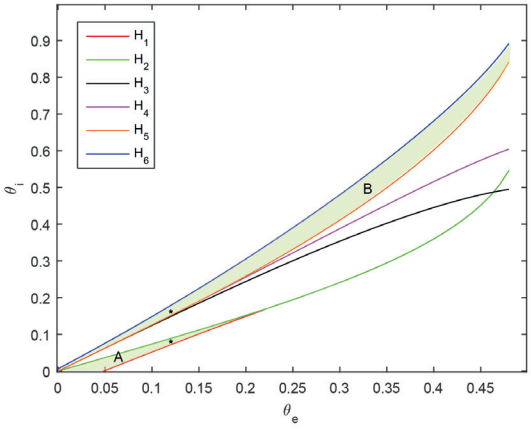

Figure 4: The image set $F_\alpha(\Sigma)$ in the weakly modulated case. Input data: $\alpha_{ee} = 0.01$, $\alpha_{ie} = 0.01$, $\alpha_{ei} = 0.025$ and $\alpha_{ii} = 0.025$. The threshold value point (θ_e, θ_i) of Set 1 in Table 1 belongs to Region A and the threshold value point (θ_e, θ_i) of Set 2 belongs to Region B. These two points are marked with $*$. The curves H_1-H_6 are defined in the same way as in Fig. 3.

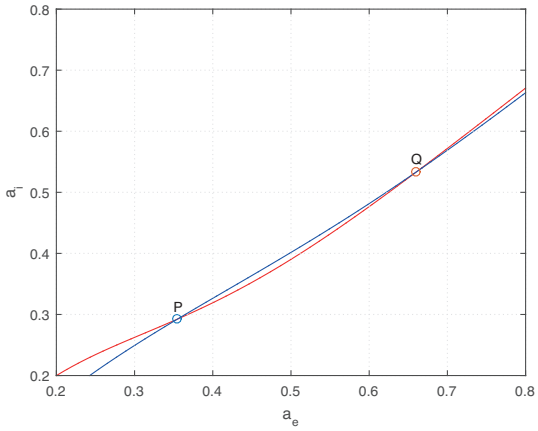

Figure 5: The intersection of level curves (15) - (16) in the weakly modulated case. $f_e = \theta_e$ (red curve) and $f_i = \theta_i$ (blue curve). Input data: $\alpha_{ee} = 0.01$, $\alpha_{ie} = 0.01$, $\alpha_{ei} = 0.025$ and $\alpha_{ii} = 0.025$, parameter Set 2 in Table 1.

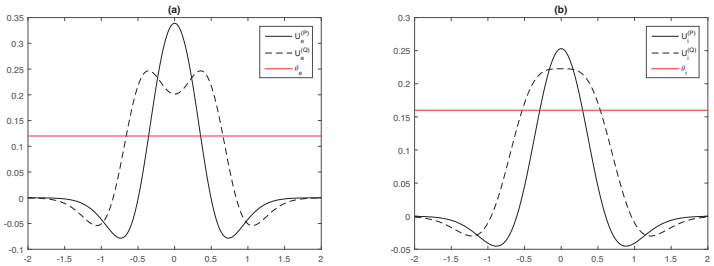

Figure 6: Excitatory components (a) and inhibitory components (b) of the bumps corresponding to intersection points P and Q in Fig. 5. The pulse width coordinates are given as $P : (a_e, a_i) = (0.3548, 0.2924)$ and $Q : (a_e, a_i) = (0.6599, 0.5330)$.

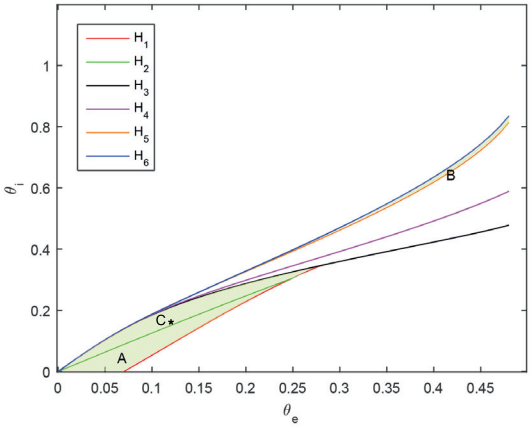

Figure 7: The image set $F_\alpha(\Sigma)$ beyond the weakly modulated case. Input data: The synaptic footprints in Table 1. Input data: $\alpha_{ee} = 0.25$, $\alpha_{ie} = 0.25$, $\alpha_{ei} = 0.83$ and $\alpha_{ii} = 0.25$. The curves H_1-H_6 are defined in the same way as in Fig. 3. The threshold value point (θ_e, θ_i) of Set 2 in Table 1 is marked with $*$. This point corresponds to Fig. 8.

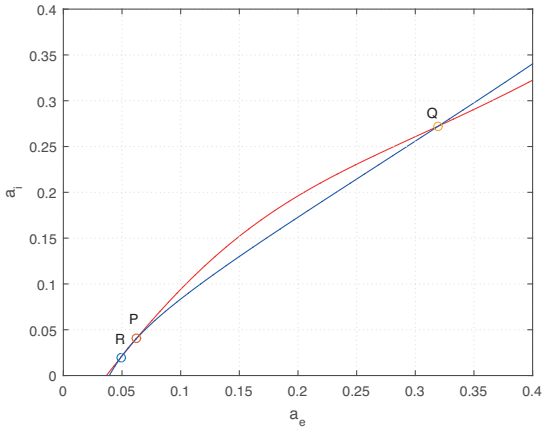

Figure 8: Intersections of the level curves $f_e = \theta_e$ and $f_i = \theta_i$ corresponding to $*$ point in Fig. 7. Input parameters: Set 2 of Table 1, $\alpha_{ee} = 0.25$, $\alpha_{ie} = 0.25$, $\alpha_{ei} = 0.83$ and $\alpha_{ii} = 0.25$.

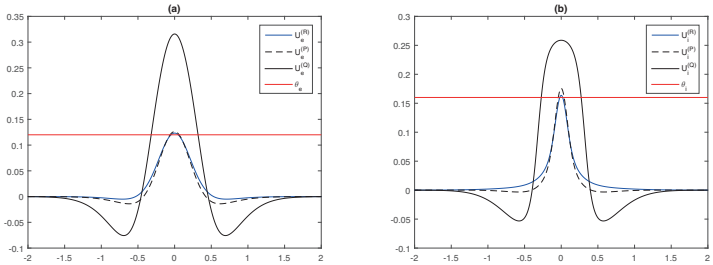

Figure 9: Excitatory components (a) and inhibitory components (b) of bumps corresponding to intersections of level curves in Fig. 8. The pulse width coordinates are given as $P : (a_e, a_i) = (0.0491, 0.0200)$, $Q : (a_e, a_i) = (0.0620, 0.0402)$ and $R : (a_e, a_i) = (0.3198, 0.2724)$.

2.2. Uniqueness of single bumps.

Since the scaling function Φ by (7) has a bounded and continuous derivative, Theorem 1 implies that the vectorfields $\{F_\alpha\}_{\alpha \in \mathcal{A}}$ constitute a 4 - parameter family of smooth vector fields.

We choose a pair of admissible threshold values θ_e and θ_i for which the pinning equation system

$$F_0(a) = \theta$$

has at least one solution $a = a_0$. Let us assume that the Jacobian of the vectorfield F_0 evaluated at this solution is non-singular. According to Blomquist *et al.* [1] the latter property can be translated into a transversal intersection between the level curves $f_e(a, \alpha_e = 0) = \theta_e$ and $f_i(a, \alpha_i = 0) = \theta_i$ defining the pinning system. The generic picture consists of two such intersection points per admissible threshold vector θ, corresponding to two bumps. It is important to stress that this is a local result. Following the line of arguments in Blomquist *et al.* [1] we conclude that the total number of intersection points per admissible threshold value is an even number.

Now, let us take into account the heterogeneity in the model. Assuming that we start out locally with two transversal intersection points per admissible threshold vector in the translational invariant case ($\alpha = 0$), we conclude by appealing to Theorem 1, that the pinning equation system

$$F_\alpha(a) = \theta$$

in the weakly modulated case ($0 < \alpha_{mn} \ll 1$) also will have two solutions which are smooth functions of the heterogeneity parameters. Hence the generic picture with two bumps for a given set of threshold values will be retained in the weakly modulated regime. This is exactly what we observe in Fig.1.

Next, let us consider the regime beyond the weakly modulated regime. We assume that there are two transversal intersections of the level curves (15)-(16) in the weakly modulated regime, corresponding to the generic situation with two bumps. By continuously changing the heterogeneity parameters beyond this regime, the shape of the level curves will go through a homotopic deformation. Since we have four scalar heterogeneity parameters which can be adjusted independently of each other, the level curves can go from a transversal intersection to no intersection. The transition phase between intersecting and non-intersecting level curves is described by means of non-transversal intersection. For the existence problem for bumps it means that two bumps merge together before vanishing. This also means that if the

bumps (corresponding to transversal crossings) do not violate the threshold condition, the limiting bump solution (corresponding to a non-transversal intersection) will by continuous dependence on the degree of heterogeneity also do the same. It may also happen that two non-intersecting level curves in the weakly modulated regime can be brought into a state of a transversal intersection by continuously adjusting the heterogeneity parameters. This can be interpreted as generation of bumps. Within the framework of the present description a non-transversal intersection point between the level curves (15)-(16) satisfies the system

$$F(a,\alpha)=\theta,\quad \det[D_aF](a,\alpha)=0 \tag{24}$$

with $\theta\in I$. Here we for the sake of convenience have expressed the non-transversality condition by means of the smooth mapping $F:\Sigma\times\mathcal{A}\to\mathbb{R}^2$ defined by (20).

For practical purposes, we can proceed as follows when determining the bifurcation point $(a,\alpha)=(a_c,\alpha_c)$ (i.e a solution of the system (24)): We fix one of the threshold values for firing, say θ_e, and all the heterogeneity parameters in α except one, say α_{ei}. The solution of the system of two equations

$$f_e(a;\alpha_e)=\theta_e,\quad \det[D_aF](a;\alpha)=0 \tag{25}$$

with $0<\theta_e\leq\frac{1}{2}$ determines a parameterised curve $\mathcal{C}$ in the a-plane, parameterised by means of α_{ei} where $\alpha_{ei}\in[0,1)$ i.e

$$\mathcal{C}:\quad f_e(a;\alpha_{ee},\alpha_{ie})=\theta_e,\quad \det[D_aF](a;\alpha_{ee},\alpha_{ie},\alpha_{ei},\alpha_{ii})=0 \tag{26}$$

The next step consists of computing the corresponding value of the component function f_i on $\mathcal{C}$. Provided

$$0<f_i(a\in\mathcal{C},\alpha_{ei},\alpha_{ii})\leq 1,\quad \alpha_{ei}\in[0,1) \tag{27}$$

we find the bifurcation threshold value curves $\theta_i=\theta_i^{(c)}(\alpha_{ei})$ producing a critical point (a_c,α_c) simply by letting

$$\theta_i^{(c)}(\alpha_{ei})=f_i(a\in\mathcal{C},\alpha_{ei},\alpha_{ii}),\quad \alpha_{ei}\in[0,1) \tag{28}$$

In this process we have ruled out the possibility that points on the curve $\mathcal{C}$ become accumulation points, by imposing the finite change of rate condition

$$\frac{d}{d\alpha_{ei}}\{\det[D_aF]\}(a \in \mathcal{C}, \alpha_{ei}, \alpha_{ii}) \neq 0 \tag{29}$$

for the determinant of the Jacobian D_aF evaluated at the bifurcation point (a_c, α_c). Notice that the outcome of this procedure is the curve $\mathcal{C}$ in Σ, representing non-transversal intersection points between the level curves $f_e = \theta_e$ and $f_i = \theta_i$. This curve is parameterized by means of the heterogeneity parameter α_{ei}.

The solutions of the system (25) can be viewed as intersections of the level curves of the functions f_e and $\det[D_aF]$ in the a-plane with level curve constants θ_e and 0, respectively. For a given θ_e and α_e, the level curve $f_e = \theta_e$ is fixed in the a-plane, whereas the level curve $\det[D_aF] = 0$ goes through a homotopic deformation where the heterogeneity parameter α_{ei} plays the role as homotopy parameter. This homotopic deformation process can result in a transversal intersection between the level curves. Now, by appealing to the similar type of reasoning as earlier, we conclude that the transversal intersection case consists of two solutions of the system (25) in the generic case. The condition for this transversal intersection can indeed be expressed as $\det[D_aG](a;\alpha) \neq 0$ where G is the vector field

$$G(a,\alpha) = \begin{bmatrix} f_e(a;\alpha_e) \\ \det[D_aF](a;\alpha) \end{bmatrix}$$

By plugging the two solutions of the system (25) into the remaining pinning function f_i, we hence obtain two critical threshold values $\theta_{i,1}^{(c)}$ and $\theta_{i,2}^{(c)}$ for each α_{ei}. Notice that these two curves correspond to the curves H_1 and H_6 in Fig. 3, Fig. 4 and Fig. 7.

In Fig. 10 the graphs of the critical threshold value $\theta_{i,1}^{(c)}$ and $\theta_{i,2}^{(c)}$ as functions of the heterogeneity parameter α_{ei} are displayed. For $\theta_i < \theta_{i,1}^{(c)}(\alpha_{ei})$ and $\theta_i > \theta_{i,2}^{(c)}(\alpha_{ei})$, we have no intersection points between the level curves $f_e = \theta_e$ and $f = \theta_i$, which means non-existence of bumps, whereas the set $0 \leq \alpha_{ei} < 1, \quad \theta_{i,1}^{(c)}(\alpha_{ee}) \leq \theta_i \leq \theta_{i,2}^{(c)}(\alpha_{ee})$ produces at least one intersection point locally. The green shaded set is the interior of this region. In that set we typically have two transversal intersection points of the level curves

$f_e = \theta_e$ and $f = \theta_i$, giving rise to two bumps. Let us fix $\alpha_{ei} = 0.5$. The point L belongs to green shaded region, whereas the point M is located at the curve $\theta_i = \theta_{i_2}^{(c)}(\alpha_{ei})$. The point N represents a state of non-existence of bumps.

For fixed $\theta_i = 0.085$, there are two disjoint α_{ei}-intervals producing points in the green shaded region (corresponding to at least two bumps). A and B are points representing transition state to the non-existence regime for $\theta_i = 0.085$. This means that we study the existence of bumps as function of the line segment in the parameter space $\mathcal{A}$. The directional vector for this line segment is the unit vector along the α_{ei}-axis.

Notice that we can equally well develop a procedure for determining non-transversal intersection points where the outcome is critical threshold value curves parameterized by one of the other heterogeneity parameters. Here we show how to construct such curves in the θ_e, α_{ie}-plane. We fix the threshold value θ_i and the heterogeneity parameters α_{ee}, α_{ei} and α_{ii}. Then the solution of the system (24) defines a curve

$$\tilde{\mathcal{C}}: \quad f_i(a; \alpha_{ei}, \alpha_{ii}) = \theta_i, \quad \det[D_a F](a; \alpha_{ee}, \alpha_{ie}, \alpha_{ei}, \alpha_{ii}) = 0$$

in the a-plane (parameterized by α_{ie}), for which the finite change of rate condition

$$\frac{d}{d\alpha_{ie}}\{\det[D_a F]\}(a \in \tilde{\mathcal{C}}, \alpha_{ee}, \alpha_{ie}) \neq 0 \tag{30}$$

is satisfied. Also in this case we get two solutions of the system $f_i = \theta_i$, $\det[D_a F] = 0$ for each α_{ie}, corresponding to the transversal crossing situation for the system (30). Then by plugging these solutions into the pinning function f_e, we find as expected the two bifurcation threshold value curves, denoted by $\theta_{e,1}^{(c)}$ and $\theta_{e,2}^{(c)}$. The result of this study is summarized in Fig. 11. Just as in the case depicted in Fig. 10 we get a band in the threshold value-heterogeneity parameter plane producing at least one bump per admissible threshold value. Moreover, we identify two disjoint non-existence regions for bumps in this plane, separated from this existence band.

Finally, but not least, we can determine bifurcation curves in the θ_i, α_{ii}- and θ_e, α_{ee}-plane by using the same procedure as the one leading to Fig. 10 and Fig. 11. The outcome of this construction is similar to the band structure

observed in Fig. 10 and Fig. 11. We do not pursue any details here, however.

To sum up, the complexity of the bifurcation process leading to the formation of bumps is increased, due to the presence of finite heterogeneity in the model. A typical feature, which is not present in the translational invariant case ($\alpha = 0$), is the existence of one-parameter families of critical bumps (corresponding to (a_c, α_c)) parameterized by means of one of the heterogeneity parameters. These bump families represent transition states between existence and non-existence of bumps. We finally notice that our results with respect to coexistence of bump states together with the weak-to-strong heterogeneity transition is similar with those ones found by Avitabile *et al.* [30] for a 1-population version of (2) without resorting to two-scale convergence.

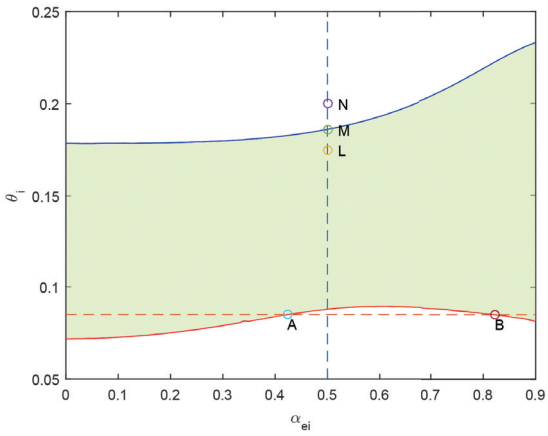

Figure 10: The graph of the critical threshold values $\theta_{i,1}^{(c)}$ (red bold curve) and $\theta_{i,2}^{(c)}$ (blue bold curve) as functions of the heterogeneity parameter α_{ei}. Input parameters: $\alpha_{ee} = \alpha_{ie} = \alpha_{ii} = 0$, $\theta_e = 0.12$ and the synaptic footprints of Table 1. Green shaded region corresponds to existence of at least one bump per admissible threshold value, white regions non-existence of bumps. In the case of $\alpha_{ei} = 0.5$, the point L produces two bumps (the generic situation), M one bump (the bifurcation point) and N no bumps. For fixed $\theta_i = 0.085$, there are two disjoint α_{ei}-intervals producing points in the green shaded region. A and B are points representing transition state to the non-existence regime for $\theta_i = 0.085$.

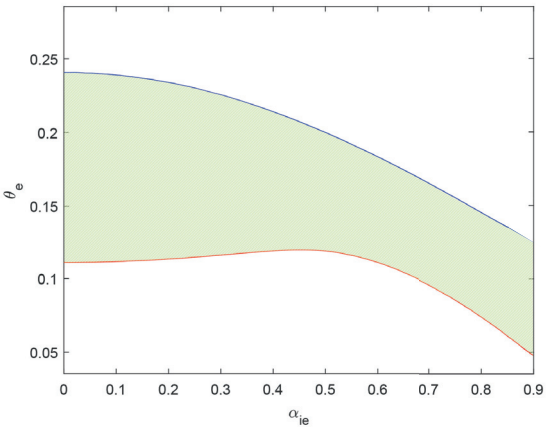

Figure 11: The graph of the critical threshold values $\theta_{e,1}^{(c)}$ (red curve) and $\theta_{e,2}^{(c)}$ (blue curve) as functions of the heterogeneity parameter α_{ie}. Input parameters: $\alpha_{ee} = \alpha_{ei} = \alpha_{ii} = 0$, $\theta_i = 0.16$ and the synaptic footprints of Table 1. Green shaded region corresponds to existence of at least one bump per admissible threshold value, white regions non-existence of bumps.

3. Stability analysis

The starting point for the stability analysis is the homogenized system (3). Given $U = (u_e, u_i)^T$ we conveniently write the system on the compact form

$$\mathbf{T}^{-1}\frac{\partial U}{\partial t} = -U + \mathcal{F}U, \tag{31}$$

with

$$\mathbf{T} = \begin{pmatrix} 1 & 0 \\ 0 & 1/\tau \end{pmatrix} \quad \text{and} \quad \mathcal{F}U = \begin{pmatrix} \mathcal{F}_{ee}u_e - \mathcal{F}_{ie}u_i \\ \\ \mathcal{F}_{ee}u_e - \mathcal{F}_{ie}u_i \end{pmatrix} \tag{32}$$

where $\mathcal{F}_{mn}$, $m, n \in \{e, i\}$ are the Hammerstein operators defined as

$$(\mathcal{F}_{mn}u)(x, y) = \int_{\mathbb{R}} \int_{Y} \omega_{mn}(x' - x, y' - y) H(u(x', y') - \theta_n) dy' dx'. \tag{33}$$

Faugeras *et al.* [31] has investigated the stability of stationary solutions to (31) on a bounded spatial domain and with a smooth sigmoid like firing rate

function using functional analytical methods. For these settings the model is well-posed and standard methods of functional analysis are applicable. Dealing with the discontinuous firing rate function H, restricts the choice of functional spaces [32, 23]. It also requires a justification of the linearization technique for studying the stability of the bumps. In Oleynik *et al.* [33] the Hammerstein operators (33) in one variable have been studied in connection with neural field models. Several results in [33] can be easily extended to the present case. Here we will formulate them without proofs.

Introduce the Banach space $\mathcal{B} = BC^1(\mathbb{R} \times Y)$ of functions U that are 1-periodic in y variables and where U and its partial derivatives are continuous functions. $\mathcal{B}$ is equipped with the norm

$$\|U\|_{\mathcal{B}} = \sup_{(x,y)\in\mathbb{R}\times Y} \left(|U(x,y)| + \left| \frac{\partial U}{\partial x}(x,y) \right| \right).$$

Let $U_0 = (U_e, U_i)^T$ be a bump solution to (31)-(33). Then from (14) we see that $U_0 \in \mathcal{B} \times \mathcal{B}$. Define the ball with center at U_0 and radius ρ as

$$B_\rho(U_0) = \{U \in \mathcal{B} \times \mathcal{B} \,|\, \|U - U_0\|_{\mathcal{B}\times\mathcal{B}} < \rho\}.$$

According to Lemma 4.1 in Oleynik *et al.* [33], there exits an $\rho > 0$ such that $\mathcal{F} : B_\rho(U_0) \to \mathcal{B} \times \mathcal{B}$. Moreover, $\mathcal{F}$ is Frechét differentiable at U_0, (see Lemma 5.6 in [32]), with the Frechét derivative given by

$$\mathcal{F}'_{U_0} V = \begin{pmatrix} L_{ee}V_e - L_{ie}V_i \\ \\ L_{ei}V_e - L_{ii}V_i \end{pmatrix}. \tag{34}$$

Here the linear operators L_{mn}, $m, n = e, i$, are defined as

$$\begin{aligned}(L_{mn}V_m)(x,y) = \frac{1}{|U'_m(a_m)|} \int_Y & (\omega_{mn}(a_m - x, y' - y)V_m(a_m, y') + \\ & \omega_{mn}(a_m + x, y' - y)V_m(-a_m, y'))\, dy'.\end{aligned} \tag{35}$$

Notice that for connectivity kernels ω_{mn} and perturbations V_m which are independent of the local variable y, the Frechét derivative (35)-(35) simplifies as expected to what one gets when applying the Evans function technique to the translational invariant case [1]. This result is also analogous to what was found in Svanstedt *et al.* [20] for single bumps in a homogenized 1-population

neural field model and Malyutina *et al.* [19] for 2-bumps in a homogenized 1-population neural field model.

The first step of the stability analysis for U_0 consists of linearizing the system (31)-(32) around the state U_0. Doing this, we get

$$\mathbf{T}^{-1}\frac{\partial V}{\partial t} = -V + \mathcal{F}'_{U_0}V \tag{36}$$

or, equivalently,

$$\frac{\partial V}{\partial t} = \mathcal{G}V, \quad \mathcal{G}V = \mathbf{T}\left(-V + \mathcal{F}'_{U_0}V\right) \tag{37}$$

The next step consists of determining the spectrum of the operator $\mathcal{G}$. The spatial structure of $\mathcal{F}'_{U_0}$ enables us to simplify this task.

Let us define two matrix value matrices

$$\mathbf{A}^{(1)}(y) = \begin{pmatrix} A(y)+B(y) & -C(y)-D(y) \\ \\ E(y)+F(y) & -G(y)-H(y) \end{pmatrix} \tag{38}$$

and

$$\mathbf{A}^{(2)}(y) = \begin{pmatrix} A(y)-B(y) & -C(y)+D(y) \\ \\ E(y)-F(y) & -G(y)+H(y) \end{pmatrix} \tag{39}$$

where

$$\begin{gathered} A(y) = \tfrac{\omega_{ee}(0,y)}{|U'_e(a_e)|}, \quad B(y) = \tfrac{\omega_{ee}(2a_e,y)}{|U'_e(a_e)|} \\ C(y) = \tfrac{\omega_{ie}(a_i-a_e,y)}{|U'_i(a_i)|}, \quad D(y) = \tfrac{\omega_{ie}(a_i+a_e,y)}{|U'_i(a_i)|} \\ E(y) = \tfrac{\omega_{ei}(a_e-a_i,y)}{|U'_e(a_e)|}, \quad F(y) = \tfrac{\omega_{ei}(a_e+a_i,y)}{|U'_e(a_e)|} \\ G(y) = \tfrac{\omega_{ii}(0,y)}{|U'_i(a_i)|}, \quad H(y) = \tfrac{\omega_{ii}(2a_i,y)}{|U'_i(a_i)|} \end{gathered} \tag{40}$$

Then the integral operator $\mathcal{H}^{(k)}$, $k = 1, 2$,

$$(\mathcal{H}^{(k)}v_k)(y) = \int_Y \mathbf{T}\mathbf{A}^{(k)}(y'-y)v_k(y')dy', \tag{41}$$

maps the Banach space $BC^1(Y) \times BC^1(Y)$ onto itself.

Moreover, the spectrum of $\mathcal{G}$ can differ from the joint spectrum of $\mathcal{H}^{(k)}$, $k = 1, 2$ only by two values. Let $Sp(L)$ and $Res(L) = \mathbb{C} \setminus Sp(L)$ denote the spectrum and resolvent of an operator L, respectively. We have the following lemma:

Lemma 1. *The spectrum $Sp(\mathcal{G})$ of the operator $\mathcal{G}$ on the right hand side of (37) can differ from $\bigcup_{k=1,2} Sp\left(-\mathbf{T} + \mathcal{H}^{(k)}\right)$ only by two values, -1 and $-1/\tau$.*

Proof. We prove these results in two steps: Firstly, we show that $\lambda \in Res(\mathcal{G})$ implies $\lambda \in \bigcap_{k=1,2} Res\left(-\mathbf{T} + \mathcal{H}^{(k)}\right)$. Secondly, we show that the converse is also valid if $\lambda \notin \{-1, -1/\tau\}$.

Step 1: Let $\lambda \in \mathbb{C}$ be in the resolvent set of the operator $\mathcal{G}$. Thus, the equation

$$(-\mathbf{T}V + \mathcal{F}'_{U_0}V) - \lambda V = \Psi \tag{42}$$

has a solution V for any Ψ, where V and Ψ belong to the complexified Banach space $\mathcal{B} \times \mathcal{B}$. Consequently, we have

$$\begin{aligned} (-\mathbf{T}V + \mathbf{T}\mathcal{F}'_{U_0}V)(\pm a_e, y) - \lambda V(\pm a_e, y) &= \Psi(\pm a_e, y), \\ (-\mathbf{T}V + \mathbf{T}\mathcal{F}'_{U_0}V)(\pm a_i, y) - \lambda V(\pm a_i, y) &= \Psi(\pm a_i, y). \end{aligned} \tag{43}$$

Thus, by rewriting (43) for $v(y) = (V_e(a_e, y), V_e(-a_e, y), V_i(a_i, y), V_i(-a_i, y))$ we obtain the system

$$-\begin{pmatrix} \mathbf{I} & \mathbf{O} \\ \mathbf{O} & \mathbf{I}/\tau \end{pmatrix} v(y) + \int_Y \mathbf{S}(y - y')v(y')dy' - \lambda v(y) = \psi(y), \tag{44}$$

with

$$\mathbf{S}(y) = \begin{pmatrix} A(y) & B(y) & -C(y) & -D(y) \\ B(y) & A(y) & -D(y) & -C(y) \\ E(y) & F(y) & -G(y) & -H(y) \\ F(y) & E(y) & -H(y) & -G(y) \end{pmatrix}$$

that has a unique solution for any $\phi(y)$ in the complexified $BC^1(Y)^4$.

Next, we exploit the similarity transformation of $\mathbf{S}$

$$\mathbf{PS}(y)\mathbf{P}^T = \begin{pmatrix} \mathbf{A}^{(1)}(y) & \mathbf{O} \\ \mathbf{O} & \mathbf{A}^{(2)}(y) \end{pmatrix}, \quad \mathbf{P} = \begin{pmatrix} \frac{1}{2} & \frac{1}{2} & 0 & 0 \\ 0 & 0 & \frac{1}{2} & \frac{1}{2} \\ \frac{1}{2} & -\frac{1}{2} & 0 & 0 \\ 0 & 0 & \frac{1}{2} & -\frac{1}{2} \end{pmatrix} \tag{45}$$

that conveniently block-diagonalizes it. Here $\mathbf{A}^{(k)}$, $k = 1, 2$, are given as in (38) and (39).

We apply this transformation to (44) and obtain the system

$$-\mathbf{T}v_k + \mathcal{H}^{(k)}v_k - \lambda v(y) = \psi_k(y), \quad k = 1, 2. \tag{46}$$

concluding that $\lambda \in \bigcap_{k=1,2} Res\left(-\mathbf{T} + \mathcal{H}^{(k)}\right)$. This implies that $\cup_k Sp(-T + \mathcal{H}^{(k)}) \subset Sp(\mathcal{G})$.

Step 2: Let us now assume that $\lambda \in \bigcap_{k=1,2} Res\left(-\mathbf{T} + \mathcal{H}^{(k)}\right)$. This implies that (44) has a unique solution $v(y)$ for any $\phi \in (BC^1(Y))^4$, or equivalently (43) has the solution $(V_e(a_e, y), V_e(-a_e, y), V_i(a_i, y), V_e(-a_i, y)) = v(y)$ for any $\Phi(x, y)$. From (42) we can express $V(x, y)$ as

$$-(\mathbf{T} + \lambda\mathbf{I})V(x, y) = \Phi(x, y) - \mathbf{T}\mathcal{F}'_{U_0}V. \tag{47}$$

Since $\mathcal{F}'_{U_0}V$ given by (34)-(35) can be calculated only by using $v(y)$, we can obtain $V(x, y)$ if $\mathbf{T} + \lambda\mathbf{I}$ is invertible, i.e., if $\lambda \neq -1$ and $\lambda \neq -1/\tau$, see (44). This yields that $Sp(\mathcal{G}) \setminus \{-1, -1/\tau\} \subset \cup_k Sp(-T + \mathcal{H}^{(k)})$. This observation concludes our proof. □

We notice here that from the previous analysis, $Sp(\mathcal{G})$ may contain the values $-1, -1/\tau$ even if they do belong to $Sp(-T + \mathcal{H}^{(k)})$. These values, however, do not influence the stability results for the bumps. Therefore, we will focus on determining the spectrum of $-\mathbf{T} + \mathcal{H}^{(k)}$, $k = 1, 2$. We observe that the 2×2-matrix functions $\mathbf{A}^{(k)}$ $k = 1, 2$ and the eigenfunctions v_k are continuous differentiable 1-periodic functions, from which it follows that the Fourier decomposition method is applicable. The Fourier coefficients of

$-\mathbf{T}+\mathcal{H}^{(k)}$ $(k=1,2)$ are given by the matrices $\mathbf{F}_n^{(k)}$, $n\in\mathbb{Z}$, where

$$\mathbf{F}_n^{(1)}=\begin{pmatrix}\widetilde{A}_n+\widetilde{B}_n-1 & -\widetilde{C}_n-\widetilde{D}_n\\ \dfrac{\widetilde{E}_n+\widetilde{F}_n}{\tau} & -\dfrac{\widetilde{G}_n+\widetilde{H}_n+1}{\tau}\end{pmatrix} \tag{48}$$

and

$$\mathbf{F}_n^{(2)}=\begin{pmatrix}\widetilde{A}_n-\widetilde{B}_n-1 & -\widetilde{C}_n+\widetilde{D}_n\\ \dfrac{\widetilde{E}_n-\widetilde{F}_n}{\tau} & -\dfrac{\widetilde{G}_n-\widetilde{H}_n+1}{\tau}\end{pmatrix} \tag{49}$$

Here $\widetilde{A}_n$, …, $\widetilde{F}_n$, $n\in\mathbb{Z}$ denote the Fourier coefficients of A, …, F in (40). The eigenvalues of the operators $\mathcal{H}^{(k)}-\mathbf{T}$ $(k=1,2)$ the are given as the eigenvalues of the matrices $\mathbf{F}_n^{(k)}$, $n\in\mathbb{Z}$.

We summarize the results above in the following theorem:

Theorem 2. *Let Λ be the set*

$$\Lambda=\{\lambda:\quad \lambda=\lambda_{\pm,n}^{(k)},\ n\in\mathbb{Z},\ k=1,2\} \tag{50}$$

where $\lambda_{\pm,n}^{(k)}$, are the eigenvalues of the matrix $\mathbf{F}_n^{(k)}$. Then

$$\Lambda\subset\sigma(\mathcal{G})\subset\Lambda\cup\{-1,-\frac{1}{\tau}\}.$$

Notice that the eigenvalues of matrices $\mathbf{F}_n^{(k)}$ are complex, i.e.

$$\lambda_{\pm,n}^{(k)}=\mu_n^{(k)}\pm i\nu_n^{(k)},\quad \mu_n^{(k)},\nu_n^{(k)}\in\mathbb{R} \tag{51}$$

Moreover, they can also be expressed in terms of the invariants $\mathrm{tr}(\mathbf{F}_n^{(k)})$ and $\det(\mathbf{F}_n^{(k)})$ of the matrices $\mathbf{F}_n^{(k)}$:

$$\lambda_{\pm,n}^{(k)}=\frac{1}{2}\{\mathrm{tr}(\mathbf{F}_n^{(k)})\pm\sqrt{(\mathrm{tr}(\mathbf{F}_n^{(k)}))^2-4\det(\mathbf{F}_n^{(k)})}\} \tag{52}$$

We readily find that

$$\begin{gathered}\mathrm{tr}(\mathbf{F}_n^{(k)})=\widetilde{A}_n-(-1)^k\widetilde{B}_n-1-\tfrac{1}{\tau}(\widetilde{G}_n-(-1)^k\widetilde{H}_n+1\\ \tau\det(\mathbf{F}_n^{(k)})=(\widetilde{C}_n-(-1)^k\widetilde{D}_n)(\widetilde{E}_n-(-1)^k\widetilde{F}_n)\\ -(\widetilde{A}_n-(-1)^k\widetilde{B}_n-1)(\widetilde{G}_n-(-1)^k\widetilde{H}_n+1)\end{gathered} \tag{53}$$

A simple computation reveals that

$$\det(\mathbf{F}_0^{(2)}) = 0 \tag{54}$$

from which it follows that

$$\lambda_{-,0}^{(2)} \equiv 0 \tag{55}$$

The derivation of this result proceeds in exactly the same way as in Blomquist *et al.* [1]. We therefore omit the details in the proof of this fact. This result is indeed expected. It reflects the translational invariance of the bump solutions within the framework of the model (3).

For real and spatial symmetric synaptic footprint functions σ_{mn} such as (6), the Fourier coefficients $\widetilde{A}_n, \ldots, \widetilde{F}_n$, $n \in \mathbb{Z}$ will be real, from which it follows that the invariants $\mathrm{tr}(\mathbf{F}_n^{(k)})$ and $\det(\mathbf{F}_n^{(k)})$ also are real. Moreover, in that case we only need to consider these invariants for $n = 0, 1, 2, ...$ In what follows we will restrict the stability analysis to the case with real and spatial symmetric synaptic footprint functions σ_{mn}.

First, let us assume that

$$\begin{gathered} \det(\mathbf{F}_n^{(2)}) < 0 \quad \text{for at least one } n \neq 0 \\ \text{or} \\ \det(\mathbf{F}_n^{(1)}) < 0 \quad \text{for at least one } n \end{gathered} \tag{56}$$

In this case we have $\lambda_{-,n}^{(k)} < 0 < \lambda_{+,n}^{(k)}$ for the corresponding eigenvalues $\lambda_{\pm,n}^{(k)}$ for all $\tau > 0$. Hence (56) is a sufficient condition for instability.

Now, let us consider the complementary regime

$$\det(\mathbf{F}_n^{(k)}) > 0 \quad \text{for all } k \text{ and } n \tag{57}$$

Here we conveniently distinguish between the following cases:

1. For the regime

$$\widetilde{G}_n - (-1)^k \widetilde{H}_n + 1 < 0 \leq \widetilde{A}_n - (-1)^k \widetilde{B}_n - 1 \tag{58}$$

for at least one n, we have $\mathrm{tr}(\mathbf{F}_n^{(k)}) > 0$ for that particular choice of n, which means that the actual bump is unstable for all τ.

2. In the regime

$$\widetilde{A}_n - (-1)^k \widetilde{B}_n - 1 \leq 0 < \widetilde{G}_n - (-1)^k \widetilde{H}_n + 1 \tag{59}$$

for all n, we have $\mathrm{tr}(\mathbf{F}_n^{(k)}) < 0$ (for all n), from which it follows that the bumps are stable for all $\tau > 0$.

3. The scenario

$$\mathrm{sgn}(\widetilde{A}_n - (-1)^k \widetilde{B}_n - 1) = \mathrm{sgn}(\widetilde{G}_n - (-1)^k \widetilde{H}_n + 1) \tag{60}$$

for n produces two sequences of positive solutions $\{\tau_{cr,n}^{(k)}\}_{n=0}^{\infty}$ given by

$$\tau_{cr,n}^{(k)} = \frac{\widetilde{G}_n - (-1)^k \widetilde{H}_n + 1}{\widetilde{A}_n - (-1)^k \widetilde{B}_n - 1}, \quad k = 1, 2 \tag{61}$$

of the equation $\mathrm{tr}(\mathbf{F}_n^{(k)}) = 0$. Let τ_{cr} be defined as

$$\tau_{cr} = \min_{k,n} \{\tau_{cr,n}^{(k)}\} \tag{62}$$

Then the corresponding bumps are stable for $\tau < \tau_{cr}$ and unstable for $\tau > \tau_{cr}$ provided (60) holds true.

The next theorem shows that it suffices to know the eigenvalues $\lambda_{\pm,0}^{(k)}$ in order to carry out the stability assessment if the norm of the heterogeneity vector α is sufficiently small:

Theorem 3. *Let the connectivity functions ω_{mn} given by (5) with $\sigma_{mn} \in BC^1(Y)$ and $\Phi \in BC^1(\mathbb{R})$ satisfying the properties (7). Then there exists $\varepsilon > 0$ such that for any $\alpha \in [0, \varepsilon]^4$ the bumps have the same stability properties as in the translational invariant case ($\alpha = 0$).*

Proof. The stability of $U_\alpha(x)$ is assessed by means of the eigenvalues of $\mathbf{F}_n^{(1)}$ and $\mathbf{F}_n^{(2)}$, $n \in \mathbb{N} \cup \{0\}$. Now, according to Theorem 1, we have $\|U_\alpha - U_0\|_{BC^1(\mathbb{R})} \to 0$ as α goes to 0 (cf. equation (13)). The norm convergence of matrices implies convergence of eigenvalues of those matrices, in accordance with Theorem 5.12 in Section II in Kato [34]. Given $X_\alpha \in BC(Y)$ for any $\alpha \in [0, 1)$ and $\|X_\alpha - X_0\|_\infty \to 0$ as $\alpha \to 0$, Riemann-Lebesques lemma implies that

$$\sup_{n \in \mathbb{N} \cup \{0\}} |\tilde{X}_{n,\alpha} - \tilde{X}_{n,0}| \leq \|X_\alpha - X_0\|_\infty \to 0,$$

where $\tilde{X}_{n,\alpha}$ and $\tilde{X}_{n,0}$ denote the Fourier series coefficients of X_α and X_0, respectively. For $X_0 = const$ we have $|\tilde{X}_{n,\alpha}| \to 0$ as $\alpha \to 0$ uniformly in $n \in \mathbb{N}$. We readily find that

$$\left\| \mathbf{F}^{(k)}_{n,\alpha} - \begin{pmatrix} -1 & 0 \\ 0 & -1/\tau \end{pmatrix} \right\|_\infty \to 0$$

uniformly in $n \in \mathbb{N}$ as $\alpha \to 0$. In addition, we get

$$\left\| \mathbf{F}^{(k)}_{0,\alpha} - \mathbf{F}^{(k)}_{0,0} \right\|_\infty \to 0, \quad \alpha \to 0.$$

Hence, there is $\varepsilon > 0$ such for all $|\alpha| \in (0, \varepsilon)^4$, the stability properties of the bumps are the same as in the translational invariant case. □

Let us study the stability properties of the bumps depicted in Fig. 2. The input parameters for this computation are $\alpha_{ee} = 0.01$, $\alpha_{ie} = 0.01$, $\alpha_{ei} = 0.025$, $\alpha_{ii} = 0.025$, Set 1 in Table 1 and $\tau = 0.5$. We plot the real parts of the eigenvalues of matrices (48) and (49) as a function of n.

The results are summarized in Fig. 12. We conclude that the narrow bumps (corresponding to the dotted curves in Fig. 2) are unstable, whereas the bold curves (representing the broad bumps) are stable for $\tau = 0.5$.

The present formalism also enables us to determine the stability properties of the two bumps depicted in Fig. 2 as a function of the relative inhibition time τ. We readily find that when τ exceeds the threshold value τ_{cr} given by

$$\tau_{cr} = \min_k \{\tau^{(k)}_{cr,0}\} \tag{63}$$

the broad bumps become unstable. Here $\tau_{cr,0}$ is given by the expression (62) for $n = 0$. With the actual input parameters we have $\tau_{cr} = 3.0292$. The narrow bumps are characterized by the negative determinant condition (56) for $n = 0, k = 1$, which means that they are unstable for all τ. The actual stability results are indeed consistent with Theorem 3 and the stability results in Blomquist *et al.* [1].

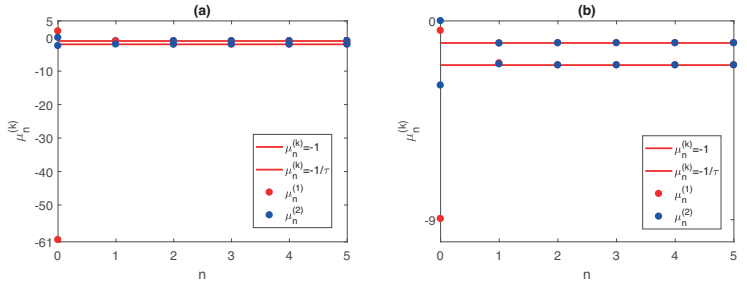

Figure 12: The real parts $\mu_n^{(k)}$ of the eigenvalues $\lambda_{\pm,n}^{(k)}$ of matrices (48) and (49) in the weakly modulated case as a function of n. Input data: Set 1 in Table 1, $\alpha_{ee} = 0.01$, $\alpha_{ie} = 0.01$, $\alpha_{ei} = 0.025$ and $\alpha_{ii} = 0.025$ and $\tau = 0.5$. $\lambda_{\pm,n}^{(1)}$ and $\lambda_{\pm,n}^{(2)}$ are the eigenvalues of the matrix (48) and the matrix (49), respectively. Eigenvalues of the matrices (48) and (49) in the case $\alpha = 0$ are equal to $(\lambda_{-,0}^{(1)}, \lambda_{+,0}^{(1)}) = (1.9405, -60.6462)$, $(\lambda_{-,0}^{(2)}, \lambda_{+,0}^{(2)}) = (0, -2.4414)$ for the narrow bumps and $(\lambda_{-,0}^{(1)}, \lambda_{+,0}^{(1)}) = (-0.4392, -8.9648)$, $(\lambda_{-,0}^{(2)}, \lambda_{+,0}^{(2)}) = (0, -2.9130)$ for the broad bumps. The translational invariance property (55) is confirmed. (a) and (b) show that real parts of the eigenvalues for the narrow and for the broad bumps, respectively.

Let us finally develop the framework for stability assessment applicable beyond the weakly modulated regime $0 < \alpha_{mn} \ll 1$. We tacitly presuppose that the bump exists in this regime. The following theorem serves as a guideline for the investigation of the stability of these bumps:

Theorem 4. *Let $\alpha \in (0,1)^4$ be fixed and let ω_{mn} satisfy the uniform bound*

$$\int_Y |\frac{\partial \omega_{mn}(x,y)}{\partial y}| dy \leq r$$

for all $m, n \in \{e, i\}$. Then the stability property of the bump $U_\alpha(x)$ is determined by the eigenvalues λ_n, $|n| \leq n_*$ where $n_* = \lceil 2r/\pi \rceil$.

Proof. Riemann-Lebesques lemma implies that the Fourier coefficients $|\tilde{X}_n| \to 0$ as $n \to \infty$ for any $X \in L_1([0,1])$. Moreover, we have the estimate

$$|\tilde{X}_n| \leq \frac{1}{2\pi n} \int_0^1 X'(y) dy. \tag{64}$$

For the functions $X = A, B, \ldots, F$ given by (40), we have the estimate

$$|\tilde{X}_n| \leq \frac{r}{2\pi n} \tag{65}$$

We observe that

$$\left\|\mathbf{F}_n^{(k)} - \mathbf{F}_\infty\right\|_\infty \leq \frac{r\max\{1, 1/\tau\}}{\pi n} \to 0. \tag{66}$$

as $n \to \infty$. This implies that the eigenvalues $\lambda_{\pm,n}^{(k)}$ $(n \in \mathbb{N})$ of the matrices $\mathbf{F}_n^{(k)}$ tend to the eigenvalues of the limiting diagonal matrix, that is, $\lambda_1 = -1$ and $\lambda_2 = -1/\tau$ as $n \to \infty$, in accordance with Theorem 5.12 in Section II in Kato [34]. In the rest of the proof we skip the superscript notations for $\mathbf{F}_n^{(k)}$ and its eigenvalues as it is valid for both $k = 1, 2$. For each fixed $n \in \mathbb{N}$, it follows from the Gershgorin circle theorem that the eigenvalues $\lambda_{\pm,n}$ belong to the union of two sets

$$D_i(n) = \{z : |z - \lambda_i| \leq |(\mathbf{F}_n)_{ij}| + |(\mathbf{F}_n)_{ii} - \lambda_i|\}, \quad i \neq j,$$

where $(\mathbf{F}_n)_{ij}$, $i, j = 1, 2$ denote the entries of $\mathbf{F}_n$.

Using the expressions for $\mathbf{F}_n$ and the estimate (65), we obtain the upper bounds for the radii of $D_i(n)$, $i = 1, 2$. Thus, the eigenvalues $\lambda_{\pm,n}^{(k)}$ are confined in the union of the two disks

$$\tilde{D}_1(n) = \left\{z : |z - (-1)| \leq \frac{2r}{\pi n}\right\},$$

$$\tilde{D}_2(n) = \left\{z : |z - (-1/\tau)| \leq \frac{2r}{\tau\pi n}\right\}.$$

It is straightforward to see that the eigenvalues $\lambda_{\pm,n}^{(k)}$ have negative real parts if $\frac{2r}{\pi n} < 1$, or equivalently $n \geq n_* \equiv \lceil 2r/\pi \rceil$. □

To illustrate Theorem 4 let us consider three bumps situation depicted in Fig. 8 - Fig. 9. The bounding constant r of this theorem is estimated to be $r = 12.5436$, from which we find that $n_* = 8$. Fig. 13 displays the real parts of the eigenvalues of matrices (48) and (49) as a function of n when $\tau = 0.2$. Also here it suffices to consider the situation with $n \geq 0$, due to the symmetry of the synaptic footprint functions σ_{mn}. We observe that for the intersection points R and Q in Fig. 8 the real parts of all the eigenvalues are negative, whereas for the intersection point P for $n = 0, k = 1$ the corresponding eigenvalue has positive real part. This means that the bumps corresponding to R and Q are stable whereas the bump corresponding to P is unstable for $\tau = 0.2$.

We can also study the stability properties of the three bumps depicted in Fig. 8 - Fig. 9 as a function of the relative inhibition time τ. We proceed as follows: For the input parameters producing the intersection point R in Fig. 8 we find that the value of τ_{cr} defined as (63) is given as $\tau_{cr} = 0.2435$, which means that the bump corresponding to R is stable for $\tau < 0.2435$. We then proceed to the intersection point P. In this case (56) is fulfilled for $n = 0, k = 1$ from which it follows that the corresponding bump is unstable for all τ-values. For the point Q in Fig. 8 we obtain $\tau_{cr} = 2.0690$, which means that the bump corresponding to Q is stable for $\tau < 2.0690$. When selecting τ in our numerical computations to a value in the range $0.2435 < \tau < 2.0690$, we thus find that only the bump corresponding to the intersection point Q in Fig. 8 is stable, the two other intersection points R and P produce unstable bumps.

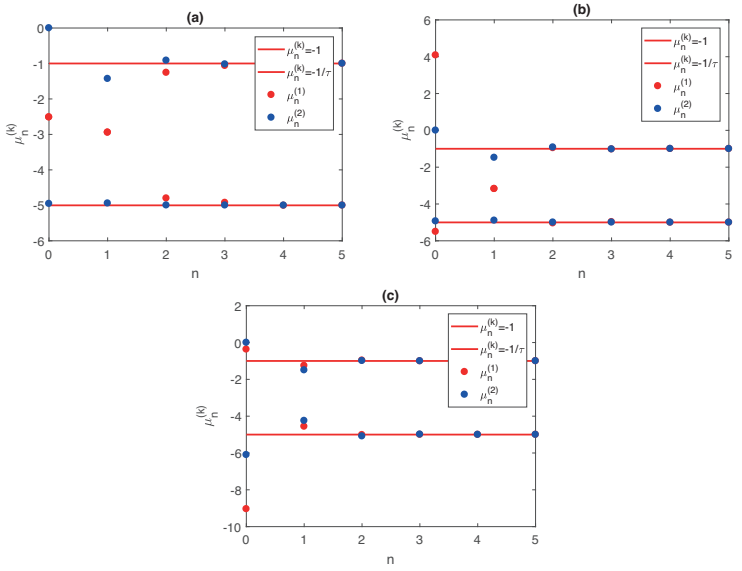

Figure 13: The real parts $\mu_n^{(k)}$ of the eigenvalues $\lambda_{\pm,n}^{(k)}$ of matrices (48) and (49) beyond the weakly modulated case as a function of n in the three bumps situation depicted in Fig. 8 - Fig. 9. Input data: $\alpha_{ee} = 0.25$, $\alpha_{ie} = 0.25$, $\alpha_{ei} = 0.83$, $\alpha_{ii} = 0.25$, the parameter Set 2 in Table 1 and $\tau = 0.2$. $\lambda_{\pm,n}^{(1)}$ and $\lambda_{\pm,n}^{(2)}$ are the eigenvalues of the matrix (48) and the matrix (49), respectively. The translational invariance property (55) is confirmed. (a), (b) and (c) show the real parts of eigenvalues for the bumps corresponding to the intersection points R, P and Q in Fig. 8, respectively.

4. Conclusions and outlook

We have shown that the homogenized model supports the same type of solutions as the translation-invariant version. Moreover, the conclusion about the number of bumps and their linear stability can be drawn from the study of the translation-invariant model when dealing with low level of heterogeneity. However, when increasing the degree of heterogeneity beyond this regime, the number of bumps and their stability is not directly related to the translation invariant case and the homogenized model needs to be analyzed in some more detail. We have shown that the methods developed for the translation invariant case could be generalized and used for the ho-

mogenized model.

In the present work we have assumed that the firing rate functions are given by the Heaviside function. It is an open question whether the results obtained in this paper can be extended to the case of smooth but steep firing rate functions. The recent study for the existence and continuous dependence of multibumps on the steepness of firing rate function in Oleynik *et al.* [33] could serve as a starting point for this type of investigation.

An extension of the analysis of the present results (as well as the multibump configuration) to $2D$ spatial geometry is both interesting and intriguing. The problem of existence and stability of travelling fronts within the framework of the 2-population homogenized neural field model (3) should also be addressed. The results obtained should then be compared with a recent paper by Folias [35] where the connectivity kernels are assumed to be homogeneous and isotropic, and external inputs are included. We also conjecture that a rigorous stability analysis could benefit from the techniques used in Folias *et al.* [36]. It would also be of interest to investigate the relationship between the present spectral stability analysis and the nonlinear stability of bump pairs, in a way analogous to Sanstede [37] for travelling waves.

Finally, but not least the impact of the periodic microstructure on pattern forming processes within the framework of the model (3) should be investigated. The outcome of this investigation will be compared with the pattern formation study carried out, using the model (1) as a starting point. In addition, it is likely that such analysis will reveal the role of bumps and traveling fronts in the pattern forming process.

5. Acknowledgements

The authors are grateful to Professor Arcady Ponosov and Professor Bjørn Fredrik Nielsen (Norwegian University of Life Sciences) for fruitful and stimulating discussions during the preparation phase of this paper. The authors would also like to thank the reviewers for constructive remarks. This research work was supported by the Norwegian University of Life Sciences and The Research Council of Norway, project number 239070.

References

[1] Patrick Blomquist, John Wyller, and Gaute T Einevoll. Localized activity patterns in two-population neuronal networks. *Physica D: Nonlinear Phenomena*, 206(3):180–212, 2005.

[2] Shun-ichi Amari. Heaviside world: Excitation and Self-Organization of Neural Fields. In *Neural Fields*, pages 97–118. Springer, 2014.

[3] S Amari. A mathematical theory of nerve nets. *Adv Biophys*, 6:75–119, 1974.

[4] Shun-ichi Amari. Dynamics of pattern formation in lateral-inhibition type neural fields. *Biological cybernetics*, 27(2):77–87, 1977.

[5] Paul C Bressloff. Spatiotemporal dynamics of continuum neural fields. *Journal of Physics A: Mathematical and Theoretical*, 45(3):033001, 2011.

[6] Jack Xin. An introduction to Fronts in Random Media. *SIAM Review*, 42:161, 2000.

[7] Jack Xin. An introduction to Fronts in Random Media. *Surveys and Tutorials in the Applied Mathematical Sciences, Springer Verlag*, 2009.

[8] Gabriel Nguetseng. A general convergence result for a functional related to the theory of homogenization. *SIAM Journal on Mathematical Analysis*, 20(3):608–623, 1989.

[9] Dag Lukkassen, Gabriel Nguetseng, and Peter Wall. Two-scale convergence. *International Journal of Pure and Applied Mathematics*, 2(1):35–86, 2002.

[10] Paul C Bressloff. Traveling fronts and wave propagation failure in an inhomogeneous neural network. *Physica D: Nonlinear Phenomena*, 155(1):83–100, 2001.

[11] Paul C Bressloff. Spatially periodic modulation of cortical patterns by long-range horizontal connections. *Physica D: Nonlinear Phenomena*, 185(3):131–157, 2003.

[12] Paul C Bressloff, Stefanos E Folias, Alain Prat, and Y-X Li. Oscillatory waves in inhomogeneous neural media. *Physical review letters*, 91(17):178101, 2003.

[13] Xiaoying Huang, William C Troy, Qian Yang, Hongtao Ma, Carlo R Laing, Steven J Schiff, and Jian-Young Wu. Spiral waves in disinhibited mammalian neocortex. *Journal of Neuroscience*, 24(44):9897–9902, 2004.

[14] Zachary P Kilpatrick, Stefanos E Folias, and Paul C Bressloff. Traveling pulses and wave propagation failure in inhomogeneous neural media. *SIAM Journal on Applied Dynamical Systems*, 7(1):161–185, 2008.

[15] Stephen Coombes and CR Laing. Pulsating fronts in periodically modulated neural field models. *Physical Review E*, 83(1):011912, 2011.

[16] Helmut Schmidt, Axel Hutt, and Lutz Schimansky-Geier. Wave fronts in inhomogeneous neural field models. *Physica D: Nonlinear Phenomena*, 238(14):1101–1112, 2009.

[17] Stephen Coombes, Carlo Laing, Helmut Schmidt, Nils Svanstedt, and John Wyller. Waves in random neural media. *Discrete and Continuous Dynamical Systems—Series A*, 32:2951–2970, 2012.

[18] Nils Svanstedt and Jean Louis Woukeng. Homogenization of a Wilson–Cowan model for neural fields. *Nonlinear Analysis: Real World Applications*, 14(3):1705–1715, 2013.

[19] Elena Malyutina, John Wyller, and Arcady Ponosov. Two bump solutions of a homogenized Wilson–Cowan model with periodic microstructure. *Physica D: Nonlinear Phenomena*, 271:19–31, 2014.

[20] Nils Svanstedt, John Wyller, and Elena Malyutina. A one-population Amari model with periodic microstructure. *Nonlinearity*, 27(6):1391–1417, 2014.

[21] Elena Malyutina, Arcady Ponosov, and John Wyller. Numerical analysis of bump solutions for neural field equations with periodic microstructure. *Applied Mathematics and Computation*, 260:370–384, 2015.

[22] Augusto Visintin. Towards a two-scale calculus. *ESAIM: Control, Optimisation and Calculus of Variations*, 12(3):371–397, 2006.

[23] Roland Potthast and Peter Beim Graben. Existence and properties of solutions for neural field equations. *Mathematical Methods in the Applied Sciences*, 33(8):935–949, 2010.

[24] Grégory Faye and Olivier Faugeras. Some theoretical and numerical results for delayed neural field equations. *Physica D: Nonlinear Phenomena*, 239(9):561–578, 2010.

[25] Stefanos E Folias and Paul C Bressloff. Breathing pulses in an excitatory neural network. *SIAM Journal on Applied Dynamical Systems*, 3(3):378–407, 2004.

[26] Stephen Coombes. Waves, bumps, and patterns in neural field theories. *Biological cybernetics*, 93(2):91–108, 2005.

[27] Markus R Owen, Carlo R Laing, and Stephen Coombes. Bumps and rings in a two-dimensional neural field: splitting and rotational instabilities. *New Journal of Physics*, 9(10):378, 2007.

[28] Richard Kollár and Robert L Pego. Spectral stability of vortices in two-dimensional Bose–Einstein condensates via the Evans function and Krein signature. *Applied Mathematics Research eXpress*, 2012(1):1–46, 2012.

[29] Stefanos E Folias and G Bard Ermentrout. Bifurcations of stationary solutions in an interacting pair of EI neural fields. *SIAM Journal on Applied Dynamical Systems*, 11(3):895–938, 2012.

[30] Daniele Avitabile and Helmut Schmidt. Snakes and ladders in an inhomogeneous neural field model. *Physica D: Nonlinear Phenomena*, 294:24–36, 2015.

[31] Olivier Faugeras, Romain Veltz, and François Grimbert. Persistent neural states: stationary localized activity patterns in nonlinear continuous n-population, q-dimensional neural networks. *Neural computation*, 21(1):147–187, 2009.

[32] Anna Oleynik, Arcady Ponosov, and John Wyller. On the properties of nonlinear nonlocal operators arising in neural field models. *Journal of Mathematical Analysis and Applications*, 398(1):335–351, 2013.

[33] Anna Oleynik, Arcady Ponosov, Vadim Kostrykin, and Alexander V Sobolev. Spatially localized solutions of the Hammerstein equation with sigmoid type of nonlinearity. *Journal of Differential Equations*, 261(10):5844–5874, 2016.

[34] Tosio Kato. Perturbation theory for linear operators. *Reprint of the corr. print. of the 2nd ed. 1980, Classics in Mathematics, Springer-Verlag*, 1995.

[35] Stefanos E Folias. Traveling waves and breathers in an excitatory-inhibitory neural field. *Physical Review E*, 95(3):032210, 2017.

[36] Stefanos E Folias and Paul C Bressloff. Stimulus-locked traveling waves and breathers in an excitatory neural network. *SIAM journal on Applied Mathematics*, 65(6):2067–2092, 2005.

[37] Björn Sandstede. Evans functions and nonlinear stability of traveling waves in neuronal network models. *International Journal of Bifurcation and Chaos*, 17(08):2693–2704, 2007.

PAPER III

Pattern formation in a 2-population homogenized neuronal network model

Karina Kolodina[a], John Wyller[a,*], Anna Oleynik[b], Mads Peter Sørensen[c]

[a] *Faculty of Science and Technology, Norwegian University of Life Sciences, P.O. Box 5003, N-1432 Ås, Norway*
[b] *Department of Mathematics, University of Bergen, P.O. Box 7803, N-5020 Bergen, Norway*
[c] *Department of Applied Mathematics and Computer Science, Technical University of Denmark, DK-2800 Kongens Lyngby, Denmark*

[*] Corresponding author
Email address: john.wyller@nmbu.no (John Wyller)

Abstract

We study pattern formation in a 2-population homogenized neural field model in one spatial dimension with periodic microstructure, in particular with respect to the formation of stationary periodic patterns and spatio temporal oscillations. The connectivity functions are periodically modulated in both the synaptic footprint and in the spatial scale. It is shown that the nonlocal synaptic interactions promote a finite band width instability, just as in the translational invariant case. The stability method which is a generalization of the method developed for the translational invariant case, relies on a sequence of wave-number dependent invariants of 2×2-matrices representing the sequence of Fourier-transformed linearized evolution equations for the perturbation imposed on the homogeneous background. The generic picture of the instability structure consists of a finite set of well-separated gain bands. We follow the instability numerically into the nonlinear regime for both steep and shallow firing rate functions for the case when the connectivity kernels are modelled by means of exponentially decaying functions, periodically modulated both in the synaptic footprints and in the spatial scale. In the weakly modulated regime the following picture emerges: For the steep firing rate functions stable oscillations are formed whereas we get spatio-temporal oscillations in the shallow regime of the firing rate functions, consistent with the findings in the translational invariant case. In the regime beyond the weakly modulated case a rich plethora of phenomena takes place. The numerical computations show that the growth rate of the linearly most unstable mode typically decreases with the degree of heterogeneity. This leads to a slowdown of the pattern forming process when increasing the degrees of heterogeneity, which is also confirmed by the numerical simulations.

Keywords: Neural field models, homogenization theory, Turing type of instability, pattern formation.

1. Introduction

It is common to investigate large-scale activity of neural tissue by means of nonlocal models. Since the seminal works of Amari [1, 2] and Wilson and Cowan [3, 4] such models have been subject to a vast number of investigations, e.g. [5] and the references therein. 1- and 2-population neural field models have been used to understand spatiotemporal dynamics of the cortex of the brain. Stationary spatially-extended patterns are related to visual hallucinations [6, 7, 8], while stationary localized structures (*bumps*) are related to short term memory [9, 10, 11]. Traveling waves (fronts, pulses, target waves and spirals) are connected to information processing [12, 13].

The nonlocal field model is defined by means of the coupled system of the two nonlinear integro-differential equations

$$\begin{aligned} \frac{\partial}{\partial t}u_e &= -u_e + \omega_{ee} \otimes P_e(u_e - \theta_e) - \omega_{ie} \otimes P_i(u_i - \theta_i) \\ \tau\frac{\partial}{\partial t}u_i &= -u_i + \omega_{ei} \otimes P_e(u_e - \theta_e) - \omega_{ii} \otimes P_i(u_i - \theta_i) \end{aligned} \tag{1}$$

where $\omega_{mn} \otimes\otimes P_m$ is the convolution of ω_{mn} and P_m $(m, n = e, i)$ defined by

$$\big(\omega_{mn}\otimes\otimes P_m(u_m-\theta_m)\big)(x,t) \equiv \int\limits_{\mathbb{R}^N} \omega_{mn}(x-x',t)P_m(u_m(x',t)-\theta_m)dy'dx', \tag{2}$$

This model describes the interaction between populations of excitatory and inhibitory neurons. u_e and u_i denote the membrane potentials of excitatory and inhibitory neurons, respectively, at the spatial point x and time $t > 0$. The functions ω_{mn} $(m, n = e, i)$ evaluated at the difference $x - x'$ measure the connectivity strengths between neurons at located at position x and x', whereas P_m $(m = e, i)$ are the firing rate functions. θ_e and θ_i are threshold values for firing of the excitatory and the inhibitory neurons, respectively. Notice here that we allow for the situation where $\theta_e \neq \theta_i$. The parameter τ is the relative inhibition time i.e. $\tau = \tau_i/\tau_e$ where τ_e (τ_i) is the excitatory (inhibitory) time constant.

The neural field model (1) which is often referred to as a 2-population model of the Amari type was proposed by Blomquist *et al.* [14]. In [14] the existence and stability of single bumps with the Heaviside firing rate functions have been studied. In Wyller *et al.* [15] pattern formation of the Turing type within the framework of (1) in one spatial dimension as a function of the steepness of the firing rate function was investigated. In particular there were considered stationary periodic patterns and spatiotemporal oscillations. The present work is mostly based on the paper [15].

However, the modeling framework (1) assumes that the cortical medium is homogeneous and isotropic. Thus, the heterogeneity in the cortical structure is not taken into account. Therefore, this modeling approach represents a simplification of the actual situation. One way to take into account the microstructure of the brain media is by using the so-called *homogenization techniques* [16, 17]. The connection between periodic microstructure of the cortex and nonlocal mean field description has been explored in the works [18, 19, 13, 20, 21, 22]. It turns out that the microstructure has an impact on the pattern forming mechanisms as well as existence and stability of traveling fronts and pulses. In homogenization techniques for neural field models it is usually assumed that the connectivity functions are represented as $\omega_{mn}^{\varepsilon}(x) = \omega_{mn}(x, x/\varepsilon)$ and have periodicity in the second variable $y = x/\varepsilon$, where the microstructure of heterogeneity is parameterized by $\varepsilon > 0$, see e.g. [23, 24, 25]. Thus, a possible extension of (1) taking this type of heterogeneity into account reads

$$\begin{aligned} \frac{\partial}{\partial t} u_e^{\varepsilon} &= -u_e^{\varepsilon} + \omega_{ee}^{\varepsilon} \otimes P_e(u_e^{\varepsilon} - \theta_e) - \omega_{ie}^{\varepsilon} \otimes P_i(u_i^{\varepsilon} - \theta_i) \\ \tau \frac{\partial}{\partial t} u_i^{\varepsilon} &= -u_i^{\varepsilon} + \omega_{ei}^{\varepsilon} \otimes P_e(u_e^{\varepsilon} - \theta_e) - \omega_{ii}^{\varepsilon} \otimes P_i(u_i^{\varepsilon} - \theta_i) \end{aligned} \tag{3}$$

The two-scale convergent method described in [26, 27, 28] has been applied by Svanstedt *et al.* [24] to a one-population neural field model with spatial microstructure. Then, by employing the same arguments as in [24], one can show that (3) two-scale weakly converges as $\varepsilon \to 0$ to the system

$$\frac{\partial}{\partial t}u_e = -u_e + \omega_{ee} \otimes\otimes P_e(u_e - \theta_e) - \omega_{ie} \otimes\otimes P_i(u_i - \theta_i)$$
$$\tau\frac{\partial}{\partial t}u_i = -u_i + \omega_{ei} \otimes\otimes P_e(u_e - \theta_e) - \omega_{ii} \otimes\otimes P_i(u_i - \theta_i) \tag{4}$$

of coupled nonlinear integro-differential equations. Here $\omega_{mn} \otimes\otimes P_m$ is the *double convolution* of ω_{mn} and P_m $(m, n = e, i)$ defined by

$$\big(\omega_{mn} \otimes\otimes P_m(u_m - \theta_m)\big)(x, y, t) \equiv$$
$$\int\limits_{\mathbb{R}^N}\int\limits_{Y} \omega_{mn}(x - x', y - y', t)P_m(u_m(x', y', t) - \theta_m)dy'dx' \tag{5}$$

where $x \in \mathbb{R}^N, y \in \mathbb{R}^N$ and $t > 0$. Here $Y = [0, 1]^N$ is a period cell in $\mathbb{R}^N$.

In the papers [23, 24, 29, 25, 30, 31] the existence and stability of single- and two-bumps within the framework of a homogenized 1-population neural field model have been studied. Here one considers the periodic microstructure variation in both the synaptic footprint and the spatial scale of the connectivity strength. We notice, however, that most investigations in inhomogeneous media use 1-population models as modelling frameworks while it is rare in between studies of 2-population nonlocal neural field models with inhomogeneities. We are not aware of any studies of the microstructure effects on the pattern formation mechanism within such modelling frameworks either. In Kolodina *et al.* [32] the existence and stability of y-independent single bumps in the homogenized 2-population model (4) in one spatial dimension ($N = 1$) were investigated, with the firing rate functions modelled by means of the Heaviside function.

This serves as a background for the present paper. Our goal is to explore pattern formation within the framework of the homogenized 2-population model (4) in the 1-dimensional spatial setting. Thus, we study the effect of the periodic microstructure on the pattern forming process in this modelling framework. We proceed in a way analogous to Wyller *et al.* [15] for the pattern formation for the translational invariant model (1). The nonlinear

development of the instability is detailed by means of numerical simulations, based on MATLAB R2018a program, demonstrating spatially and spatiotemporally periodic patterns as final outcomes of the instability.

This investigation complements the papers [14], [15] and [32] as well as the works [24], [29], [30] and [23].

The paper is organized as follows: In Section 2 we specify the properties of the input functions of the model (4). Section 3 is devoted to the existence theory for constant solutions of the homogenized 2-population model. We also develop the framework for analyzing the linear stability of these constant solutions. Section 4 is devoted to a numerical study of the nonlinear stage of the instability, whereas Section 5 contains the conclusions and an outlook.

2. Model

Let us design the input data for the model (3) and (4):

The firing rate functions P_m, $m = e, i$ which are expressed in terms of a scaling function S and parameterised by means of the steepness parameter β_m satisfy the following properties:

$$\begin{gathered} P_m(u) = S(\beta_m u) \\ P_m(u) \to H(u) \quad \text{as} \quad \beta_m \to \infty \\ S : \mathbb{R} \to [0,1] \\ S' \in BC(\mathbb{R}), \quad S'(u) \geq 0 \end{gathered} \tag{6}$$

Here H is the Heaviside function.

The connectivity kernels ω_{mn} are expressed in terms of the scaling function Φ and the footprint functions σ_{mn}, $m, n = e, i$ as

$$\omega_{mn}(x,y;\alpha_{mn}) = \frac{1}{\sigma_{mn}(y;\alpha_{mn})}\Phi\bigg(\frac{x}{\sigma_{mn}(y;\alpha_{mn})}\bigg), \tag{7}$$

where

$$\sigma_{mn}(y;\alpha_{mn}) = s_{mn}(1+\alpha_{mn}\cos(2\pi y)), \quad s_{mn}>0, \quad 0\leq\alpha_{mn}<1 \tag{8}$$

The parameters α_{mn}, $m,n = e,i$ are referred to as the *heterogeneity parameters*. (7) and (8) mean that the connectivity kernels are assumed to be periodically modulated in both the spatial scales and the synaptic footprints. Notice that we recover the translational invariant case when $\alpha_{mn}=0$.

The scaling function Φ is assumed to satisfy the following conditions

$$\Phi(\xi)=\Phi(-\xi), \quad \Phi(\xi)\geq 0, \quad \int\limits_{\mathbb{R}}\Phi(\xi)d\xi = 1 \tag{9}$$

Moreover, we also impose the extra localization condition

$$\int\limits_{\mathbb{R}}\xi^2\Phi(\xi)d\xi<\infty \tag{10}$$

for the scaling function Φ. This condition will ensure that the growth and decay rate curves detected in Section 3 are two times continuously differentiable functions of the wave number.

Notice that the normalization condition imposed on the scaling function Φ implies that the connectivity functions are normalized i.e.

$$\int\limits_{\mathbb{R}}\int\limits_{Y}\omega_{mn}(x,y;\alpha_{mn})dydx = \int\limits_{\mathbb{R}}\Phi(\xi)d\xi = 1 \tag{11}$$

Introduce the Banach space $\mathcal{B} = BC(\mathbb{R}\times Y)$ of bounded continuous functions on $\mathbb{R}\times Y$ equipped with the norm

$$\|f\|_{\mathcal{B}} \equiv \sup_{(x,y)\in\mathbb{R}\times Y}|f(x,y)|.$$

Now, by proceeding in a way analogous to Potthast *et al.* [33] one can prove that the initial value problem of (4) with the connectivity kernels ω_{mn}

and the firing rate functions P_m designed as (6) and (8)-(9), respectively, is globally well-posed in $\mathcal{B}$ and bounded.

Let us investigate the consequences of this property in some detail. Introduce τ_m defined by

$$\tau_m \equiv \begin{cases} 1, & m = e \\ \tau, & m = i \end{cases}$$

and let $u_m^{(0)}, m = e, i$ denote the components of the solution of (4) with all the nonlocal terms omitted. We readily find that

$$u_m^{(0)}(x, y, t) = U_m(x, y) \exp[-t/\tau_m], \quad m = e, i$$

where $U_m \in \mathcal{B}, m = e, i$ are the components of the initial condition of (4). Now, by using (6)-(11) we find the uniform bounds

$$0 \leq [\omega_{mn} \otimes \otimes P_m(u_m - \theta_m)](x, y, t) \leq 1, \quad (x, y, t) \in \mathbb{R} \times Y \times \mathbb{R}_0^+$$

for $m, n = e, i$, from which it follows that each component of the solution of (4) satisfies the comparison property

$$\|u_m - u_m^{(0)}\|_\infty(t) \leq 1 - \exp[-t/\tau_m], \quad m = e, i \tag{12}$$

Hence we arrive at the following result: If $|U_m(x, y)| \leq 1$ for all $(x, y) \in \mathbb{R} \times Y$, then $|u_m(x, y, t)| \leq 1$ for all $(x, y, t) \in \mathbb{R} \times Y \times \mathbb{R}_0^+$. This means that the subset $A = \{u_m; |u_m| \leq 1\}$ of the phase space is a global attractor for the evolution prescribed by the model (4). By appealing to the property (12) we also conclude that the nonlinear stage of any instabilities leading to pattern formation will eventually be saturated within the present modelling framework. This property is indeed important to bear in mind in the forthcoming sections of the present paper. Notice that these results are exactly the same as the attractor- and boundedness results deduced in the translational invariant case [15]. Finally, but not least, these results also hold true in the multidimensional situation i.e. when $N > 1$.

3. Linear stability analysis

In this section we review the existence theory for constant solutions and develop the linear stability theory for the constant solutions . The stability technique is a generalization of the method presented in Wyller *et al.* [15].

Introduce $U = (u_e, u_i)^T$. We conveniently rewrite the homogenized system (4) on the compact form

$$\mathbf{T}^{-1}\frac{\partial U}{\partial t} = -U + \mathcal{F}U, \tag{13}$$

with

$$\mathbf{T} = \begin{pmatrix} 1 & 0 \\ 0 & 1/\tau \end{pmatrix} \text{ and } \mathcal{F}U = \begin{pmatrix} \mathcal{F}_{ee}u_e - \mathcal{F}_{ie}u_i \\ \\ \mathcal{F}_{ei}u_e - \mathcal{F}_{ii}u_i \end{pmatrix} \tag{14}$$

where $\mathcal{F}_{mn}$, $m, n \in \{e, i\}$ are the Hammerstein operators defined as

$$(\mathcal{F}_{mn}u_m)(x, y) = \int_{\mathbb{R}} \int_{Y} \omega_{mn}(x' - x, y' - y) P_m(u_m(x', y') - \theta_m) dy' dx'. \tag{15}$$

Let $V_0 = (v_0, v_0)^T$ denote a constant solution to (13)-(15). We readily find that v_0 satisfies the fixed point problem

$$\begin{gathered} F(v_0) = 0, \quad -1 < v_0 < 1 \\ F(v_0) \equiv v_0 + P_i(v_0 - \theta_i) - P_e(v_0 - \theta_e) \end{gathered} \tag{16}$$

.

In Wyller *et al.* [15] it is shown that the 2-population model possesses at least one constant solution. Moreover, the maximal number of constant solutions is five.

We impose a perturbation on the constant background V_0 i.e.

$$U(x, y, t) = V_0 + V(x, y, t), \quad V = (V_e, V_i)^T \tag{17}$$

where we assume that component functions $V_m, m = e, i$ belong to the subset of $\mathcal{B}$ for which the elements are absolute integrable functions with respect to x and piecewise smooth, continuous and 1-periodic in the second variable y. We linearize the evolution equation for V and get

$$\mathbf{T}^{-1}\partial_t V = -V + \mathcal{F}'_{V_0} V \tag{18}$$

Here $\mathcal{F}'_{V_0}$ is the Frechét derivative

$$\mathcal{F}'_{U_0} V = \begin{pmatrix} L_{ee}V_e - L_{ie}V_i \\ \\ L_{ei}V_e - L_{ii}V_i \end{pmatrix}. \tag{19}$$

where

$$(L_{mn}V_m)(x,y,t) = P'_m(v_0 - \theta_m)(\omega_{mn} \otimes \otimes V_m)(x,y,t)$$

$$\equiv P'_m(v_0 - \theta_m) \int\limits_{\mathbb{R}} dx' \int\limits_{Y} dy' \omega_{mn}(x'-x, y'-y) V_m(x', y', t) dx'$$

In order to analyze the system of linearized evolution equations (18) we proceed as follows: First, let us introduce the Fourier transformations with respect to the macroscale variable x and their respective inversion formulas

$$\tilde{V}_m(k,y,t) = \int\limits_{\mathbb{R}} V_m(x,y,t) \exp(-i2\pi xk) dx$$

$$V_m(x,y,t) = \int\limits_{\mathbb{R}} \tilde{V}_m(k,y,t) \exp(i2\pi xk) dk$$

$$\tilde{\omega}_{mn}(k,y) = \int\limits_{\mathbb{R}} \omega_{mn}(x,y) \exp(-i2\pi xk) dx$$

$$\omega_{mn}(x,y) = \int\limits_{\mathbb{R}} \tilde{\omega}_{mn}(k,y) \exp(i2\pi xk) dk$$

The assumptions imposed on both ω_{mn} and V_m guarantee that the Fourier-transforms $\tilde{\omega}_{mn}$ and $\tilde{V}_m$ exist for all y and t.. From (7) it follows that

$$\tilde{\omega}_{mn}(k,y) = \tilde{\Phi}(k\sigma_{mn}(y)), \quad \tilde{\Phi}(k) = \int\limits_{\mathbb{R}} \Phi(\xi) \exp(-i2\pi\xi k) d\xi \tag{20}$$

Since the connectivity kernels ω_{mn} for each $y \in Y$ are even and real functions of x, the Fourier transforms $\tilde{\omega}_{mn}$ are even and real functions of k.

By the convolution theorem we obtain the system of linear nonlocal evolution equations

$$\mathbf{T}^{-1}\partial_t \tilde{V} = -\tilde{V} + \tilde{\mathcal{F}'}_{V_0}\tilde{V} \tag{21}$$

from (18). Here

$$\tilde{V} = (\tilde{V}_e, \tilde{V}_i)^T$$

$$\tilde{\mathcal{F}'}_{U_0}\tilde{V} = \begin{pmatrix} \tilde{L}_{ee}\tilde{V}_e - \tilde{L}_{ie}\tilde{V}_i \\ \\ \tilde{L}_{ei}\tilde{V}_e - \tilde{L}_{ii}\tilde{V}_i \end{pmatrix}$$

with

$$(\tilde{L}_{mn}\tilde{V}_m)(k,y,t) = P'_m(v_0-\theta_m)\int\limits_Y \tilde{\omega}_{mn}(k,y'-y)\tilde{V}_m(k,y',t)dy'$$

The next step consists of inserting Fourier series in the local variable y i.e.

$$\tilde{V}_m(k,y,t) = \sum_{\mu=-\infty}^{\mu=\infty} \hat{V}_m^{(\mu)}(k,t)\exp(i2\pi\mu y)$$

$$\hat{V}_m^{(\mu)}(k,t) = \int\limits_Y \tilde{V}_m(k,y,t)\exp(-i2\pi\mu y)dy$$

$$\tilde{\omega}_m(k,y) = \sum_{\mu=-\infty}^{\mu=\infty} \hat{\omega}_{mn}^{(\mu)}(k)\exp(i2\pi\mu y)$$

$$\hat{\omega}_{mn}^{(\mu)}(k) = \int\limits_Y \tilde{\omega}_{mn}(k,y)\exp(-i2\pi\mu y)dy$$

into (21). We notice that these Fourier-decompositions also exist due to the assumptions imposed on ω_{mn} and V_m.

Notice that since $\tilde{\omega}_{mn}$ is a real, even in k and 1-periodic function of y, the Fourier-coefficients $\hat{\omega}_{mn}^{(\mu)}(k)$ are real. Moreover, since $\tilde{\omega}_{mn}(k,y) = \tilde{\omega}_{mn}(-k,y)$

for all y, we have $\hat{\omega}_{mn}^{(\mu)}(k) = \hat{\omega}_{mn}^{(\mu)}(-k)$. Hence $\hat{\omega}_{mn}^{(\mu)}$ is a well-defined, realvalued function of $\eta = k^2$. Finally, but not least, we have $\hat{\omega}_{mn}^{(\mu)}(k) = \hat{\omega}_{mn}^{(-\mu)}(k)$ from which it follows that we can let $\mu \in \mathbb{N}_0 = \{0, 1, 2, 3, ...\}$ without loss of generality.

We readily find a sequence of linear 2×2 ODE systems

$$\begin{gathered} \partial_t \hat{V}_\mu = \mathbf{A}_\mu \hat{V}_\mu, \quad \mu \in \mathbb{N}_0, \quad \eta = k^2 \\ \mathbf{A}_\mu \equiv \mathbf{T}(-\mathbf{I} + \mathbf{C}_\mu) \end{gathered} \tag{22}$$

for the Fourier coefficients $\hat{V}_\mu = (\hat{V}_e^{(\mu)}, \hat{V}_i^{(\mu)})^T$. Here $\{\mathbf{C}_\mu\}_{\mu \in \mathbb{N}_0}$ is the sequence of 2×2-matrices defined by

$$\mathbf{C}_\mu = \begin{pmatrix} P'_e \hat{\omega}_{ee}^{(\mu)} & -P'_i \hat{\omega}_{ie}^{(\mu)} \\ \\ P'_e \hat{\omega}_{ei}^{(\mu)} & -P'_i \hat{\omega}_{ii}^{(\mu)} \end{pmatrix}$$

where the parameters P'_m $(m = e, i)$ are defined as

$$P'_m \equiv \frac{dP_m}{du}(v_0 - \theta_m), \quad m = e, i \tag{23}$$

Simple computation reveals that

$$\mathbf{A}_\mu = \begin{pmatrix} -1 + P'_e \hat{\omega}_{ee}^{(\mu)} & -P'_i \hat{\omega}_{ie}^{(\mu)} \\ \\ \frac{1}{\tau} P'_e \hat{\omega}_{ei}^{(\mu)} & -\frac{1}{\tau}(1 + P'_i \hat{\omega}_{ii}^{(\mu)}) \end{pmatrix}$$

Notice that the structure of the sequence of stability matrices $\{\mathbf{A}_\mu\}_{\mu=0}^{\infty}$ resembles the stability matrix of the translational invariant case.

The linear stability problem thus boils down to a study of the linear ODE system (22) in a way analogous to Wyller *et al.* [15] for the translation invariant case. The eigenvalues $\lambda_\mu^{\pm}$ of the coefficient matrix $\mathbf{A}_\mu$ are expressed in terms of the determinant and trace of the matrix $\mathbf{A}_\mu$ i.e.

$$\lambda_\mu^{(\pm)}(\eta) = \frac{1}{2}\big(\varphi_\mu(\eta) \pm \sqrt{(\varphi_\mu(\eta))^2 - 4\psi_\mu(\eta)}\big) \tag{24}$$

where the sequences of functions $\{\varphi_\mu\}_{\mu=0}^{\infty}$ and $\{\psi_\mu\}_{\mu=0}^{\infty}$ are defined as

$$\varphi_\mu(\eta) \equiv \big(\,\mathrm{tr}(\mathbf{A}_\mu)\big)(\eta) = P'_e\hat{\omega}_{ee}^{(\mu)}(k) - 1 - \tfrac{1}{\tau}(1 + P'_i\hat{\omega}_{ii}^{(\mu)}(k))$$

$$\psi_\mu(\eta) \equiv \big(\,\det(\mathbf{A}_\mu)\big)(\eta) \tag{25}$$

$$= \tfrac{1}{\tau}\big((1 - P'_e\hat{\omega}_{ee}^{(\mu)}(k)\big)\big(1 + P'_i\hat{\omega}_{ii}^{(\mu)}(k)) + P'_eP'_i\hat{\omega}_{ie}^{(\mu)}(k)\hat{\omega}_{ei}^{(\mu)}(k)\big)$$

We introduce the sequence of parameterized curves $\Gamma_\mu : \mathbb{R}_0^+ \to \mathbb{R}^2, \mu \in \mathbb{N}_0$ defined as

$$\Gamma_\mu(\eta) = \big(\varphi_\mu(\eta), \psi_\mu(\eta)\big), \quad \eta = k^2 \geq 0 \tag{26}$$

in the invariant plane. Each point on this curve represents a Fourier component in the perturbation imposed on the constant background. Thus, the stability problem boils down to the study of the sequence of composite maps

$$\eta \overset{\Gamma_\mu}{\longmapsto} \big(\varphi_\mu(\eta), \psi_\mu(\eta)\big) \overset{\lambda_\mu^{(\pm)}}{\longmapsto} \lambda_\mu^{(\pm)}(\eta), \quad \mu \in \mathbb{N}_0 \tag{27}$$

Notice the difference between the present case and the one treated in Wyller *et al.* [15]: The effect of the microstructure on the linear stability properties is taken care of by a sequence of parameterized curves in the invariant plane and not a single curve as in the translational invariant case. Based on the sequence of composite maps (27), we thus arrive at the following conclusion: V_0 is stable if all the parameterized curves $\{\Gamma_\mu\}_{\mu\in\mathbb{N}_0}$ remain in the second quadrant of the invariant plane for all η, whereas we get instability if at least one curve Γ_μ visits at least one of the other quadrants for some η-interval.

Therefore, let us investigate the properties of the sequence of parameterized curves $\Gamma_\mu : \mathbb{R}_0^+ \to \mathbb{R}^2, \mu \in \mathbb{N}_0$:

1. (*The initial points of the curves* $\{\Gamma_\mu\}_{\mu\in\mathbb{N}_0}$.)

   We readily find that

$$\tilde{\omega}_m(0, y) = \int_{\mathbb{R}} \omega_{mn}(x, y)dx = \int_{\mathbb{R}} \frac{1}{\sigma_{mn}(y)}\Phi(\frac{x}{\sigma_{mn}(y)})dx = \int_{\mathbb{R}} \Phi(\xi)d\xi = 1$$

Hence the Fourier coefficients $\hat{\omega}_{mn}^{(\mu)}$ at $k = 0$ are given as

$$\hat{\omega}_{mn}^{(\mu)}(0) = \begin{cases} 1, & \mu = 0 \\ 0, & \mu > 0 \end{cases}$$

from which it follows that the sequence of matrices $\{\mathbf{C}_\mu\}_{\mu\in\mathbb{N}_0}$ evaluated at $k = 0$ is given by

$$\mathbf{C}_\mu = \begin{pmatrix} 0 & 0 \\ 0 & 0 \end{pmatrix}$$

for $\mu \neq 0$ and

$$\mathbf{C}_0 = \begin{pmatrix} P_e' & -P_i' \\ P_e' & -P_i' \end{pmatrix}$$

The corresponding sequence of matrices $\{\mathbf{A}_\mu\}_{\mu\in\mathbb{N}_0}$ evaluated at $k = 0$ is given as

$$\mathbf{A}_\mu = \begin{pmatrix} -1 & 0 \\ 0 & -\frac{1}{\tau} \end{pmatrix}$$

for $\mu \neq 0$ and

$$\mathbf{A}_0 = \begin{pmatrix} -1 + P_e' & -P_i' \\ \frac{1}{\tau}P_e' & -\frac{1}{\tau}(1 + P_i') \end{pmatrix}$$

for $\mu = 0$. Notice that the role of the matrix $\mathbf{A}_0$: The local dynamical counterpart of (13)-(14) is given by

$$\frac{\partial U}{\partial t} = -\mathbf{T}U + \mathbf{T}\mathcal{F}_0 U, \tag{28}$$

with

$$\mathbf{T} = \begin{pmatrix} 1 & 0 \\ 0 & 1/\tau \end{pmatrix} \text{ and } \mathcal{F}_0 U = \begin{pmatrix} P_e(u_e - \theta_e) - P_i(u_i - \theta_i) \\ \\ P_e(u_e - \theta_e) - P_i(u_i - \theta_i) \end{pmatrix} \tag{29}$$

$\mathbf{A}_0$ is the Jacobian of the vector field defining this $2D$ autonomous dynamical system evaluated at the equilibrium point $V_0 = (v_0, v_0)$.

We readily find that the initial points of $\{\Gamma_\mu\}_{\mu\in\mathbb{N}_0}$ have the following properties:

$$\Gamma_\mu(0) = \big(-1 - \tfrac{1}{\tau}, \tfrac{1}{\tau} \big) \quad \text{for} \quad \mu > 0$$

$$\Gamma_0(0) = \big(-1 + P_e' - \tfrac{1}{\tau}(1 + P_i'), \tfrac{1}{\tau}(1 + P_i' - P_e') \big)$$

Hence all the parameterized curves $\{\Gamma_\mu\}_{\mu>0}$ start in the second quadrant in the invariant plane. The initial point of the curve Γ_0 is in the second quadrant if

$$-1 + P_e' - \tfrac{1}{\tau}(1 + P_i') < 0$$

$$F'(v_0) = 1 + P_i' - P_e' > 0$$

Let assume that $1 + P_i' - P_e' > 0$. For $P_e' \leq 1$, the condition $-1 + P_e' - \frac{1}{\tau}(1 + P_i') < 0$ is fulfilled for all $\tau > 0$, whereas in the complementary regime $P_e' > 1$, we must have $1 < P_e'$ and $0 < \tau < \tau_H$ where

$$\tau_H \equiv \frac{P_i' + 1}{P_e' - 1} \tag{30}$$

The threshold value τ_H for the relative inhibition time τ with the constraint $1 < P_e' < 1 + P_i'$ yields

$$\varphi_0(\eta=0)=0, \quad \tfrac{d\varphi_0}{d\tau}(\eta=0,\tau=\tau_H)=\tfrac{1}{\tau_H^2}(1+P_i')>0$$

$$\psi_0(\eta=0,\tau=\tau_H)=\tfrac{1}{\tau_H}(1+P_i'-P_e')$$

In the corresponding local dynamics this point corresponds to a Hopf-bifurcation. Therefore τ_H is referred to as the Hopf-point in this local description. For $\tau < \tau_H$ with $P_e' > 1$, the equilibrium point V_0 is asymptotically stable. Assume that $F'(v_0) > 0$ and introduce

$$\tau_\pm \equiv \frac{(\sqrt{F'(v_0)} \pm \sqrt{P_i' P_e'})^2}{(P_e'-1)^2} \tag{31}$$

In accordance with [15] V_0 will in this case be a node if $0 \le \tau \le \tau_-$ or $\tau \ge \tau_+$ ($P_e' \neq 1$), while in the complementary regime it will be a focus within the same dynamical framework.

2. (*Translational invariant case.*)

Assume that the connectivity kernels ω_{mn} are independent of the local variable y. This is equivalent with the requirement that all the degrees of heterogeneity are equal to zero: $\alpha_{mn} = 0$. In that case

$$\mathbf{C}_\mu = \begin{pmatrix} 0 & 0 \\ & \\ 0 & 0 \end{pmatrix}$$

for $\mu \neq 0$ and

$$\mathbf{C}_0 = \begin{pmatrix} P_e'\tilde{\omega}_{ee} & -P_i'\tilde{\omega}_{ie} \\ & \\ P_e'\tilde{\omega}_{ei} & -P_i'\tilde{\omega}_{ii} \end{pmatrix}$$

In this case the matrices $\mathbf{A}_\mu$ for $\mu \neq 0$ are diagonal matrices with -1 and $-1/\tau$ on the diagonal whereas the matrix $\mathbf{A}_0$ is given as

$$\mathbf{A}_0 = \begin{pmatrix} -1+P_e'\tilde{\omega}_{ee} & -P_i'\tilde{\omega}_{ie} \\ & \\ \frac{1}{\tau}P_e'\tilde{\omega}_{ei} & -\frac{1}{\tau}(1+P_i'\tilde{\omega}_{ii}) \end{pmatrix}$$

We notice that $\mathbf{A}_0$ is the stability matrix in the translational invariant case [15].

3. (*Finite band width instability.*)

Let us explore the property of the sequence of parameterized curves $\{\Gamma_\mu\}_{\mu\in\mathbb{N}_0}$ in some detail. First of all, we find the uniform bound

$$|\hat{\omega}_{mn}^{(\mu)}(k)| \leq \int_0^1 |\tilde{\Phi}(k\sigma_{mn}(y))|dy \leq \int_0^1 \int_{\mathbb{R}} \Phi(\xi)d\xi dy = 1, \quad k \in \mathbb{R}$$

for the Fourier coefficients $\hat{\omega}_{mn}^{(\mu)}$, $\mu = 0, \pm 1, \cdots$. Secondly, since the scaling function Φ of the connectivity kernels ω_{mn} is absolute integrable, the Fourier transform $\tilde{\Phi}$ of Φ is a uniformly continuous function of k. Hence by (20), the composite mapping $\tilde{\Phi} \circ S_{mn}^{(k)} : Y \to \mathbb{R}$ defined by

$$y \overset{S_{mn}^{(k)}}{\longmapsto} k\sigma_{mn}(y) \overset{\tilde{\Phi}}{\longmapsto} \tilde{\Phi}\big(k\sigma_{mn}(y)\big) = \tilde{\omega}_{mn}(k, y)$$

is a continuous function on Y for all $k \in \mathbb{R}$. Here $S_{mn}^{(k)}(y) \equiv k\sigma_{mn}(y)$. Therefore, in accordance with Riemann-Lebesque's lemma, the Fourier coefficients $\hat{\omega}_{mn}^{(\mu)}$ will satisfy the property

$$\hat{\omega}_{mn}^{(\mu)}(k) \to 0 \quad \text{as} \quad \mu \to \infty \quad \text{for all } k \in \mathbb{R}$$

Moreover, we find also according to Riemann-Lebesque's lemma $\tilde{\Phi}(k) \to 0$ as $|k| \to \infty$. By (20), we find that $\tilde{\omega}_{mn}(k, y) \to 0$ as $|k| \to \infty$ uniformly in $y \in Y$. Hence we also have

$$\hat{\omega}_{mn}^{(\mu)}(k) \to 0 \quad \text{as} \quad |k| \to \infty \quad \text{for all } \mu \in \mathbb{N}_0$$

Interestingly, this result implies that all the curves $\{\Gamma_\mu\}_{\mu>0}$ are closed curves: They start and terminate at the same point $\big(-1 - \frac{1}{\tau}, \frac{1}{\tau}\big)$ in the second quadrant in the invariant plane. This result also enables us to detail the instability structure. First of all, we find that when μ exceeds a certain threshold μ_0, the corresponding curves $\{\Gamma_\mu\}_{\mu\geq\mu_0}$ remain in the second quadrant for all $\eta \geq 0$. Secondly, the remaining

curves $\{\Gamma_\mu\}_{0\leq\mu<\mu_0}$ will terminate in the second quadrant in the invariant plane. The latter result simply means that the instability structure is of a finite band width type. Notice that the translational invariant case corresponds to $\mu_0 = 1$ within the present stability methodology.

The assumption (10) implies that the derivative $\tilde{\Phi}' = \frac{d\tilde{\Phi}}{dk}$ and the second derivative $\tilde{\Phi}'' = \frac{d^2\tilde{\Phi}}{dk^2}$ are uniformly continuous functions of k with the property

$$\tilde{\Phi}'(k), \tilde{\Phi}''(k) \to 0 \quad \text{as} \quad |k| \to \infty \tag{32}$$

Hence, since

$$\begin{aligned} \partial_k\omega_{mn}(k,y) &= \sigma_{mn}(y)\tilde{\Phi}'\big(k\sigma_{mn}(y)\big) \\ \partial_k^2\omega_{mn}(k,y) &= \sigma_{mn}^2(y)\tilde{\Phi}''\big(k\sigma_{mn}(y)\big) \end{aligned} \tag{33}$$

we conclude that the partial derivatives $\partial_k\omega_{mn}$ and $\partial_k^2\omega_{mn}$ are uniformly continuous functions of k for all $y \in Y$. From (32) and (33) it then follows that

$$\partial_k\omega_{mn}, \partial_k^2\omega_{mn} \to 0 \quad \text{as} \quad |k| \to \infty \tag{34}$$

uniformly for $y \in Y$. Finally, but not least, we have from (33) that the 1-parameters families of mappings $\varphi_k : Y \to \mathbb{R}$ and $\vartheta_k : Y \to \mathbb{R}$ defined by

$$\varphi_k(y) = \partial_k\omega_{mn}(k,y), \quad \vartheta_k(y) = \partial_k^2\omega_{mn}(k,y)$$

are continuous functions on Y for all $k \in \mathbb{R}$. From this we find that the derivatives $\frac{d}{dk}\hat{\omega}_{mn}^{(\mu)}$ and $\frac{d^2}{dk^2}\hat{\omega}_{mn}^{(\mu)}$ of the Fourier-coefficients $\hat{\omega}_{mn}^{(\mu)}$ are continuous functions of $k \in \mathbb{R}$ and that

$$\begin{aligned} \tfrac{d}{dk}\hat{\omega}_{mn}^{(\mu)}(k) &= \int_Y \partial_k\omega_{mn}(k,y)\exp(-i2\pi\mu y)dy \\ \tfrac{d^2}{dk^2}\hat{\omega}_{mn}^{(\mu)}(k) &= \int_Y \partial_k^2\omega_{mn}(k,y)\exp(-i2\pi\mu y)dy \end{aligned}$$

By making use of these expressions and the uniform limit (34), we find that

$$\frac{d}{dk}\hat{\omega}_{mn}^{(\mu)}(k), \frac{d^2}{dk^2}\hat{\omega}_{mn}^{(\mu)}(k) \to 0 \quad \text{as} \quad |k| \to \infty \quad \text{for all } \mu \in \mathbb{N}_0$$

We conclude that $\{\Gamma_\mu\}_{\mu\in\mathbb{N}_0}$ forms a sequence of smooth curves in the invariant plane. In the unstable situation, these curves exhibit a finite number of transversal crossings with the positive determinant axis and the negative trace axis in this plane. Thus the generic picture of the instability structure consists of a finite set of well-separated gain bands, just as in the translational invariant case investigated in Wyller *et al.* [15].

4. (*Weakly modulated case.*)

Let us consider the situation where the degrees of heterogeneity α_{mn} satisfy $0 < \alpha_{mn} \ll 1$. This case is referred to as *the weakly modulated case*. The stability properties depend continuously on the degrees of heterogeneity. From the previous analysis of the translational invariant case and the behavior of the matrices $\mathbf{A}_\mu, \mu \in \mathbb{N}_0$ for large $|k|$, it follows that the linear stability of the equilibrium V_0 depends solely on the matrix $\mathbf{A}_0$. Hence, the gain band structure in the weakly modulated case emerges as a homotopic deformation of the instability structure detected in the translational invariant case. This result means that we have to search beyond the weakly modulated regime to find significant qualitative changes in the gain band structure as compared with the translational invariant case. We will demonstrate this in Section 4.

Notice that this result can be shown rigorously to hold true by appealing to the following continuous dependence on parameter result, which holds true under a more restrictive condition on the scaling function Φ than imposed in Section 2:

Theorem 1. *Let the connectivity kernel ω_{mn} be given by (7) with $\sigma_{mn} \in BC^1(Y), \sigma_{mn}(y) > 0$ for all y and assume that $\Phi \in BC^1(\mathbb{R})$ in addition to (9). Then there is an $\varepsilon > 0$ such that for any $\alpha \in [0, \varepsilon]^4$ the solutions U_α have the same stability properties as the solution in the translation invariant case ($\alpha = 0$).*

The proof of Theorem 1 proceeds in the way as the proof of Theorem 3 in Kolodina *et al.* [32]. We omit the details here.

5. (*Generation and coalescence of gain bands.*)

We detect the generation and coalescence of gain bands by viewing such phenomena as bifurcation processes with one of the degrees of heterogeneity α_{mn} as control parameter. Just as in Wyller *et al.* [15] we get two types of bifurcations, a continuous version of the static codimension-one bifurcation and a continuous version of the Hopf type of bifurcation. The former one is referred to as the *Turing bifurcation*, whereas the latter one is called the *Turing-Hopf bifurcation*. We determine these two bifurcations in the following way: Fix $\mu \in \mathbb{N}_0$ and assemble three of the heterogeneity parameters into a single parameter vector which we denote by $a \in [0,1)^3$. The remaining degree of heterogeneity is denoted by α_{mn}. We fixate a. By assumption both φ_μ and ψ_μ are smooth functions of α_{mn}. Moreover, due to (10) the same functions are two times continuously differentiable with respect to η. We will make use of these properties when describing the Turing- and the Turing-Hopf bifurcation.

(a) (*Turing type bifurcation*) In this case the bifurcation point is determined by means of the non-transversality condition

$$\begin{gathered}\psi_\mu(\eta_c, \alpha_{mn,c}) = 0, \quad \tfrac{d\psi_\mu}{d\eta}(\eta_c, \alpha_{mn,c}) = 0 \\ \varphi_\mu(\eta_c, \alpha_{mn,c}) < 0\end{gathered} \tag{35}$$

Here $(\eta_c, \alpha_{mn,c})$ (where $\eta_c = k_c^2$) is the bifurcation point. This means that the corresponding eigenvalue $\lambda_\mu^{(+)}$ changes sign as we pass the bifurcation point. Here we have tacitly imposed the finite velocity condition

$$\frac{\partial \psi_\mu}{\partial \alpha_{mn}}(\eta_c, \alpha_{mn,c}) \neq 0$$

in order to ensure that the bifurcation point $(\eta_c, \alpha_{mn,c})$ is not an accumulation point. Since

$$\frac{d^2\lambda_\mu^{(+)}}{d\eta^2}(\eta_c, \alpha_{mn,c}) = \frac{d^2\psi_\mu}{d\eta^2}(\eta_c, \alpha_{mn,c})/\varphi_\mu(\eta_c, \alpha_{mn,c})$$

we get generation of gain bands if

$$\frac{d^2\psi_\mu}{d\eta^2}(\eta_c, \alpha_{mn,c}) > 0$$

and coalescence of gain bands if

$$\frac{d^2\psi_\mu}{d\eta^2}(\eta_c, \alpha_{mn,c}) < 0$$

(b) (*Turing-Hopf type bifurcation*) In this case the bifurcation is described by means of the non-transversality condition

$$\begin{gathered}\varphi_\mu(\eta_c, \alpha_{mn,c}) = 0, \quad \tfrac{d\varphi_\mu}{d\eta}(\eta_c, \alpha_{mn,c}) = 0 \\ \psi_\mu(\eta_c, \alpha_{mn,c}) > 0\end{gathered} \tag{36}$$

Here $(\eta_c, \alpha_{mn,c})$ (where $\eta_c = k_c^2$) is the bifurcation point. This means that the real part of the corresponding eigenvalues $\lambda_\mu^{(\pm)}$

changes sign at the bifurcation point. Also here we have assumed the finite velocity condition

$$\frac{\partial \varphi_\mu}{\partial \alpha_{mn}}(\eta_c, \alpha_{mn,c}) \neq 0$$

in order to avoid the bifurcation point to become an accumulation point. Since

$$Re\{\lambda_\mu^{(\pm)}\}(\eta) = \frac{1}{2}\varphi_\mu(\eta)$$

we get generation of gain bands if

$$\frac{d^2\varphi_\mu}{d\eta^2}(\eta_c, \alpha_{mn,c}) < 0$$

and coalescence of gain bands if

$$\frac{d^2\varphi_\mu}{d\eta^2}(\eta_c, \alpha_{mn,c}) > 0$$

Notice that this analysis implies that even though we have no bifurcation point for $\mu = 0$ of the type (a) and (b), it might happen that some $\mu = \mu_*$ for which $0 < \mu_* \leq \mu_0$ we will have such a point. This is caused by the presence of the periodic microstructure in the modelling framework.

4. Numerical simulations

The present section is devoted to a numerical study of the linear stage of the instability discussed in the previous section and the nonlinear stage of this instability.

We assume that the scaling function S of the firing rate functions P_m ($m = e, i$) is given as

$$S(u) = \frac{1}{2}(1 + \tanh(u)) \tag{37}$$

Then by (6) and (37) we obtain

$$P_m' = \frac{1}{2}\beta_m \cosh^{-2}(\beta_m(v_0 - \theta_m)), \quad m = e, i \tag{38}$$

Parameters	β_e	β_i	θ_e	θ_i	v_0	P'_e	P'_i	τ_H	τ_-	τ_+
Set A	20	30	0.10	0.12	0.129	7.26	13.94	2.39	1.36	4.20
Set B	5	10	0.05	0.10	0.106	2.31	4.98	4.56	1.27	16.35

Table 1: The single equilibrium points $V_0 = (v_0, v_0)$ are determined by (16) for the listed parameters β_m and θ_m $(m = e, i)$, P'_e and P'_i are defined by (38) and τ_H and $\tau_\pm$ are defined by (30) and (31), respectively.

Set A represents a scenario with steep firing-rate functions, whereas Set B gives an example of shallow firing-rate functions. This choice of input parameters yields a single equilibrium point $V_0 = (v_0, v_0)$. The values of v_0 are also listed in Table 1. Next, we compute the corresponding steepness parameters $P'_m, m = e, i$ by means of the formula (38) and thereafter the Hopf-time τ_H and the relative inhibition times $\tau_\pm$ by means of the expressions (30) and (31), respectively. The input parameters P'_m, P'_m, τ_H and $\tau_\pm$ are also listed in Table 1.

Let the scaling function Φ of the connectivity kernels ω_{mn} be given as an exponentially decaying function, i.e.

$$\Phi(\xi) = \frac{1}{2}\exp(-|\xi|) \tag{39}$$

with

$$\tilde{\Phi}(k) = \frac{1}{(2\pi k)^2 + 1}$$

as the corresponding Fourier- transform. Thus, we readily get

$$\tilde{\omega}_{mn}(k, y) = \tilde{\Phi}(\sigma_{mn}(y)k) = \tfrac{1}{(2\pi k\sigma_{mn}(y))^2+1}, \tag{40}$$

where $\sigma_{mn}(y)$ is defined by (8). The corresponding Fourier coefficients $\hat{\omega}^{(\mu)}_{mn}$ are given by means of the integrals

$$\hat{\omega}^{(\mu)}_{mn}(k) = \int_Y \frac{1}{(2\pi k\sigma_{mn}(y))^2 + 1}\exp(-i2\pi\mu y)dy \tag{41}$$

In all numerical simulations the averaged synaptic footprints s_{mn} are fixated as

$$s_{ee} = 0.35, \quad s_{ei} = 0.48, \quad s_{ie} = 0.60 \quad \text{and} \quad s_{ii} = 0.69. \tag{42}$$

We aim at examining the effect of the heterogeneity on the gain band structure in four different cases. These cases are listed in Table 2.

Parameters	α_{ee}	α_{ie}	α_{ei}	α_{ii}
Set 1	0.01	0.025	0.01	0.025
Set 2	0.35	0.4	0.4	0.35
Set 3	0.6	0.55	0.5	0.65
Set 4	0.9	0.85	0.85	0.9

Table 2: Sets of heterogeneity parameters α_{mn}. Set 1 represents the weakly modulated case $0 < \alpha_{mn} \ll 1$, Set 2 and Set 3 represent scenarios of the medium degree of heterogeneity whereas Set 4 is an example on the strong heterogeneity.

Fig. 1 shows the curves Γ_0 in the invariant plane together with the corresponding growth rate curves for the parameter sets in Table 1 and Table 2. For the weakly modulated case ($0 < \alpha_{mn} \ll 1$), represented by Set 1 in Table 2, we observe as expected that the curve Γ_0 and the corresponding growth rate curve, appear as slight deformation of the corresponding curves produced in the translational invariant case. By adjusting the degree of heterogeneity beyond the weakly modulated case, the following features are notable in the case of steep firing-rate functions: Except for Set 2 in Table 2, the maximal growth rate of the instability decreases with the degree of heterogeneity. This property is accompanied by a broadening of the single gain band. In the shallow firing-rate regime, we readily observe that the gain band structure is suppressed by the degree of heterogeneity.

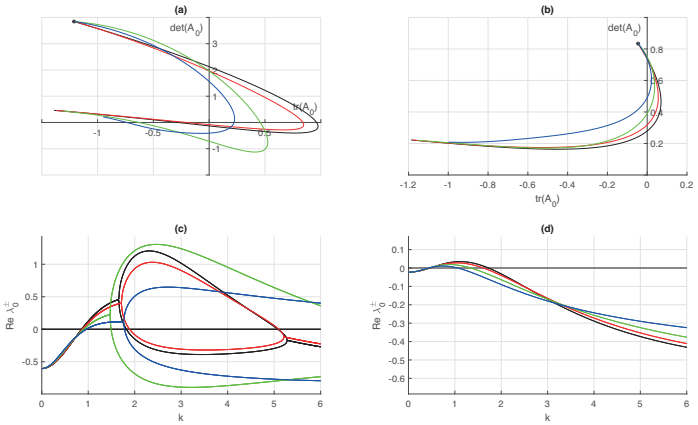

Figure 1: Examples of single gain-band structure as a function of the heterogeneity for the Fourier component corresponding to $\mu = 0$. The connectivity functions are given by (7) with (39), the averaged synaptic footprints are fixed as (42). In (a) the parameterized curves Γ_0 in the invariant plane defined by means of (25) and (26) are shown for $\tau = 2$ and parameter set A (cf. Table 1). In (c) the corresponding growth rates ($Re\{\lambda_0^{(\pm)}\}$ in (24)) are shown as a function of the wave number k. In (b) the curves Γ_0 is shown for $\tau = 4.4$ and parameter Set B (cf. Table 1). The corresponding growth rates are shown in (d). The black stars in (a) and (b) denote the initial point of the curves Γ_0, $\eta = k^2 = 0$. The heterogeneity parameters producing the black-, red-, green- and blue curves are Set 1, Set 2, Set 3 and Set 4 in Table 2, respectively.

In Fig. 2 the curves Γ_1 in the invariant plane are displayed together with the corresponding growth- and decay rate curves for the parameter sets in Table 1 and Table 2. We first notice that the curves Γ_1 are closed, in agreement with the general theory elaborated in Section 3. For the weakly modulated case, represented by Set 1 in Table 2, we show a zoomed version of the parameterized curve in a separate figure (Fig. 5). This figure clearly demonstrates the closed orbit structure of the curve Γ_1 in the vicinity of the point $(-1 - 1/\tau, 1/\tau)$ in the invariant plane, consistent with the analysis presented in Section 3: The closed curve Γ_1 deforms continuously to the single point $(-1 - 1/\tau, 1/\tau)$ as the degrees of heterogeneity tend to zero. Next, for the shallow firing-rate regime, the curves are for all the sets of heterogeneity located in total in the second quadrant of the invariant plane,

thus showing that the corresponding Fourier component does not contribute to the instability and the subsequent nonlinear stage of the evolution in this case. Interestingly, the curves Γ_1 visit the third quadrant in the invariant plane before returning to the second quadrant in the case of medium-to-strong degree of heterogeneity (represented by the Sets 3 and Set 4 in Table 2 for the steep firing-rate function regime represented by Set A in Table 1. In this case the heterogeneity contributes to the linear instability. It is indeed of interest to explore the impact of this instability on the pattern formation process. Here one should notice that it must compete with the $\mu = 0$-mode, and as we will see it will only have an impact on the initial phase of the pattern forming process, and not the final stage of the pattern forming process.

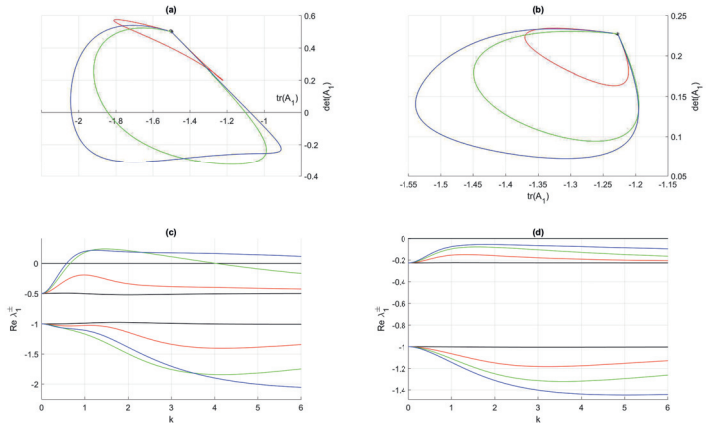

Figure 2: Examples of single gain-band structure as a function of the heterogeneity for the Fourier component corresponding to $\mu = 1$. The connectivity functions are given by (7) with (39), the averaged synaptic footprints are fixed as (42). In (a) the parameterized curves Γ_1 in the invariant plane defined by means of (25) and (26) are shown for $\tau = 2$ and Set A (cf. Table 1). In (c) the corresponding growth rates ($Re\{\lambda_1^{(\pm)}\}$ in (24)) are shown as a function of the wave number k. In (b) the curves Γ_1 is shown for $\tau = 4.4$ and Set B (cf. Table 1). The corresponding growth rates are shown in (d). The black stars in (a) and (b) denote the initial point of the curves Γ_1, $\eta = k^2 = 0$. The heterogeneity parameters producing the red-, green- and blue curves are Set 2, Set 3 and Set 4 in Table 2, respectively. Zoomed black curves corresponding to Set 1 presented in the separate figure, see (a) and (b) of fig. 5.

Fig. 2 clearly indicates that a gain band is generated in the steep firing-rate function regime when the degree of heterogeneity exceeds a certain threshold. We can analyze the generation mechanism as a Turing type of bifurcation phenomenon i.e. by means of the non-transversality condition (35). In Fig. 3 we have demonstrated this phenomenon by plotting the closed parameterized curve Γ_1 for three different sets of heterogeneity parameters. We have fixed all the heterogeneity parameters except α_{ii}.

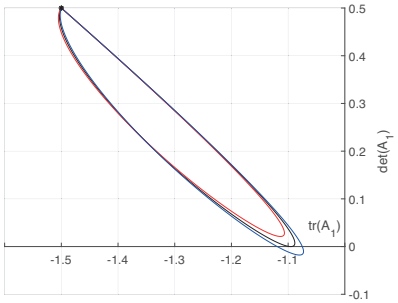

Figure 3: Example on a Turing type of bifurcation as a function of the heterogeneity for the Fourier component corresponding to $\mu = 1$. The connectivity functions are given by (7) with (39), the averaged synaptic footprints are fixed as (42). The parameterized curves Γ_1 defined by means of (25) and (26) are shown for $\tau = 2$ for Set A (cf. Table 1). Black star denote the initial point of Γ_1. Input parameters for red curve are $(\alpha_{ee}, \alpha_{ie}, \alpha_{ei}, \alpha_{ii}) = (0.1, 0.1, 0.1, 0.29)$, black curve (bifurcation) $(\alpha_{ee}, \alpha_{ie}, \alpha_{ei}, \alpha_{ii}) = (0.1, 0.1, 0.1, 0.3009)$ and blue curve $(\alpha_{ee}, \alpha_{ie}, \alpha_{ei}, \alpha_{ii}) = (0.1, 0.1, 0.1, 0.31)$.

We have also investigated the parameterised curves Γ_2 given by (25)-(26), see Fig. 4. The outcome of this investigation is summarized in Fig. 4. We find that all these curves are located in the second quadrant of the invariant plane, thus supporting numerically the conclusion of the stability analysis of Section 3 that only the lowest order Fourier components have an impact on the gain band structure. We have depicted separately the parameterized curves Γ_2 for the weakly modulated case, represented by Set 1 in Table 2 in Fig. 5. This figure clearly demonstrates the closed orbit structure of the

curve Γ_2 in the vicinity of the point $(-1-1/\tau, 1/\tau)$ in the invariant plane, consistent with the findings of the previous section: Just as the curve Γ_1, the closed curve Γ_2 deforms continuously to the single point $(-1-1/\tau, 1/\tau)$ as the degrees of heterogeneity tend to zero.

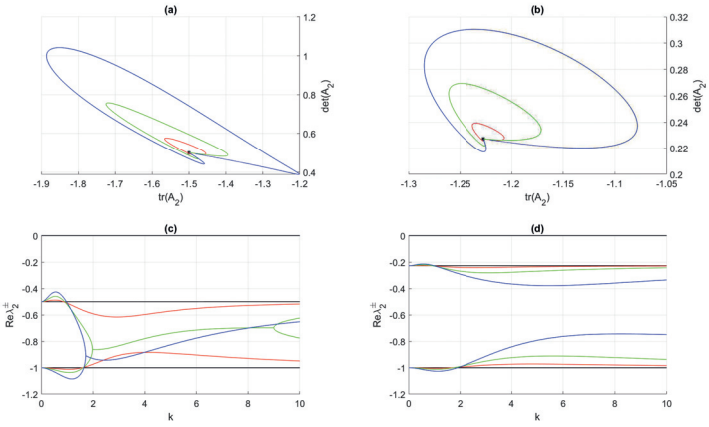

Figure 4: The parameterized curves Γ_2 defined by means of (25) and (26). The connectivity functions are given by (7) with (39), the averaged synaptic footprints are fixed as (42). In (a) $\tau = 2$ for the firing-rate function corresponding to Set A (cf. Table 1). In (b) the curve Γ_2 is shown for $\tau = 4.4$ and Set B (cf. Table 1). The black stars in (a) and (b) denote the initial point of the curves Γ_2, $\eta = k^2 = 0$. The heterogeneity parameters producing the black-, red-, green- and blue curves are Set 1, Set 2, Set 3 and Set 4 in Table 2, respectively. The decay rates corresponding to (a) and (b) are plotted in (c) and (d), respectively. Zoomed black curves corresponding to Set 1 are presented in (c) and (d) of Fig. 5.

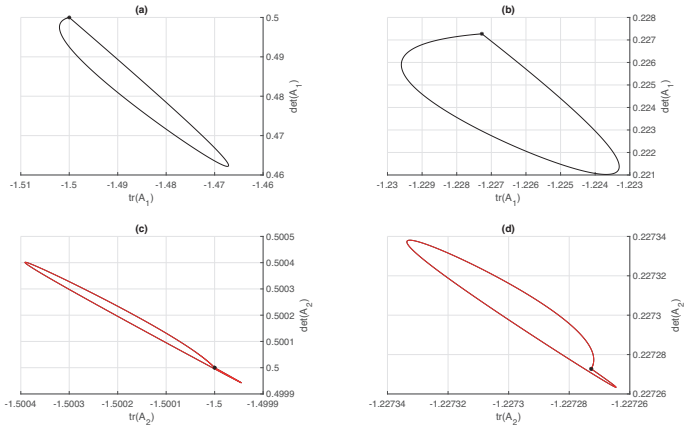

Figure 5: Zoomed versions of the curves Γ_1 and Γ_2 in Fig.2 and Fig.4 representing the weakly modulated case, i.e. Set 1 in Table 2, show the closed orbit structure. The connectivity functions are given by (7) with (39), the averaged synaptic footprints are fixed as (42). In (a) and (c) the parameterized curves Γ_1 and Γ_2 in the invariant plane defined by means of (25) and (26) is shown for $\tau = 2$ and Set A (cf. Table 1). In (b) and (d) the curves Γ_1 and Γ_2 are shown for $\tau = 4.4$ and Set B (cf. Table 1). The black stars in (a) and (b) denote the initial point of the curves Γ_1, $\eta = k^2 = 0$.

Finally, we carry out numerical simulations in order to illustrate the effect of the periodic microstructure on the pattern forming process. We do this by exploring the nonlinear stage of the instability as a function of the degree of heterogeneity α_{mn}. The present simulations are based on build-in function *ode*45 in MATLAB, where the initial condition consists of a homogeneous solution v_0 with small perturbation on the form of a narrow centered rectangular box superimposed on $-0.5 \leq x \leq 0.5$, $u_e = u_i = 0.2$. Besides, we use the build-in function *conv*2 in MATLAB to calculate the double convolutions (5) in (4). Here the function *conv*2 defines the discrete double convolution of functions ω_{mn} and $P_m(u_m - \theta_m)$, that uses a finite spatial domain, $-L < x < L$. To avoid an accumulation of errors at the end points of the interval $(-L, L)$, we assume that the initial condition for (13) is periodic in x variable with a period $T = 2L$.

We present the outcome of these simulations as snap shots of the projec-

tion of the numerical solutions onto the x, y-plane for 4 different sets of the heterogeneity parameters α_{mn} given in Table 2. Here we divide investigations into two subsections corresponding to steep firing rate regime, i.e. Set A in Table 1 (Subsection 4.2), and shallow firing rate regime, i.e. Set B in Table 1 (Subsection 4.3).

4.1. Translation invariant case

For the sake of convenience we first recall the pattern formation results of the translation invariant case explored in Wyller *et al.* [15]. We visualize the numerical solution by projecting it onto the (x, t)-plane. The results of this investigation is depicted in Fig. 6. For Set A, representing the steep firing rate function case, we see that gain band instability develops into a purely, spatial periodic pattern after a relatively short transient phase, whereas for Set B, which represents the shallow firing rate function case, the instability develops into spatiotemporal oscillations after a relatively slow transient phase.

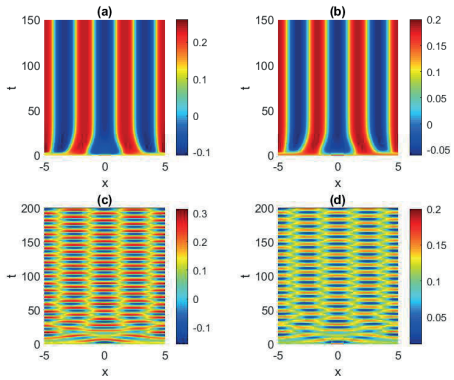

Figure 6: The pattern formation results for the translational invariant case ($\alpha_{mn} = 0, \quad m, n = e, i$) obtained in Wyller *et al.* [15]. The connectivity functions ω_{mn} are given by (7) with (39) and fixed synaptic footprints as (42). The firing rate functions are given by (6) with (37). (a) and (b) correspond to Set A in Table 1. (c) and (d) correspond to Set B in Table 1.

4.2. Steep firing rate regime (Set A)

In the weakly modulated case represented by Set 1 in Table 2 we observe as expected that the solution emerging from the instability consists of x-dependent spatial oscillations, see Fig.7. This can indeed be viewed as a continuous deformation of the translational invariant case.

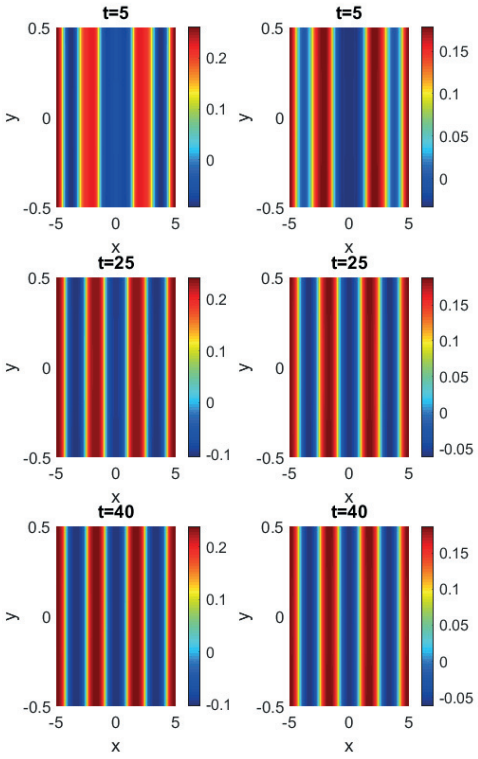

Figure 7: Dynamical evolution for parameter Set A in Table 1 and Set 1 in Table 2 (weakly modulated case) at different fixed times. Excitatory activity levels u_e and inhibitory activity levels u_i corresponds to left plots and right plots, respectively. The initial condition consists of a homogeneous solution v_0 with small perturbation in the form of a narrow centred rectangular box superimposed $-0.5 \leq x \leq 0.5$, $u_e = u_i = 0.2$

We observe the following features in Fig. 7: The first row in this figure shows the snapshot of the numerical solution in the initial, transient phase. The snapshot in the second row is repeated in the third row, thus indicating that the pattern has stabilized on spatial oscillations i.e. on periodically distributed bumps. The wavelength in x-direction is approximately equal to the wavelength of the linearly most unstable mode. Each bump in this oscillatory structure resembles the y-independent stable single bump of the Heaviside limit of the firing rate functions obtained by means of the pinning function technique developed in Kolodina *et al.* [32]. This is confirmed by means of the plots in Fig. 8: In (a) and (b) we show the excitatory and the inhibitory component of the single stationary bump in the Heaviside limit of the firing rate functions, whereas in (c) and (d) we illustrate the corresponding components of the spatially oscillating pattern restricted to one period for the heterogeneity parameter Set 1 in Table 2. This result suggests that stable bumps can be the final outcome of a pattern forming process in the steep firing rate regime.

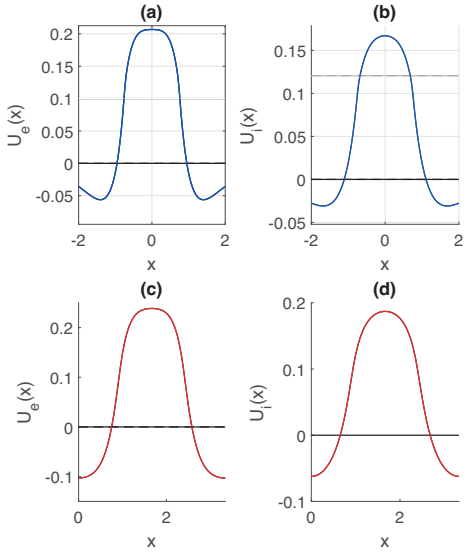

Figure 8: Comparison between stationary broad bump with the Heaviside firing rate function, where (a) and (b) correspond to the excitatory and the inhibitory components, respectively, with the stationary oscillations (c) and (d) restricted to one period for Set 1 in Table 2. Input data: $\theta_e = 0.10$, $\theta_i = 0.12$.

When increasing the degrees of heterogeneity, the patterns exhibit as expected a dependence of the local coordinate y. A rich plethora of phenomena then takes place. This is depicted in Fig. 9, Fig. 10 and Fig. 11. Here the impact of the heterogeneity is measured by means of the y-dependence in the emerging patterns. A common and prominent feature in these patterns consists of stable spatial oscillatory behavior both in the x- and y-direction, the y-dependence being as expected most pronounced in the strongly heterogeneous case depicted in Fig. 11. Again the wavelength in x-direction is approximately equal to the wavelength of the linearly most unstable mode whereas the 1-periodicity in the y-direction is retained. The numerical results also indicate that the transient phase of the dynamical evolution increases with the degree of heterogeneity, except for the notable case of the strong heterogeneity, e.g. Set 4 in Table 2. This is indeed consistent with the fact

that the maximal growth rate of the linear instability decreases with the degree of heterogeneity. See Fig. 1. The linearly most unstable $\mu = 0$-mode will grow on the expense of all the remaining modes in the unstable band in the nonlinear stage of the dynamical evolution. Due to the fact that the maximal growth rate of the unstable $\mu = 1$-modes is much less than the maximal growth rate of the unstable $\mu = 0$-modes, the linearly most unstable $\mu = 0$-mode will extract energy from all the unstable $\mu = 1$-modes as well. Fig. 1 and Fig. 2 show that there is a magnitude of order difference between the maximal growth of the $\mu = 0$-gain band and the growth rates represented in the $\mu = 1$-gain band. Thus we expect the unstable $\mu = 1$-modes to be hardly visible, even in the transient linear phase of the evolution.

Interestingly, we also detect two characteristic times, t_1 and t_2 (with $t_2 > t_1$) in the pattern forming process as demonstrated in Fig. 9 and Fig. 10: The stable patterns which emerge at the time t_1 consists of a two band structure. The latter structure remains unchanged for the intermediate time interval (t_1, t_2). At the time t_2 each of these two bands divides into two new bands. The final stage of the pattern forming process thus consists of four stable bands.

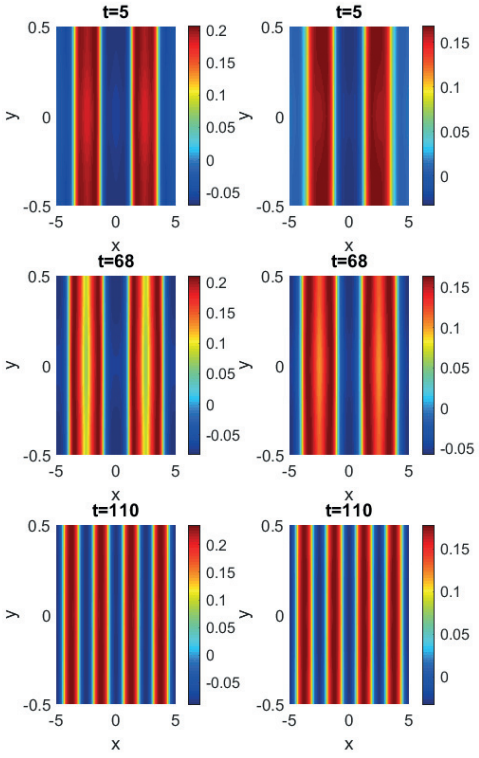

Figure 9: Dynamical evolution for parameter Set A in Table 1 and Set 2 in Table 2 at different fixed times. Excitatory activity levels u_e and inhibitory activity levels u_i corresponds to left plots and right plots, respectively. The initial condition consists of a homogeneous solution v_0 with small perturbation in the form of a narrow centred rectangular box superimposed $-0.5 \leq x \leq 0.5$, $u_e = u_i = 0.2$.

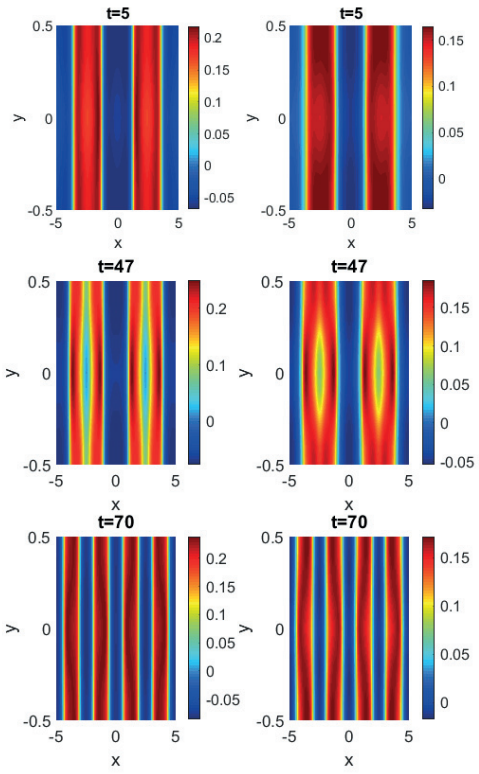

Figure 10: Dynamical evolution for parameter Set A in Table 1 and Set 3 in Table 2 at different fixed times. Excitatory activity levels u_e and inhibitory activity levels u_i corresponds to left plots and right plots, respectively. The initial condition consists of a homogeneous solution v_0 with small perturbation in the form of a narrow centred rectangular box superimposed $-0.5 \leq x \leq 0.5$, $u_e = u_i = 0.2$.

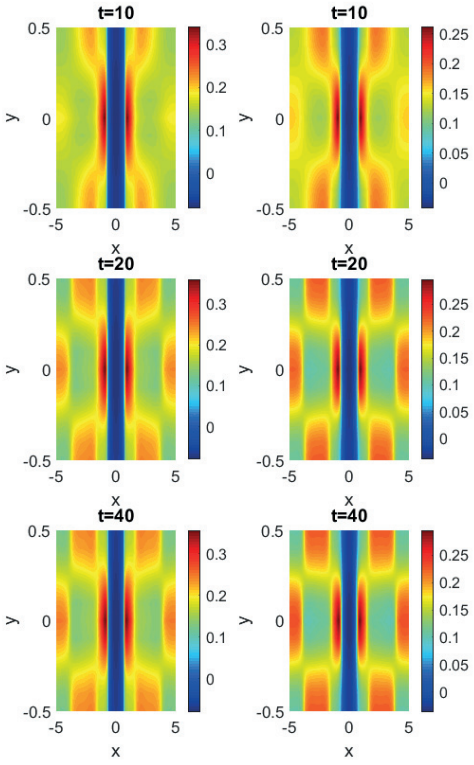

Figure 11: Dynamical evolution for parameter Set A in Table 1 and Set 4 in Table 2 at different fixed times. Excitatory activity levels u_e and inhibitory activity levels u_i corresponds to left plots and right plots, respectively. The initial condition consists of a homogeneous solution v_0 with small perturbation in the form of a narrow centred rectangular box superimposed $-0.5 \leq x \leq 0.5$, $u_e = u_i = 0.2$.

4.3. Shallow firing rate regime (Set B)

For the shallow firing rate functions case (Set B in Table 1) the outcome of the dynamical evolution is shown in Fig. 12-15 in terms of snapshots of the numerical solutions projected onto (x, y)-plane. We observe that the

instability develops into a spatiotemporal oscillations. This is consistent with the transient phase described by two complex conjugate eigenvalues of the matrix $\mathbf{A}_0$, where the imaginary part determines the frequency of the oscillations. The wave length of the emerging spatiotemporal oscillations is approximately given by the wave length corresponding to the maximal growth rate, whereas the frequency is given by the imaginary part of the eigenvalues producing the maximal growth rate. This is also consistent with findings in the translational invariant case. Thus, the numerical runs suggest that the nonlinear stage of the instability in the weakly modulated regime appears as continuous deformation of the nonlinear stage in the translational invariant case. A notable feature is, however, that the stabilization on spatiotemporal oscillations is slow compared with the emergence of stable spatial oscillations for the steep firing rate case i.e. for Set A. This is indeed a consequence of the magnitude of order difference between the maximal growth rate in the steep firing rate regime and the maximal growth in the shallow firing rate regime, as shown in Fig. 1. We proceed as follows in order to detect the times for the emergence the stable patterns for each heterogeneity parameter set: Numerical solution is projected onto the x, y-plane for a fixed time in the transient, initial stage of the temporal development. This is shown in the first row of each of the snapshots in Fig. 12-15. We notice that the second row in these plots repeats itself in the third row, thus indicating that the patterns have stabilized as spatio-temporal oscillations. In addition, we observe the effect of the 1-periodicity in the y-variable in Fig. 13-15.

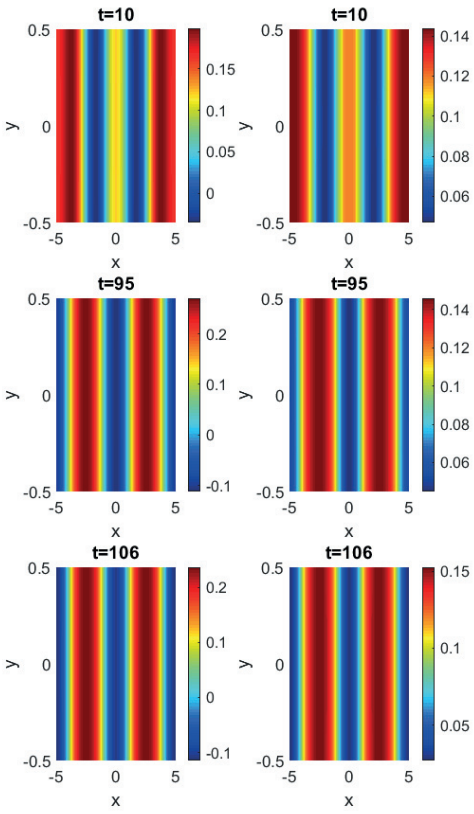

Figure 12: Dynamical evolution for parameter Set B in Table 1 and Set 1 in Table 2 (weakly modulated case) at different fixed times. Excitatory activity levels u_e and inhibitory activity levels u_i corresponds to left plots and right plots, respectively. The initial condition consists of a homogeneous solution v_0 with small perturbation in the form of a narrow centred rectangular box superimposed $-0.5 \leq x \leq 0.5$, $u_e = u_i = 0.2$.

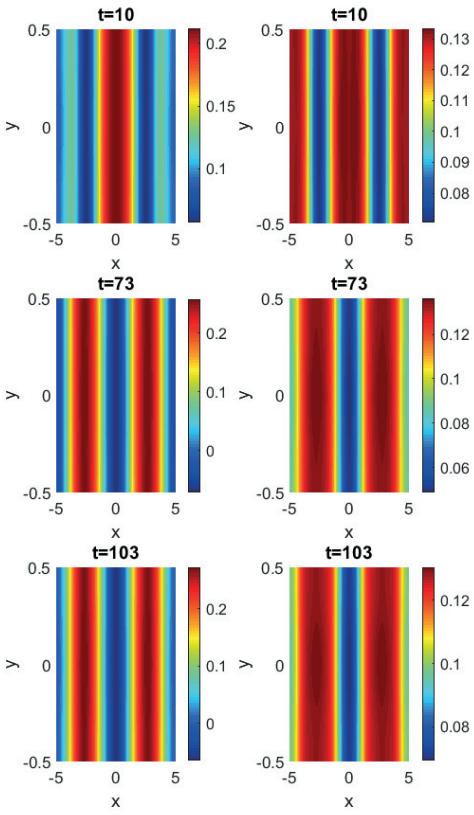

Figure 13: Dynamical evolution for parameter Set B in Table 1 and Set 2 in Table 2 at different fixed times. Excitatory activity levels u_e and inhibitory activity levels u_i corresponds to left plots and right plots, respectively. The initial condition consists of a homogeneous solution v_0 with small perturbation in the form of a narrow centred rectangular box superimposed $-0.5 \leq x \leq 0.5$, $u_e = u_i = 0.2$.

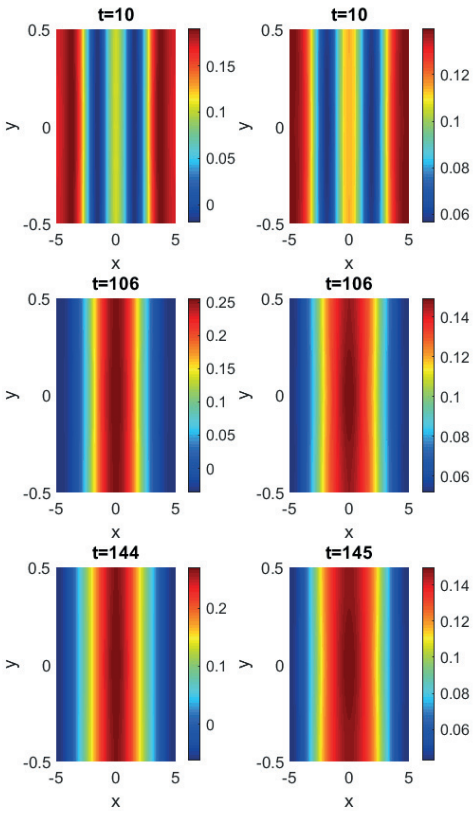

Figure 14: Dynamical evolution for parameter Set B in Table 1 and Set 3 in Table 2 at different fixed times. Excitatory activity levels u_e and inhibitory activity levels u_i corresponds to left plots and right plots, respectively. The initial condition consists of a homogeneous solution v_0 with small perturbation in the form of a narrow centred rectangular box superimposed $-0.5 \leq x \leq 0.5$, $u_e = u_i = 0.2$.

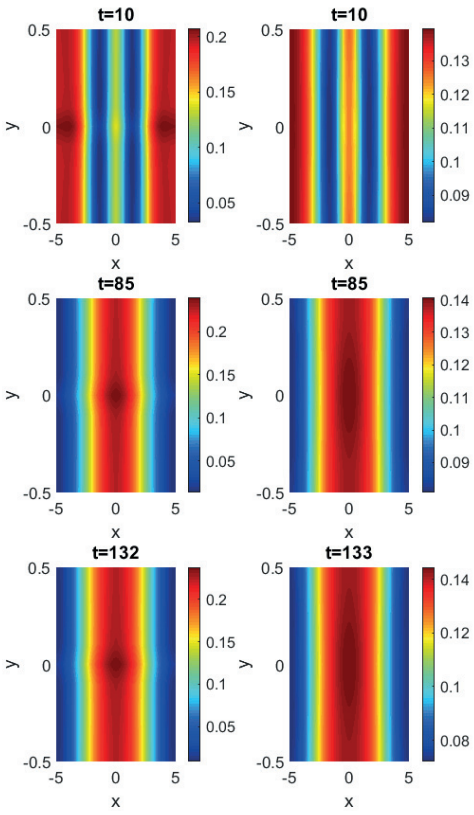

Figure 15: Dynamical evolution for parameter Set B in Table 1 and Set 4 in Table 2 at different fixed times. Excitatory activity levels u_e and inhibitory activity levels u_i corresponds to left plots and right plots, respectively. The initial condition consists of a homogeneous solution v_0 with small perturbation in the form of a narrow centred rectangular box superimposed $-0.5 \leq x \leq 0.5$, $u_e = u_i = 0.2$.

5. Conclusions and outlook

In the present paper we have investigated the effect of periodic microstructure on the pattern formation mechanism in a 2-population neural field model. This work presents an extension of the previous paper by Wyller *et al.* [15] on Turing type of instability and pattern formation within the framework of a 2-population neural field model with homogeneous and isotropic connectivity strengths.

The structure of the linear instability consists of a finite set of well-separated gain bands. In the weakly modulated case the gain band structure emerges as a homotopic deformation of gain band structure in the translational invariant case, due to the continuous dependence of the heterogeneity parameters. We have also examples for which gain bands are generated. We have also demonstrated coalescence of gain bands. The process of generation and coalescence of such bands typically takes place in the regime beyond the weakly modulated regime and is as such a microstructure effect. It is revealed as a bifurcation process. Notice that the instability structure which we have detected for the model (4) resembles the gain band structure obtained for modulational instability (MI) in the nonlocal, nonlinear Schrödinger equation [34] and for modulational instability in the nonlocal $\chi^{(2)}$-model [35]. The existence of several coexisting gain bands thus seems to be a generic feature of nonlocal models.

We have also detailed numerically the development of the linear instability into the nonlinear regime. We have considered examples with steep and shallow firing rate functions. In order to compare with previously obtained results for the 2-population neural translational invariant model, we have used the same parameter sets for the steep and shallow regimes as in Wyller *et al.* [15]. We have presented the result of the pattern forming process as snap shots of the projection of the numerical solutions onto the x, y-plane for the 4 specific sets of the heterogeneity parameters α_{mn} listed in Table 2. These sets represent scenarios with weak- , intermediate- and strong heterogeneity. We have divided the investigation into two subsections corresponding to the outcomes in the steep firing rate regime and in the shallow regime. Here we will emphasize that the actual choices of steepness parameters and the heterogeneity parameters will of course not cover all possible outcomes, since all these parameters can be varied independently of each other.

The results of these simulations can be summarized as follow:

In the steep firing rate regime (Set A)) we get as expected spatial oscillations. In the weakly modulated case (Set 1) the oscillations consist of periodically distributed bump like structures where the solution restricted to one period is quite similar to the bumps detected in Kolodina *et al.* [32]. The wavelength of these oscillations is as expected approximately equal to the wave length of the linearly most unstable mode. We also observe that it takes relatively longer time to form the stable stationary patterns than in the translational invariant case. This was indeed expected since the growth rate of the linearly most unstable mode in this case is less than the corresponding growth rate in the translational invariant case. When increasing the degrees of heterogeneity beyond the weakly modulated case, our numerical examples indicate a further slowdown of the pattern forming process. When the patterns are formed in the regime of strong heterogeneity, we readily observe that the impact of the periodic heterogeneity manifests itself in 1-periodicity in y-variable, in addition to the spatial oscillatory behavior in the x-direction.

In the shallow firing rate regime (Set B) we obtain spatiotemporal oscillations. In the weakly modulated case (Set 1) spatiotemporal oscillations appear as homotopic deformation of the spatiotemporal oscillations of the translational invariant case. This follows from the linear stability analysis, namely, we have got complex conjugate eigenvalues of the stability matrix for the linearly most unstable mode. Even in this case the increase in the degree of heterogeneity will decrease the growth rate of the fastest growing mode, thus explaining the slowdown of the pattern forming process when increasing the degree of heterogeneity. We have also observed that the pattern forming process in the shallow firing rate regime takes much longer time than in the steep regime. This result can easily be understood as a consequence of the magnitude of order difference between the maximal growth rate in the steep firing rate regime versus the shallow firing rate regime. We also observe that the strong heterogeneity results in 1-periodicity in the y-direction of the emerging patterns in addition to the spatiotemporal oscillations in the x, t-direction.

A natural extension of the present work consists of studying pattern formation within the modelling framework (4) when $N = 2$. This means that

a 2-population model with a periodic microstructure built into the connectivity kernels is defined on a two-dimensional domain. This extension can be viewed as a step towards a more realistic description of the actual situation in the cortical tissue. Other realistic effects which could be included in the present homogenized modelling framework (and its generalisations to Volterra type of models) is finite axonal and dendritic delays effect. Here we will follow the line of thought as in Venkov *et al.* [36] and Faye *et al.* [37]. Finally, but not least, possible modifications of the present model consist of assuming other types of microstructure effects and then investigate existence and stability of coherent structures as well as pattern formation within the framework of the corresponding homogenized problems.

Acknowledgements

The present work was initiated and completed in 2018 when J. Wyller was a Guest Professor at Department of Applied Mathematics and Computer Science, Technical University of Denmark (DTU) and at Department of Mathematics, Natural Sciences and Information Technologies, Tambov State University, Russia. J. Wyller will like to express his sincere gratitude to DTU and Tambov State University for kind hospitality during the stays. The authors are grateful to Professor Arcady Ponosov, Professor Bjørn Fredrik Nielsen (Norwegian University of Life Sciences) and Dr Evgenii Burlakov (Tambov State University) for fruitful and stimulating discussions during the preparation phase of this paper. This research work was supported by the Norwegian University of Life Sciences and The Research Council of Norway, project number 239070.

References

[1] Shun-Ichi Amari. Homogeneous nets of neuron-like elements. *Biological cybernetics*, 17(4):211–220, 1975.

[2] Shun-ichi Amari. Dynamics of pattern formation in lateral-inhibition type neural fields. *Biological cybernetics*, 27(2):77–87, 1977.

[3] Hugh R Wilson and Jack D Cowan. Excitatory and inhibitory interactions in localized populations of model neurons. *Biophysical journal*, 12(1):1–24, 1972.

[4] Hugh R Wilson and Jack D Cowan. A mathematical theory of the functional dynamics of cortical and thalamic nervous tissue. *Kybernetik*, 13(2):55–80, 1973.

[5] Paul C Bressloff. Spatiotemporal dynamics of continuum neural fields. *Journal of Physics A: Mathematical and Theoretical*, 45(3):033001, 2011.

[6] Paul C Bressloff, Jack D Cowan, Martin Golubitsky, and Peter J Thomas. Scalar and pseudoscalar bifurcations motivated by pattern formation on the visual cortex. *Nonlinearity*, 14(4):739, 2001.

[7] Paul C Bressloff, Jack D Cowan, Martin Golubitsky, Peter J Thomas, and Matthew C Wiener. Geometric visual hallucinations, euclidean symmetry and the functional architecture of striate cortex. *Philosophical Transactions of the Royal Society of London B: Biological Sciences*, 356(1407):299–330, 2001.

[8] G Bard Ermentrout and Jack D Cowan. A mathematical theory of visual hallucination patterns. *Biological cybernetics*, 34(3):137–150, 1979.

[9] Patricia S Goldman-Rakic. Cellular basis of working memory. *Neuron*, 14(3):477–485, 1995.

[10] Carlo R Laing, William C Troy, Boris Gutkin, and G Bard Ermentrout. Multiple bumps in a neuronal model of working memory. *SIAM Journal on Applied Mathematics*, 63(1):62–97, 2002.

[11] Carlo R Laing and William C Troy. Two–bump solutions of amari–type models of working memory. *Physica D: Nonlinear Phenomena*, 178:190–218.

[12] G Bard Ermentrout and J Bryce McLeod. Existence and uniqueness of travelling waves for a neural network. *Proceedings of the Royal Society of Edinburgh Section A: Mathematics*, 123(3):461–478, 1993.

[13] Xiaoying Huang, William C Troy, Qian Yang, Hongtao Ma, Carlo R Laing, Steven J Schiff, and Jian-Young Wu. Spiral waves in disinhibited mammalian neocortex. *Journal of Neuroscience*, 24(44):9897–9902, 2004.

[14] Patrick Blomquist, John Wyller, and Gaute T Einevoll. Localized activity patterns in two-population neuronal networks. *Physica D: Nonlinear Phenomena*, 206(3):180–212, 2005.

[15] John Wyller, Patrick Blomquist, and Gaute T Einevoll. Turing instability and pattern formation in a two-population neuronal network model. *Physica D: Nonlinear Phenomena*, 225(1):75–93, 2007.

[16] Jack Xin. An introduction to fronts in random media. *SIAM Review*, 42:161, 2000.

[17] Jack Xin. An introduction to fronts in random media. *Surveys and Tutorials in the Applied Mathematical Sciences, Springer Verlag*, 2009.

[18] Paul C Bressloff. Spatially periodic modulation of cortical patterns by long-range horizontal connections. *Physica D: Nonlinear Phenomena*, 185(3):131–157, 2003.

[19] Paul C Bressloff, Stefanos E Folias, Alain Prat, and Y-X Li. Oscillatory waves in inhomogeneous neural media. *Physical review letters*, 91(17):178101, 2003.

[20] Zachary P Kilpatrick, Stefanos E Folias, and Paul C Bressloff. Traveling pulses and wave propagation failure in inhomogeneous neural media. *SIAM Journal on Applied Dynamical Systems*, 7(1):161–185, 2008.

[21] Stephen Coombes and CR Laing. Pulsating fronts in periodically modulated neural field models. *Physical Review E*, 83(1):011912, 2011.

[22] Helmut Schmidt, Axel Hutt, and Lutz Schimansky-Geier. Wave fronts in inhomogeneous neural field models. *Physica D: Nonlinear Phenomena*, 238(14):1101–1112, 2009.

[23] Stephen Coombes, Carlo Laing, Helmut Schmidt, Nils Svanstedt, and John Wyller. Waves in random neural media. *Discrete and Continuous Dynamical Systems—Series A*, 32:2951–2970, 2012.

[24] Nils Svanstedt and Jean Louis Woukeng. Homogenization of a wilson–cowan model for neural fields. *Nonlinear Analysis: Real World Applications*, 14(3):1705–1715, 2013.

[25] Nils Svanstedt, John Wyller, and Elena Malyutina. A one-population amari model with periodic microstructure. *Nonlinearity*, 27(6):1391–1417, 2014.

[26] Gabriel Nguetseng. A general convergence result for a functional related to the theory of homogenization. *SIAM Journal on Mathematical Analysis*, 20(3):608–623, 1989.

[27] Dag Lukkassen, Gabriel Nguetseng, and Peter Wall. Two-scale convergence. *International Journal of Pure and Applied Mathematics*, 2(1):35–86, 2002.

[28] Augusto Visintin. Towards a two-scale calculus. *ESAIM: Control, Optimisation and Calculus of Variations*, 12(3):371–397, 2006.

[29] Elena Malyutina, John Wyller, and Arcady Ponosov. Two bump solutions of a homogenized wilson–cowan model with periodic microstructure. *Physica D: Nonlinear Phenomena*, 271:19–31, 2014.

[30] Elena Malyutina, Arcady Ponosov, and John Wyller. Numerical analysis of bump solutions for neural field equations with periodic microstructure. *Applied Mathematics and Computation*, 260:370–384, 2015.

[31] Evgenii Burlakov, John Wyller, and Arcady Ponosov. Two-dimensional amari neural field model with periodic microstructure: Rotationally symmetric bump solutions. *Communications in Nonlinear Science and Numerical Simulation*, 32:81–88, 2016.

[32] Karina Kolodina, Anna Oleynik, and John Wyller. Single bumps in a 2-population homogenized neuronal network model. *Physica D: Nonlinear Phenomena*, 370:40–53, 2018.

[33] Roland Potthast and Peter Beim Graben. Existence and properties of solutions for neural field equations. *Mathematical Methods in the Applied Sciences*, 33(8):935–949, 2010.

[34] John Wyller, Wieslaw Krolikowski, Ole Bang, and Jens Juul Rasmussen. Generic features of modulational instability in nonlocal kerr media. *Physical Review E*, 66(6):066615, 2002.

[35] John Wyller, Wiesław Z Królikowski, Ole Bang, Dan Erik Petersen, and Jens Juul Rasmussen. Modulational instability in the nonlocal $\chi^{(2)}$-model. *Physica D: Nonlinear Phenomena*, 227(1):8–25, 2007.

[36] Nikola Atanasov Venkov, Stephen Coombes, and Paul C Matthews. Dynamic instabilities in scalar neural field equations with space-dependent delays. *Physica D: Nonlinear Phenomena*, 232(1):1–15, 2007.

[37] Grégory Faye and Olivier Faugeras. Some theoretical and numerical results for delayed neural field equations. *Physica D: Nonlinear Phenomena*, 239(9):561–578, 2010.

4 Errata list

Side	Line	Original text	Corrected text
vii		Need to include Æ, Ø, Å in the Norwegian summary	

Table 1

ISBN: 978-82-575-1583-6
ISSN: 1894-6402

Norwegian University
of Life Sciences

Postboks 5003
NO-1432 Ås, Norway
+47 67 23 00 00
www.nmbu.no